

Hypertrophic cardiomyopathy: Development of new molecular strategies for mutation analysis and therapy

Dissertation

In fulfillment of the requirements for the degree

Doctor of Natural Sciences

Submitted to the Department of Biology, Faculty of Mathematics,

Informatics and Natural Sciences

University of Hamburg

by

Christina Gedicke

from Waren/Müritz

Hamburg, 2011



Universitätsklinikum
Hamburg-Eppendorf

Zentrum für Molekulare
Neurobiologie

Falkenried 94
20251 Hamburg

Research Group:
Neuronal Translational
Regulation

Dr. Kent Duncan
Telefon: (040) 7410-56274
Telefax: (040) 7410-53436

kent.duncan@zmnh.uni-hamburg.de
www.zmnh.uni-hamburg.de

Universitätsklinikum Hamburg-Eppendorf Martinistraße 52 20246 Hamburg
Zentrum für Molekulare Neurobiologie - Forschergruppen

To whom it may concern:

27 July 2011

Certification

I hereby certify that the English language used by Christina Gedicke in her dissertation 'Hypertrophic cardiomyopathy: development of new molecular strategies for mutation analysis and therapy' is correct.

Dr. Kent Duncan
Universität Hamburg
Universitätsklinikum Hamburg-Eppendorf
Zentrum für Molekulare Neurobiologie
AG Duncan
Falkenried 94 · D-20251 Hamburg

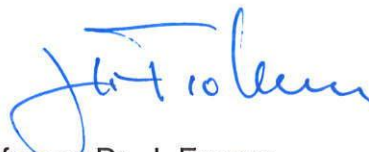
Universitätsklinikum Hamburg-Eppendorf
Körperschaft des öffentlichen Rechts
Gerichtsstand: Hamburg

Vorstandsmitglieder:
Prof. Dr. Jörg F. Debatin (Vorsitzender)
Dr. Alexander Kirstein
Joachim Pröls
Prof. Dr. Dr. Uwe Koch-Gromus

Bankverbindung:
HSH Nordbank
Kto.-Nr.: 104 364 000
BLZ: 210 500 00

Genehmigt vom Fachbereich Biologie
der Fakultät für Mathematik, Informatik und Naturwissenschaften
an der Universität Hamburg
auf Antrag von Prof. Dr. T. ESCHENHAGEN
Weiterer Gutachter der Dissertation:
Prof. Dr. W. STREIT
Tag der Disputation: 30. September 2011

Hamburg, den 15. September 2011



Professor Dr. J. Fromm
Vorsitzender des Promotionsausschusses
Biologie

Table of contents

List of figures	VII
List of tables	IX
1 Introduction	1
1.1 Heart anatomy and function.....	1
1.2 Hypertrophic cardiomyopathy	5
1.2.1 Clinical aspects.....	5
1.2.2 Common mutations in sarcomeric proteins.....	6
1.3 Cardiac myosin-binding protein-C (cMyBP-C)	8
1.3.1 Structural role of cMyBP-C	8
1.3.2 Regulatory role of cMyBP-C	10
1.3.3 <i>MYBPC3</i> mutations in hypertrophic cardiomyopathy	11
1.4 Mechanisms of RNA splicing.....	12
1.5 Nonsense-mediated mRNA decay	14
1.6 The ubiquitin-proteasome system.....	16
1.7 Treatment and potential novel therapies for hypertrophic cardiomyopathy.....	18
1.7.1 Pharmacological and surgical treatments of hypertrophic cardiomyopathy ..	18
1.7.2 Innovative therapies for hypertrophic cardiomyopathy	18
1.7.2.1 Targeting the NMD or UPS?.....	19
1.7.2.2 Targeting nonsense mRNA?	20
1.7.2.3 Targeting mutant pre-mRNA?	20
1.8 Objectives	21
2 Material and Methods	23
2.1 Material.....	23
2.1.1 Cell lines and neonatal mouse cardiac myocytes	23
2.1.2 Targeted <i>Mybpc3</i> -knock-in mouse model.....	23
2.1.3 Treatments applied to HEK293 cells and neonatal mouse cardiac myocytes	25

2.2	Methods	25
2.2.1	Molecular biological methods.....	25
2.2.1.1	Generation of minigenes by directional TOPO® cloning.....	25
2.2.1.2	Preparation of plasmid DNA.....	27
2.2.1.3	Restriction digestion.....	28
2.2.2	Cell biology, transfections, treatments and microscopy	28
2.2.2.1	HEK293 cell line.....	28
2.2.2.2	Isolation and culture of neonatal mouse cardiac myocytes.....	32
2.2.3	Purification, analysis and sequencing of DNA and RNA	34
2.2.3.1	Agarose gel electrophoresis	34
2.2.3.2	Preparative agarose gels	35
2.2.3.3	Sequencing of DNA	35
2.2.3.4	RNA isolation.....	35
2.2.3.5	Determination of the RNA and DNA concentration.....	35
2.2.3.6	Reverse transcription.....	36
2.2.3.7	Polymerase chain reaction (PCR)	36
2.2.3.8	Determination of mRNA level by quantitative PCR.....	38
2.2.4	Protein analysis	42
2.2.4.1	Protein isolation and concentration determination.....	42
2.2.4.2	Immunoprecipitation of proteins.....	42
2.2.4.3	Western blot	43
2.2.4.4	Determination of the half-lives of cMyBP-C wild-type and knock-in proteins.....	44
2.3	Statistical analysis.....	45
3	Results.....	46
3.1	Establishment of a cell-based system to analyse the expression of <i>MYBPC3</i> mutations.....	46
3.1.1	Choice of <i>MYBPC3</i> mutations	46
3.1.2	Generation of minigenes encoding human mini-cMyBP-Cs	49
3.1.3	Evaluation of the expression of human minigenes after transient transfection into HEK293 cells	51
3.1.4	Evaluation of human mini-cMyBP-C proteins after transient transfection....	53
3.1.5	Establishment of stable cell lines expressing human minigenes	54

3.1.5.1	Evaluation of minigenes' expression at the level of mRNA	55
3.1.5.2	Evaluation of the contribution of NMD in the regulation of gene mutation expression	57
3.1.5.3	Evaluation of NMD inhibition in clonal Flp-In293 cells	59
3.1.5.4	Evaluation of minigenes' expression at the protein level	61
3.1.6	Summary of the chapter	66
3.2	Evaluation of an RNA-based approach to remove the mutated exon in cardiac myocytes from <i>Mybpc3</i> knock-in mice	67
3.2.1	Validation of an alternative spliced isoform in WT mice	69
3.2.2	Stability and localisation of spliced variant-4	69
3.2.3	The exon-skipping strategy and choice of the target.....	71
3.2.4	Design of antisense oligoribonucleotides.....	72
3.2.5	Intracellular localisation of antisense oligoribonucleotides	74
3.2.6	Evaluation of the skipping efficiency in AON-treated NMCMS	75
3.2.7	Half-lives of WT- and KI-cMyBP-C proteins.....	77
3.2.8	Determination of the mRNA levels in AON-treated NMCMS	78
3.2.9	Evaluation of the cMyBP-C protein levels in AON-treated NMCMS	82
3.2.10	Summary of the chapter	85
4	Discussion	86
4.1	HEK293 cells stably expressing human <i>MYBPC3</i> minigenes are suitable for analysis of the expression of <i>MYBPC3</i> mutations	86
4.2	Modified antisense oligoribonucleotides induce exon skipping in cardiac myocytes from wild-type and <i>Mybpc3</i> -knock-in mice	91
4.2.1	Outlook.....	95
4.2.2	Summary	96
5	Appendix	99
5.1	Material.....	99
5.1.1	Adenovirus	99
5.1.2	Antibodies	99
5.1.3	Bacterial strains	100
5.1.4	Chemicals	100
5.1.5	Consumable material.....	103

5.1.6	Kits	104
5.1.7	Laboratory equipment	105
5.1.8	Restriction enzymes	106
5.1.9	Oligonucleotides.....	107
5.1.9.1	<i>MYBPC3</i> primers and probes	107
5.1.9.2	<i>Mybpc3</i> primers and probes	108
5.1.9.3	Antisense oligoribonucleotide sequences.....	109
5.1.10	Vectors	109
5.2	Protein and DNA markers	110
5.3	List of abbreviations	110
6	Literature	114
7	Acknowledgement.....	120

List of figures

Figure 1.1. Anatomy of the heart.	1
Figure 1.2. The cardiac conduction system.	2
Figure 1.3. Ultrastructure of the sarcomere.	3
Figure 1.4. Functional unit of the sarcomere.	5
Figure 1.5. Characteristics of hypertrophic cardiomyopathy.	6
Figure 1.6. The cardiac myosin-binding protein C domain structure.	9
Figure 1.7. Proposed arrangement of the thick filament associated cMyBP-C.	10
Figure 1.8. Classical splicing signals.	12
Figure 1.9. Exonic and intronic splicing enhancer and silencer motifs.	13
Figure 1.10. The nonsense-mediated mRNA decay pathway.	15
Figure 1.11. The ubiquitin-proteasome system.	17
Figure 2.1. Targeting strategy of the <i>Mybpc3</i> -knock-in mouse model.	24
Figure 2.2. Minigene construct generated by PCR.	25
Figure 2.3. TOPO® cloning.	26
Figure 2.4. The Flp-In™-System.	30
Figure 2.5. Example of screening of Flp-In™ cell lines transfected with different minigene plasmids after <i>lacZ</i> -staining.	31
Figure 2.6. TaqMan® probe and SYBR® green chemistries for RT-qPCR analysis.	39
Figure 2.7. Amplification plot.	40
Figure 3.1. Consequences of a splicing mutation in <i>MYBPC3</i>	47
Figure 3.2. Consequences of a 4-bp-insertion in <i>MYBPC3</i>	48
Figure 3.3. Analyses of a 4-bp-insertion in <i>MYBPC3</i> at both the mRNA and protein level in patient samples.	48
Figure 3.4. Evaluation of generated minigenes by restriction digestion and sequencing. ...	50
Figure 3.5. Evaluation of generated minigenes by PCR.	51
Figure 3.6. cMyBP-C expression in non-transfected HEK293 cells.	52
Figure 3.7. Expression of human minigenes after transient transfection.	53
Figure 3.8. Protein expression of human minigenes after transient transfection.	54
Figure 3.9. β-Galactosidase activity in clonal Flp-In™ cell lines.	55
Figure 3.10. Expression of human minigenes in clonal Flp-In293 cell lines.	56

Figure 3.11. Determination of the minigene expression level.	57
Figure 3.12. NMD reporter genes.	58
Figure 3.13. NMD-inhibition by emetine in clonal WT-Flp-In293 cells transfected with NMD reporter plasmids.	59
Figure 3.14. Effect of NMD inhibition in Flp-In293 cells.	60
Figure 3.15. Evaluation of protein levels in Flp-In293 cells.	61
Figure 3.16. Validation of protein expression in Flp-In293 cells after immunopreci- pitation.	62
Figure 3.17. Evaluation of protein levels in Flp-In293 cells after proteasome inhibition. ..	63
Figure 3.18. Determination of the steady-state levels of ubiquitinated proteins.	64
Figure 3.19. Validation of protein expression in Flp-In293 cells after proteasome inhibition.	65
Figure 3.20. Cardiac phenotype of cMyBP-C knock-in mice.	67
Figure 3.21. Consequences of a G>A transition in <i>Mybpc3</i> -KI mice.	68
Figure 3.22. Validation of an alternative spliced isoform.	69
Figure 3.23. Evaluation of the stability of aberrant cMyBP-C proteins in HEK cells.	70
Figure 3.24. Intracellular localisation of the variant-4 protein in KI-NMCMs.	71
Figure 3.25. Protein structures resulting from the G>A transition in <i>Mybpc3</i> -KI mice.	72
Figure 3.26. Predicted ESE sequences of <i>Mybpc3</i> -exon 5.	73
Figure 3.27. Exon-skipping strategy.	74
Figure 3.28. Fluorescence analysis of AON-5-treated NMCMs by confocal microscopy. .	75
Figure 3.29. Targeting specificity of AONs in WT-NMCMs.	76
Figure 3.30. Identification of the required AON amount to induce exon skipping in KI- NMCMs.	77
Figure 3.31. Determination of the protein half-life of WT- and KI-cMyBP-C proteins.	78
Figure 3.32. AON-induced exon skipping in WT- and KI-NMCMs.	79
Figure 3.33. RT-PCR of KI-NMCMs after AON-treatment.	80
Figure 3.34. RT-qPCR analysis of KI-NMCMs after AON-treatment.	81
Figure 3.35. Protein expression of cMyBP-C variants.	83
Figure 3.36. Determination of the level of total cMyBP-C of KI-cMyBP-C mutants.	84
Figure 5. 1. Markers.	110

List of tables

Table 1.1. Mutations in sarcomeric genes causing HCM.	7
Table 2.1. Standard PCR program used for PrimeSTAR® HS DNA polymerase.	37
Table 2.2. PCR program adapted to RT-qPCR conditions for use with PrimeSTAR®.....	37
Table 2.3. Standard PCR program (touch-down) used for AmpliTaq Gold® polymerase..	38
Table 2.4. PCR program for qPCR analysis with TaqMan probes	41
Table 2.5. PCR program for qPCR analysis with SYBR® green	41
Table 5.1. Antibodies used for Western blotting.	99
Table 5.2. Antibodies used for immunofluorescence staining.	100

1 Introduction

1.1 Heart anatomy and function

The heart plays a central role in meeting the metabolic requirements of all tissues by assuring adequate blood circulation through the vasculature. In the normal resting state this involves pumping the entire circulating blood volume about once every minute. The heart is divided into four chambers – the two upper left and right atria and the two lower left and right ventricles. Each ventricle has two one-way valves: the atrioventricular valve (left mitral and right tricuspid) between atrium and ventricle and the semilunar valve (left aortic and right pulmonary) between ventricle and outflow. The left and right side of the heart are separated by the interatrioventricular septum. While the right side receives deoxygenated blood from the whole body (except the lungs) and pumps it through the lungs, the left side of the heart receives oxygenated blood from the lungs and pumps it into the body (Figure 1.1).

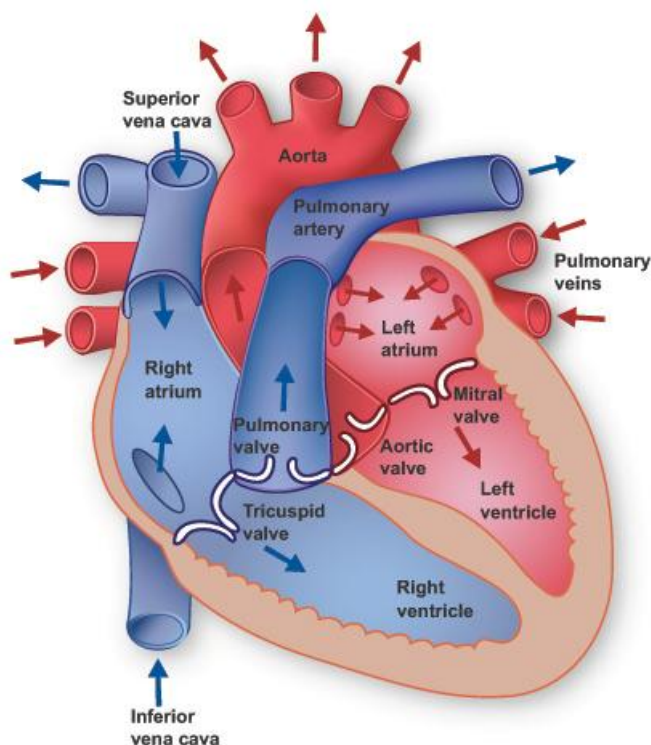


Figure 1.1. Anatomy of the heart.

The image represents a lateral section of the heart with its internal structures and shows the blood flow through the organ. The blue components and arrows indicate pathways of the deoxygenated blood coming from the body and pumped through the lungs for oxygen uptake. The red components and arrows illustrate the pathways of the oxygenated blood coming from the lungs and pumped into the body (picture from the Texas Heart Institute website.)

The contractile force of the heart is generated by the cardiac muscle, which varies from both skeletal and smooth muscles e.g. in that the cardiac cells (cardiomyocytes) intertwine with each other by intercalated discs. This linkage allows a consecutive contraction from the apex to the base of the heart to facilitate maximal ejection outflow from the ventricles during contraction.

The heart is innervated by both sympathetic and parasympathetic nerves of the autonomous nervous system (Mitchell 1953), which controls the strength and frequency of the heart beat. To induce contraction/relaxation of the heart a unique group of cells within the heart generate and propagate electrical signals. The so called conduction system is composed of five units (Figure 1.2): the sinoatrial node, the atrioventricular node, the bundle of His, the Purkinje fibers and the left and right bundle branches. The primary pacemaker of the heart is the sinus node, which regularly generates electrical impulses that induce contraction of the atria. The electrical signal then passes the atrioventricular node before traversing through the bundle of His and Purkinje fibers to finally induce contraction of the ventricles.

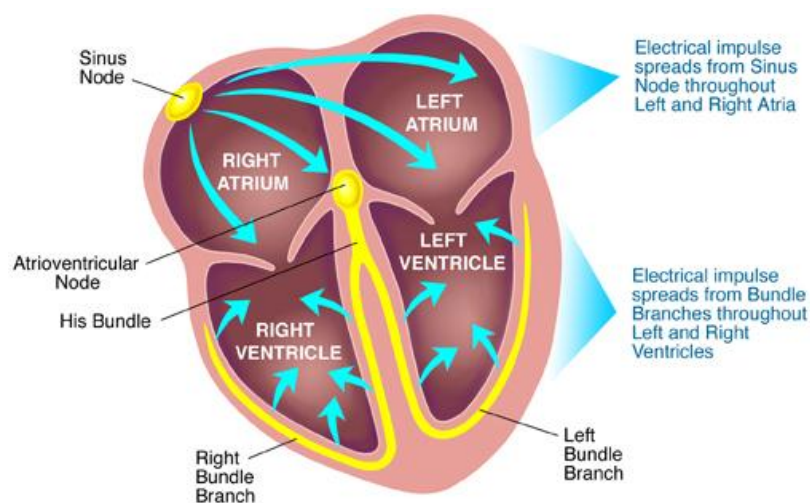


Figure 1.2. The cardiac conduction system.

Without any neural stimulation the sinus node generates electrical impulses that induce contraction of the left and right atria. A special conducting tissue conveys the impulse to the atrioventricular node, which conducts the atrial impulse to the ventricles. This allows the ventricles to relax and fill with blood, while the atria contracts. Rapid conduction proceeds through the bundle of His, which divides into the right and left bundle branches and extends down either side of the interventricular septum to cause contraction of the ventricles (picture from the "UpToDate" website).

Cardiac muscle contains three types of cells - fibroblasts, endothelial cells and cardiomyocytes. Cardiomyocytes constitute about 20% of the total cell population but 80% of the total mass. They are made up of myofibrils, which are composed of repeated

sarcomeres, the basic contractile units. Each sarcomere (Figure 1.3) mainly consists of three types of myofilaments: the thin filament (contains predominantly actin), the thick filament (contains primarily myosin) and the elastic filament (contains primarily titin). Sarcomeres are restricted by Z-discs, where the thin filament and titin are anchored. Titin in turn extends to the M-band where it interacts with the thick filament and attaches it to the Z-disc (Labeit et al., 1992). Titin is involved in the passive tension of the cardiac myocytes by connecting the Z-disc with the M-band *via* its elastic properties (Linke et al., 1999; Linke et al., 2000; Solaro et al., 2010). The thick filament-associated protein cardiac myosin-binding protein-C (cMyBP-C) has both functional and structural roles in the sarcomere. Like cMyBP-C several other proteins such as nebulin and M-protein play an important role in the stability of the sarcomeric structure. They are mainly located in the Z-disc and in the M-band of the sarcomere.

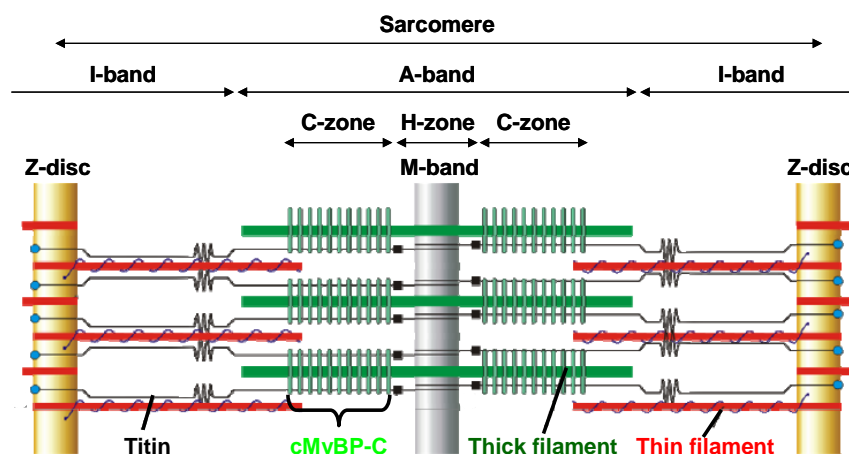


Figure 1.3. Ultrastructure of the sarcomere.

The sarcomere is restricted by the Z-discs, which are surrounded by the regions of the I-bands in proximity to the A-band. Z-discs are anchors for thin filaments (red) and titin (black). Thick filaments (green) are located at the A-band and cross the M-band. A thick filament associated protein, the cardiac myosin-binding protein-C (cMyBP-C), is illustrated in light green as transverse lines within the thick filament (adapted from Gregorio et al., 1999).

Both the thin and thick filaments are arranged in a manner that they can slide over each other during the process of muscle contraction (sliding filament theory; see Figure 1.4). The molecular motor of the heart is the myosin molecule, which is composed of two myosin heavy chains (MHC) and two pairs of myosin light chains (MLC). Together, they form 3 regions, which are the globular heads (S1 domain), the neck (S2 domain) and the tail (light meromyosin, LMM). The MHCs form a coiled-coil structure, and form distinct globular heads at the N-terminus. The heads project from the thick filament and each

contain an actin binding site and an enzymatic site, which catalyses the hydrolysis of ATP (Adelstein, 1983). The binding of myosin to actin is regulated by tropomyosin, which, in tandem with the troponin complex, associates with actin in muscle fibers. Troponin is a hetero-trimer composed of an inhibitory (TnI), tropomyosin-binding (TnT) and Ca^{2+} -binding (TnC) subunit.

Cardiac muscle contraction is initiated when extracellular calcium ions enter the cytoplasm through voltage-gated L-type calcium channels during the action potential. This inward flux induces the opening of calcium release channels (ryanodine receptors) of the intracellular sarcoplasmic reticulum. The combination of calcium influx and calcium release results in an increase of the free calcium concentration (calcium-induced calcium release; Weiss et al., 2011). The calcium can then bind to the calcium-sensitive protein TnC, which triggers systole and induces a conformational change of TnC. This allows the C-terminus of TnI to bind to TnC and changes in turn the position of TnT, such that it pulls Tm into the groove of the actin filament (Kass et al., 2006; Aktories et al., 2009). Thus, the binding sites for the myosin heads are fully uncovered from the actin filament and myosin can bind. The binding of ATP to myosin-S1 detaches the S1-crossbridge from actin followed by hydrolysis of ATP in ADP and P_i . In the presence of Ca^{2+} , which binds to TnC, myosin-S1 undergoes a conformational change and can weakly interact with actin. This interaction enhances the release of P_i , which produces a strong interaction between myosin-S1 and actin due to conformational changes of myosin. Further conformational changes of myosin-S1 result in a stroke of the crossbridge and shift the thick filament against the thin filament pulling the actin filament into the middle of the sarcomere. ADP is then released to return to the rigor-like state. The repeated release and binding of myosin heads of the series-connected sarcomeres forms the contraction. The movement of the myosin molecules is regulated by interactions with myosin light chain and cMyBP-C, depending on their phosphorylation state (Colson et al., 2010).

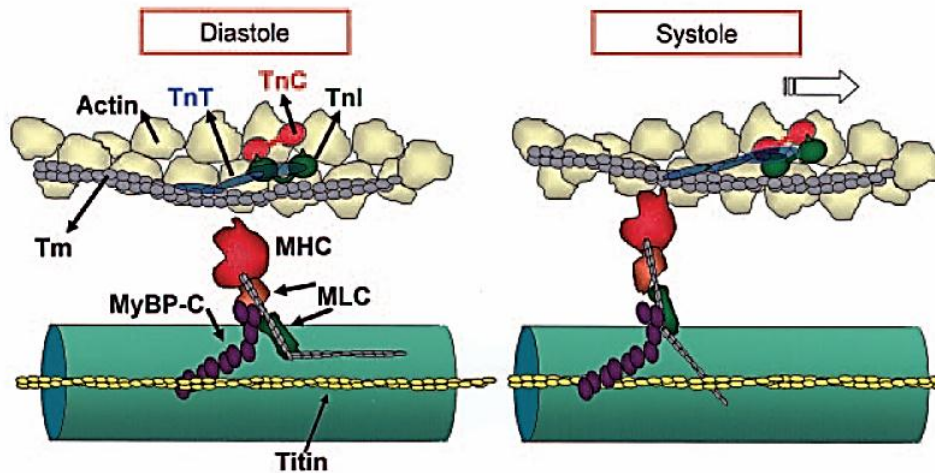


Figure 1.4. Functional unit of the sarcomere.

Scheme of the structural unit of the sarcomere showing one cross-bridge in diastole (left) and one in systole (right). In diastole, the tropomyosin (Tm) blocks the cross-bridge formation of the myosin heads (MHC) with actin by protein-protein interactions with troponin I (TnI, green) and troponin T (TnT, blue). The calcium-sensitive troponin C (TnC, red) does not interact with the C-terminal region of TnI. In the presence of calcium, which triggers systole, TnC is deformed such that TnI can bind to it. This in turn changes the position of TnT so that it pulls Tm into the groove of the actin filament. Consequently, the binding sites for the myosin heads are uncovered from the actin filament. If ATP binds to the myosin head and is hydrolysed, the actin filament is pulled into the center of the sarcomere. The repeated release and binding of myosin heads in the series-connected sarcomeres constitutes the contraction. Regulation of the cross-bridge interaction by myosin light chain (MLC) and cMyBP-C depends on their phosphorylation state (picture from Kass et al., 2006).

1.2 Hypertrophic cardiomyopathy

1.2.1 Clinical aspects

Hypertrophic cardiomyopathy (HCM) was initially described in 1958 by Donald Teare (Teare 1958). It is an autosomal-dominant disease, which is clinically characterized by an asymmetric left ventricular hypertrophy, left ventricular outflow tract obstruction and diastolic dysfunction without any obvious cause (Richardson et al., 1996; Nanni et al., 2003; Carrier et al., 2010). Histopathologically, HCM is associated with myocyte hypertrophy, myocardial disarray and interstitial fibrosis (see Figure 1.5; Nanni et al., 2003). The disease is characterised by an incomplete penetrance with inter- and intrafamilial variabilities showing both benign and malignant manifestations (Richard et al., 2003). HCM is known to be the major cause of sudden death in young individuals, especially competitive athletes, and mutation-carriers require implantable cardioverter-defibrillator placement (for review, see Carrier et al., 2010). It is also associated with a significant risk of heart failure and stroke.

The clinical diagnosis of HCM is established with 2-dimensional echocardiography by imaging the hypertrophied but nondilated left ventricular (LV) chamber in the absence of another cardiac or systemic disease, which results in hypertrophy. In diagnosed patients the increased LV wall thicknesses ranges from mild (13-15 mm) to massive (≥ 30 mm; for review, see Maron 2002).

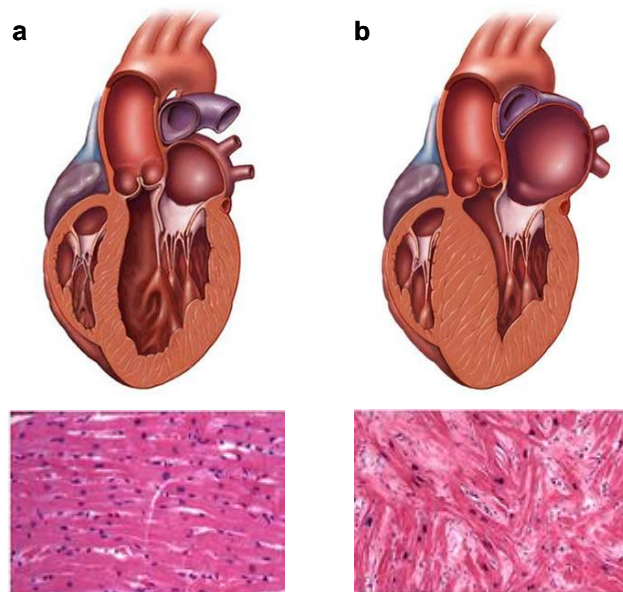


Figure 1.5. Characteristics of hypertrophic cardiomyopathy.

The upper part represents lateral sections of a normal heart (a) and a hypertrophied heart (b). In the hypertrophied heart the walls are thickened, most prominently the septum. In the lower part histological sections stained with hematoxylin and eosin are represented. While in the normal heart the myocytes are properly arranged (a), the hypertrophied heart reveals myocardial disarray and fibrosis (b). Upper pictures from the Mayo Clinic website; lower pictures from Springer Images website, Dr. Robert Padera, Boston.

1.2.2 Common mutations in sarcomeric proteins

With a prevalence of 1:500 HCM is the most frequent genetic cardiovascular disease (Maron et al., 1995). It is caused by mutations in different sarcomeric genes (for review, see Carrier et al., 2010). More than 500 different mutations in 19 different genes have been causally related to HCM (see Table 1.1; for review, see Schlossarek et al., 2011). One of the most affected gene is *MYBPC3* encoding cMyBP-C (Richard et al., 2003). Mutations in *MYBPC3* are found in 20-25% of screened patients (Richard et al., 2003; Van Driest et al., 2004). More than 185 different mutations have been reported for this gene (for review, see Schlossarek et al., 2011). Most of them are listed on the website Cardio Genomics (Disease-causing mutations in the human *MYBPC3*; Harvard Medical School Boston).

Table 1.1. Mutations in sarcomeric genes causing HCM.

Number of mutations found in different genes encoding sarcomeric proteins. Table from Schlossarek et al., 2011.

Gene name	Symbol	Number of mutations
β -myosin heavy chain	<i>MYH7</i>	218
Cardiac myosin-binding protein C	<i>MYBPC3</i>	185
Cardiac troponin T	<i>TNNT2</i>	36
Cardiac troponin I	<i>TNNI3</i>	30
α -tropomyosin	<i>TPM1</i>	12
Regulatory myosin light chain	<i>MYL2</i>	10
Cardiac α -actin	<i>ACTC1</i>	7
Essential myosin light chain	<i>MYL3</i>	5
α -actinin 2	<i>ACTN2</i>	4
Muscle LIM protein	<i>CSRP3</i>	3
Muscle RING-finger protein 1	<i>TRIM63</i>	3
Myozenin 2 (calsarcin 1)	<i>MYOZ2</i>	2
Nexilin	<i>NEXN</i>	2
Telethonin	<i>TCAP</i>	2
Titin	<i>TTN</i>	2
Vinculin	<i>VCL</i>	2
Cardiac troponin C	<i>TNNC1</i>	1
α -myosin heavy chain	<i>MYH6</i>	1
Obscurin	<i>OBSCN</i>	1

In contrast to mutations in the other most frequently mutated gene *MYH7* coding for β -myosin heavy chain, mutations in *MYBPC3* are commonly associated with delayed onset (middle or old age), lower penetrance, milder degree of hypertrophy and better survival (Niimura et al., 1998; Charron et al., 1998; Yu et al., 1998). Furthermore in 3-5% of cases patients exhibited two mutations, either in the same gene or in two different genes encoding sarcomeric proteins. These patients develop a more severe form of HCM than patients with a single mutation (Richard et al. 2003). Interestingly, 20–30% of affected patients are healthy carriers, suggesting the presence of other factors such as environment, epigenetic, micro RNAs, posttranslational modifications or gene polymorphisms (for reviews, see Richard et al., 2006; Schlossarek et al., 2011). As potential modifier genes that modulate the phenotypic expression of HCM studies described polymorphisms in genes encoding angiotensin I-converting enzyme, AT1 and AT2 receptors and in the promotor of calmodulin III (Tesson et al., 1997; Osterop et al., 1998; Deinum et al., 2001; Friedrich et al., 2009; for review, see Carrier et al. 2010).

1.3 Cardiac myosin-binding protein-C (cMyBP-C)

Myosin-binding protein-C (MyBP-C, C-protein) is a thick filament-associated protein (Offer et al., 1973). Three isoforms of MyBP-C, encoded by different genes, were found in adult muscle: slow skeletal (*MYBPC1*), fast skeletal (*MYBPC2*) and cardiac MyBP-C (*MYBPC3*). The *MYBPC3* gene encoding cardiac myosin-binding protein C (cMyBP-C) is located on human chromosome 11p11.2 (Gautel et al., 1995). The organization and sequence of *MYBPC3* was determined by Carrier et al. (1997). It contains >21000 bp and 35 exons, of which only the first 34 exons are coding.

The core structure of all three isoforms is similar: it is composed of seven I-class immunoglobulin (IgI) domains and three fibronectin type III (FnIII) domains (motif 1 to 10). Nevertheless, the cardiac isoform (cMyBP-C) differs from the others with an additional Ig-like domain at the N-terminus (C0), four phosphorylation sites located in the MyBP-C motif, a 28-amino acid loop insertion in the C5 domain and two proline-rich linker between domains C0-C1 and C4-C5 (Figure 1.6; for reviews, see Ramburan et al., 2010; Flashman et al., 2004; Oakley et al., 2004).

1.3.1 Structural role of cMyBP-C

The cMyBP-C protein of 150 kDa (Carrier, 2007) interacts with several sarcomeric proteins via specific motifs/domains: the MyBP-C motif interacts with the subfragment S2 of myosin (Gruen et al., 1999a), the C10 domain with light mero-myosin (Okagaki et al., 1993) and the C8-C10 domains with titin (Freiburg et al., 1996). In addition, the interaction with actin was shown in several publications, binding either to: the linker between C0 and C1 domains (Squire et al., 2003), the C0 domain (Kulikovskaya et al., 2003) or the domains C1 to C2 (Razumova et al., 2006). cMyBP-C contains four phosphorylation sites (Figure 1.6). Phosphorylation of cMyBP-C is assumed to sustain thick filament stability (Kulikovskaya et al., 2007).

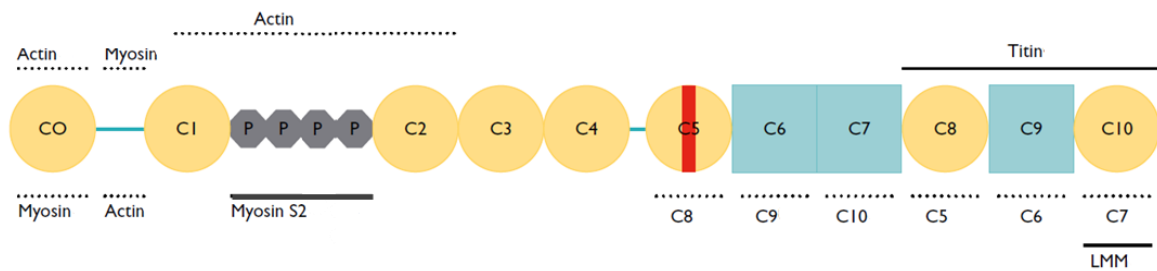


Figure 1.6. The cardiac myosin-binding protein C domain structure.

The cMyBP-C protein belongs to the intracellular immunoglobulin superfamily and is composed of 11 domains (C0 - C10), eight of them are I-class immunoglobulin domains (Ig-1; yellow circles) and three of them are fibronectin type III (Fn-3; blue boxes) domains. Protein domains implicated in protein interactions are indicated. These include regions known to interact with sarcomeric proteins (solid black lines: the subfragment-2 (S2) of myosin, titin and light mero-myosin (LMM)), as well as additional putative interaction domains that remain to be confirmed (broken black lines: actin, myosin, cMyBP-C interdomain interactions referring to the “trimeric collar” model). The blue lines between domains C0-C1 and C4-C5 indicate the Pro-Ala-rich regions. The cardiac specific 28 amino acid loop insertion in domain C5 is indicated by the red stripe and the specific four phosphorylation sites located in the MyBP-C motif are indicated by gray octagons (picture adapted from Ramburan et al., 2010).

During human and murine development and in adulthood cMyBP-C is exclusively expressed in the heart (Gautel et al., 1998; Fougousse et al., 1998). The protein is located in doublets in the C-zone of the A-band of the sarcomere where it forms a series of 7 to 9 transverse stripes of 43 nm spacing in each half A-band (Luther et al., 2008; Bennett et al., 1986; Craig et al., 1976; for review, see Oakley et al. 2004). The spacing indicates that only one-third of the myosin heads are associated with cMyBP-C (Gruen et al., 1999b).

The precise cMyBP-C protein arrangement in the sarcomere is not fully elucidated, but two models have been proposed, the trimeric collar model and an axial model (for review, see Oakley et al., 2004). The most accepted model is the trimeric collar model. In this model three staggered cMyBP-C molecules are ordered around the backbone of the thick filament in a “trimeric collar” (Moolman-Smook et al., 2002). This form is suggested to be stabilized by interactions between cMyBP-C domains C5 with C8, C7 with C10 and C10 with the myosin rod (Figure 1.7). Therefore the N-terminal located domains C0 to C4 are assumed to project for interaction with myosin and actin (Moolman-Smook et al., 2002; for review, see Ramburan et al., 2010).

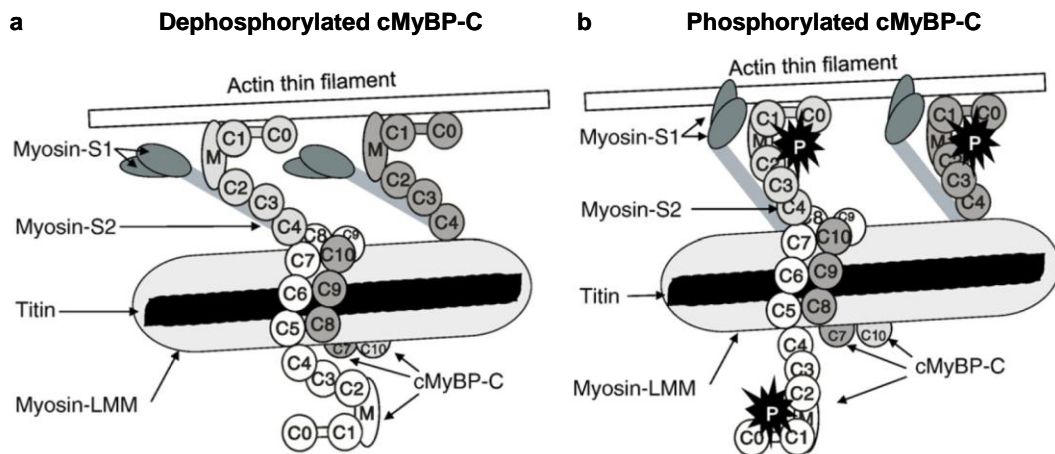


Figure 1.7. Proposed arrangement of the thick filament associated cMyBP-C.

The C5-C10 domains of three staggered cMyBP-C molecules are supposed to trimerize around the backbone of the filament of light meromyosin (myosin-LMM) and titin (black) in a "trimeric collar". This form is suggested to be stabilized by interdomain interaction of C5 with C8, C7 with C10 and C10 with the myosin rod. The N-terminal domains C0 to C4 can therefore project to interact with the myosin-S2 and actin. (a) When the MyBP-C motif (M) of cMyBP-C is dephosphorylated the cross-bridge formation of myosin-S2 and actin is prevented, since the C1-M-C2 domains are reversibly bound to myosin-S2 (grey rectangle) and actin (white rectangle). (b) Phosphorylation of the MyBP-C motif releases this interaction allowing the myosin heads (myosin-S1) to extend to the thin filament, which results in a strong actin-myosin interaction (picture from Schlossarek et al., 2011).

1.3.2 Regulatory role of cMyBP-C

The cMyBP-C protein contains phosphorylation sites, which are located in the MyBP-C motif. For both the human and murine cMyBP-C isoforms four cAMP-dependent protein kinase A (PKA) sites were identified (Ser-275, Ser-284, Ser-304, Ser-311 and Ser-281, Ser-290, Ser-310, Ser-315, respectively; for review, see Schlossarek et al., 2011). Phosphorylation of cMyBP-C occurs in response to β -adrenergic agonists via PKA, by increases in intracellular Ca^{2+} levels via an endogenous Ca^{2+} /calmodulin-dependent kinase, by protein kinase C ϵ in a Ca^{2+} -independent manner, by protein kinase D and by p90 ribosomal S6 kinase (RSK; Barefield et al., 2010; Cuello et al., 2010). It was shown that phosphorylated cMyBP-C improves force of contraction and is essential for normal cardiac function (Sadayappan et al., 2005).

The phosphorylation of cMyBP-C is involved in the regulation of cross-bridge cycling. It is therefore suggested to be the primary regulator of contractility in the thick filament by reversibly binding the S2 region of myosin in the dephosphorylated state (for reviews, see Ramburan et al., 2010; Flashman et al. 2004). Phosphorylation prevents this binding resulting in the cross-bridge formation of myosin and actin (Gruen et al., 1999b). In addition, cMyBP-C is suggested to serve as an internal load by tethering myosin-S2 to

the thick filament, thereby limiting cross-bridge formation and promoting relaxation of the sarcomere during diastole (Hofmann et al., 1991; Kulikovskaya et al., 2003; Colson et al., 2007; Pohlmann et al., 2007). The resulting reduced ATP consumption and slowed cross-bridge formation may contribute to a prolonged systolic ejection associated with an increased contractile efficiency as well as facilitating the diastolic filling rates *in vivo* (Razumova et al., 2006; Stelzer et al., 2007; for review, see Ramburan et al., 2010). In addition, by providing mechanical stability to the myofilament lattice, cMyBP-C influence the transmission of force across the sarcomere and sustain systolic stiffening (Palmer et al., 2004).

1.3.3 MYBPC3 mutations in hypertrophic cardiomyopathy

The mechanism by which mutations in *MYBPC3* cause HCM is not fully elucidated. But two mechanisms have been proposed: i) haploinsufficiency, i.e. the functional loss of one allele of the gene cannot be compensated by the healthy allele and ii) poison peptide effect, where mutant proteins interfere with the normal sarcomere function. Whereas several missense mutations were found, which result in amino acid exchanges, about 61% of the known *MYBPC3* mutations are frameshift or nonsense mutations leading to a putative null allele. While nonsense mutations are point mutations which directly results in a premature termination codon (PTC), frameshift mutations are caused by insertions, deletions or point mutations, which result in the disruption of the open reading frame and a PTC downstream of the mutation in the transcribed mRNA (for reviews, see Richard et al., 2006; Alcalai et al., 2008; Carrier et al., 2010). Frameshift and nonsense mutations are expected to produce C-terminal truncated proteins. Nevertheless, these expected shortened cMyBP-C proteins have not been detected after gene transfer in cardiac myocytes (Sarikas et al., 2005) or in myocardial tissue of patients (Rottbauer et al., 1997; Moolman et al., 2000; van Dijk et al., 2009). On the other hand, aberrant mRNAs and a lowered relative level of full-length protein content was detected for both truncation and missense mutations in affected heterozygous patients (Marston et al., 2009; van Dijk et al. 2009), suggesting that haploinsufficiency can cause HCM. The absence of truncated proteins also suggests that aberrant mRNAs or proteins are highly unstable and rapidly degraded.

Some of the described mutations are located in the consensus sequences of splice sites, suggesting an alteration of pre-mRNA splicing (Nanni et al., 2003; Andersen et al., 2004; Rottbauer et al. 1997). Splice-site mutations frequently result in skipping of the neighbouring exon or create a new splice site and thus change the splicing pattern of the transcript (for review, see Cartegni et al., 2002).

1.4 Mechanisms of RNA splicing

After gene transcription the created pre-mRNA is processed into mRNA by splicing out of the introns and joining of the exons to obtain a continuous reading frame for the translation machinery. Pre-mRNA splicing is a highly complex process in the nucleus that is orchestrated by the spliceosome and involves hundreds of different proteins and small nuclear RNAs (snRNAs). The complex of proteins and snRNAs is called small nuclear ribonucleoprotein (snRNP). Five snRNPs are involved in the splicing process (U1, U2, U4-U6). The snRNAs of the snRNPs in turn recognize three weakly conserved intronic *cis*-elements located in the pre-mRNA, which signal the presence of an intron (Figure 1.8): the 5'- and 3'-splice sites, which define the exon-intron boundaries and the branch point located 20-50 bases upstream of the 3'-splice site. Recognition of the branch point and 3'-splice site region by U2 snRNP is enhanced by the presence of an adjacent polypyrimidine tract (Clark, 2006; Gil et al., 1991). At the 5'-splice site the introns start with the nucleotides GU and end at the 3'-splice site with AG.

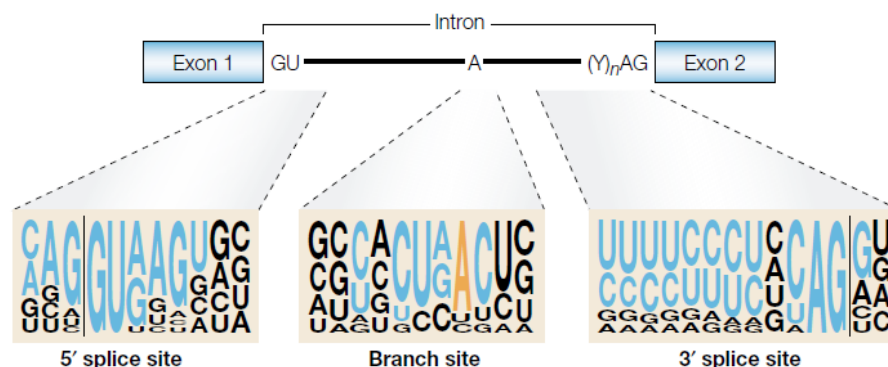


Figure 1.8. Classical splicing signals.

The upper part of the illustration shows the conserved nucleotides of the 5'-splice site (GU), the branch site (A) and the 3'-splice site (AG). The polypyrimidine tract is indicated by (Y)_n. The sequence motifs surrounding these nucleotides are depicted in the lower part. Here the height of a nucleotide reflects its frequency determined in an alignment of conserved sequences from 1683 human introns. Nucleotides that belong to classical consensus motifs are shown in blue and orange. The vertical lines indicate the exon-intron boundaries (picture from Cartegni and Krainer, 2002).

All these elements are necessary, but clearly by no means sufficient to define exon–intron boundaries as eukaryotic cells can sometimes use different splice sites within the same gene. This process, called alternative splicing, is common in mammals and results in a highly complex proteome. To regulate the complex process additional regulatory signals contribute to modulation of splicing in a developmental and/or cell-type-specific manner, typically by shifting the balance between enhancement or silencing of specific splice sites. Activation or repression of alternative splice sites is based on antagonistic effects of activator (enhancer) and repressor (silencer) complexes onto a variety of *cis*-acting enhancer and silencer motifs (Dreumont et al., 2010). This in turn is mainly based on the tissue-specific levels of the splicing activators and repressors (Barnard et al., 2002). In addition, the intrinsic strength of the flanking splice sites plays a role (for review, see Cartegni et al., 2002). Two major families of proteins regulate the interaction between *cis*-regulatory elements and the splicing machinery: serine/arginine-rich (SR) proteins (Bourgeois et al., 2004; for review, see Long et al., 2009) and heterogeneous nuclear ribonucleoproteins (hnRNP; Martinez-Contreras et al., 2007). SR proteins (e.g. SF2/ASF) facilitate the recognition of proper exons by binding to exonic/intronic splicing enhancer sequences (E/ISEs) and recruit the splicing machinery directly (Figure 1.9; Lavigne et al., 1993; Graveley et al., 2001). In contrast, the heterogeneous nuclear ribonucleoproteins (e.g. hnRNP A1) antagonize the activity of SR proteins on the selection of 5'-splice sites and can bind to intronic/exonic splicing silencers (I/ESSs) to prevent the use of adjacent 3'-splice sites (for review, see Smith et al., 2000). Therefore they prevent the inclusion of pseudo-exons (pre-mRNA sequence that resembles an exon, but that is never recognized as an exon by the spliceosome; Cartegni et al., 2002).

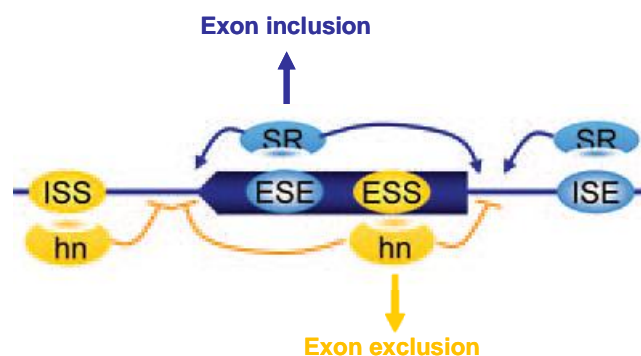


Figure 1.9. Exonic and intronic splicing enhancer and silencer motifs.

In addition to the classical splicing signals, *cis*-acting exonic and intronic enhancer (ESE/ISE) and silencer (ESS/ISS) motifs regulate the process of splicing/alternative splicing. Serine/arginine-rich (SR) proteins allow the recognition of proper exons by binding to ESEs or ISEs. Heterogeneous nuclear ribonucleoproteins (hn) suppress inclusion of pseudo-exons by binding to exonic or intronic silencer sequences (I/ESS). In exons containing both ESE and ESS the tissue-specific levels of splicing activators and repressors regulate the inclusion or exclusion of the exons from the transcript (picture from Aartsma-Rus and van Ommen, 2010).

The incorrect recognition of exon-intron boundaries or the failure to remove an intron results in aberrant mRNAs, which may encode mutant proteins that have a deleterious role in cell structure and function. However, three major quality control systems are known to lower the level of aberrant mRNAs and/or proteins: nonsense-mediated mRNA decay (NMD), which degrades highly unstable mRNAs carrying a premature termination codon; the ubiquitin-proteasome system (UPS) which selectively degrades damaged, misfolded or mutant proteins having an abnormal conformation and autophagy, which degrades/recycles membrane proteins and organelles through the lysosomal machinery.

1.5 Nonsense-mediated mRNA decay

Nonsense-mediated mRNA decay (NMD) is an mRNA surveillance mechanism found in all eukaryotes. NMD ensures mRNA quality by selectively targeting mRNAs that contain a PTC for degradation (Maquat 1995; Hentze et al., 1999). PTCs can arise from mutations (frameshift, nonsense) or errors during transcription or splicing and could result in non-functional or deleterious proteins. These C-terminal truncated proteins in turn could act as poison peptides via dominant-negative or gain-of-function effects.

During the splicing process of pre-mRNA into mRNA, an exon junction complex (EJC) is deposited 20-24 nucleotides upstream of each exon-exon junction (Figure 1.10; Le Hir et al., 2000). These complexes are important to facilitate mRNA export and to provide an anchor for up-frameshift suppressor proteins (UPFs; for review, see Cartegni et al., 2002; Chang et al., 2007). On a normal mRNA EJCs are displaced by the elongating ribosome when it crosses the mRNA during the pioneer round of translation in the cytoplasm (Ishigaki et al., 2001; Lejeune et al., 2002). In this case translation stops when the ribosome reaches the normal stop codon and newly recruited ribosomes no longer encounter EJCs. Therefore the mRNA becomes protected from degradation via the NMD machinery. During subsequent rounds of translation the nuclear cap-binding complex is replaced by eukaryotic initiation factor 4E (eIF4E) and poly-(A)-binding protein II (PABPII), which shuttles between the nucleus and cytosol, is replaced by PABPI, which is active in the cytoplasm (Ishigaki et al., 2001; for review, see Cartegni et al., 2002; Dreyfuss et al., 2002). However, in mRNAs that contain a PTC, the ribosome stops at the PTC during the pioneer round of translation and release factors of the post-termination

complex are able to interact with any undisplaced EJC, which initiates degradation of the mRNA (Czaplinski et al., 1998). The general rule is that NMD degrades PTC-containing transcripts when the PTC is located at least 50 nucleotides upstream of the last exon-exon junction (Nagy et al., 1998).

Since NMD acts during the pioneer round of translation, it can be inhibited by translation inhibitors such as emetine or cycloheximide. While emetine binds to the 40S ribosomal subunit and inhibits the EF-2-dependent translocation of ribosomes, cycloheximide binds to the 60S subunit and blocks the movement of peptidyl-tRNA from acceptor (aminoacyl) site to the donor (peptidyl) site (Schneider-Poetsch et al., 2010; Sanchez et al., 1977; McKeehan et al., 1969; Carter et al., 1995).

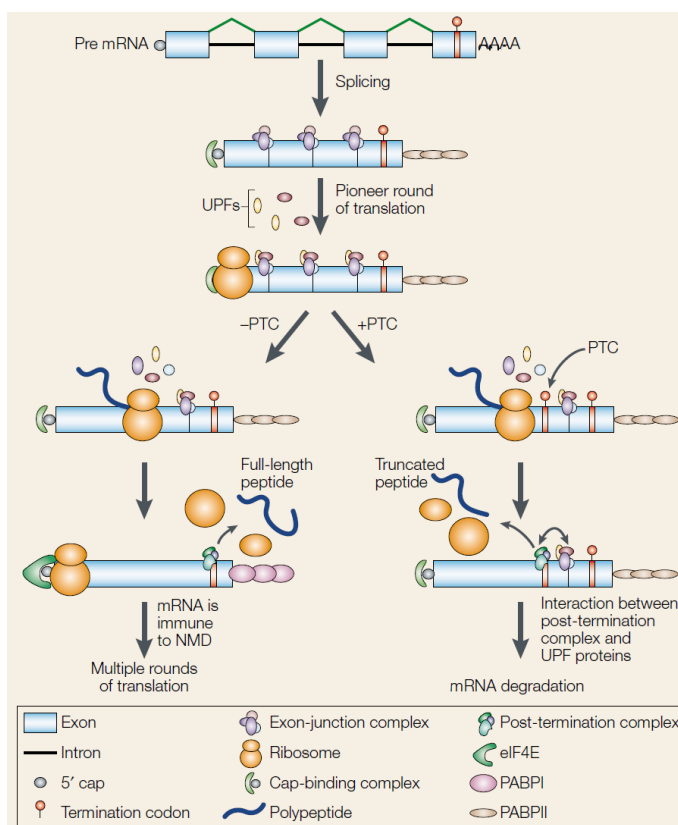


Figure 1.10. The nonsense-mediated mRNA decay pathway.

During splicing of pre-mRNA into mRNA, an exon-junction complex (EJC) is deposited 20-24 nucleotides upstream of each exon-exon junction. EJCs serve as anchors for up-frameshift suppressor proteins (UPFs). During the pioneer round of translation of a normal mRNA the EJCs are displaced by elongating ribosomes as they proceed to the normal stop codon. Since EJCs were displaced during the first round of translation, new ribosomes do not encounter EJCs and the mRNA is immune to NMD (lower left part of figure). During subsequent rounds of translation the cap-binding complex is exchanged by eukaryotic initiation factor 4E (eIF4E) and poly-(A)-binding protein II (PABPII) is replaced by PABPI. However, in a PTC-containing mRNA the ribosome terminates at the PTC during the pioneer round of translation. Subsequent interaction between any undisplaced EJCs and components of the post-termination complex triggers mRNA decay (lower right part of figure). Picture from Cartegni and Krainer (2002).

1.6 The ubiquitin-proteasome system

Like NMD, which acts at the mRNA level the ubiquitin-proteasome system (UPS) is a quality-control system that selectively degrades aberrant proteins. In mammalian cells about 85% of intracellular proteins (nuclear, cytosolic, myofibrillar) are degraded by the UPS, whereas the lysosomes degrade mainly membrane and extracellular proteins by endocytosis as well as cytosolic proteins and organelles via autophagy (for reviews, see Zolk et al., 2006; Mearini et al., 2008). The UPS is located in both the nucleus and cytosol and has both regulatory and cell-protective functions. For example it is involved in controlling the concentration of key signalling proteins, degradation of short-lived proteins, stress responses, antigen processing, DNA repair, apoptosis and transcriptional regulation (Wilkinson 1999; Zolk et al., 2006). In addition it protects the cell against damaged, misfolded or mutant proteins (for reviews, see Zolk et al., 2006; Carrier et al., 2010). On the other hand the UPS is involved in forms of malignancy, pathogenesis of several genetic diseases, in immune surveillance or viral pathogenesis and pathology of neurodegenerative disorders such as Alzheimer's or Parkinson's (for review, see Ciechanover et al., 2003). In cardiac diseases, such as heart failure, myocardial ischemia and cardiac hypertrophy activation or impairment of the UPS has been demonstrated (for review, see Mearini et al., 2008). Recent data suggest that accumulation of ubiquitinated proteins is a feature of HCM in humans and in a mouse model carrying a cMyBP-C point mutation (Vignier et al., 2009).

The UPS is an ATP-dependent proteolytic system that requires the polyubiquitination of target proteins prior to their degradation by the intracellular 26S proteasome (for reviews, see Mearini et al. 2008; Schlossarek et al. 2011). In the process of ubiquitination three enzymes (E1, E2 and E3) are involved (Figure 1.11). In eukaryotic cells there is only one E1 enzyme, but multiple E2s and E3s exist. The latter are tissue-specific. The initial activation step is catalyzed by the ubiquitin-activating enzyme (E1), which activates ubiquitin in an ATP-dependent manner. One of the ubiquitin-conjugating enzymes (E2) conjugates thereafter the ubiquitin molecules to the substrate. The ubiquitin ligase E3 acts thereby either as a bridging factor or forms an ubiquitin-thiol-ester intermediate before transferring the ubiquitin chain to the targeted protein (Zolk et al., 2006). The resulting polyubiquitin chains are recognized by the 19S cap of the 26S proteasome, degraded and the released amino acids and ubiquitin molecules are recycled.

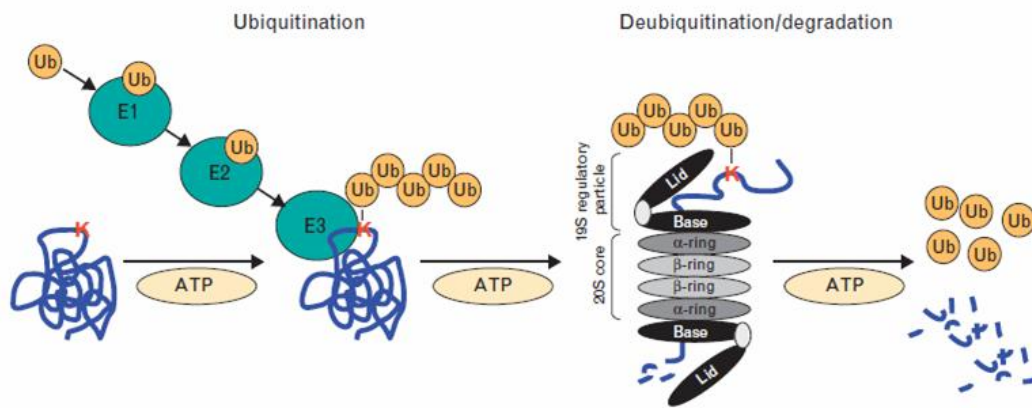


Figure 1.11. The ubiquitin-proteasome system.

Target proteins are marked for degradation through the ATP-dependent 26S proteasome by linking an ubiquitin chain. The ubiquitin molecules in turn are connected via Lys48 of ubiquitin. Three enzymes are involved in the process of ubiquitination: the ubiquitin-activating enzyme (E1), the ubiquitin-conjugating enzymes (E2) and the ubiquitin ligase (E3). The latter transfers the polyubiquitin chain to the target protein, which is recognized at the 19S cap of the large 26S proteasome. The 26S proteasome is composed of the 20S proteasome, where the proteins are cleaved by peptidase activities and two regulatory 19S complexes (picture from Schlossarek, 2011a).

The proteasome contains one 20S particle structure and two 19S regulatory caps, which recognize, de-ubiquitinate and unfold targeted proteins before they reach the hollow core of the 20S catalytic centre (Figure 1.11; Herrmann et al., 2004). The 20S particle features four layered heptameric ring structures, which consist themselves of two different types of subunits (α and β ; Hedhli et al., 2010). The α -subunit has structural functions while the β -subunit primarily performs catalytic functions. The major catalytic subunits β 1, β 2 and β 5, prefer to cleave amino acid chains after hydrophobic, alkaline and acidic amino acids, respectively. In accordance with the denotation of monospecific proteases (chymotrypsin, trypsin and caspase) these activities are named chymotrypsin-like, trypsin-like and caspase-like activities (Tanaka et al., 1988; for review, see Mearini et al. 2008). Thus, the 20S particle is responsible for cleaving the proteins into their amino acid components and releasing ubiquitin, which will be recycled.

The proteolytic activities of the 20S particle are targeted by several inhibitors such as peptide aldehydes (e.g. MG132), peptide boronates (e.g. MG262), β -lactone derivatives (e.g. β -lacton), peptide vinyl sulfones (e.g. NLVS) or peptide epoxyketones (e.g. epoxomicin; for review, see Mearini et al., 2008; Hedhli et al., 2010).

1.7 Treatment and potential novel therapies for hypertrophic cardiomyopathy

The clinical outcome of HCM is highly variable and ranges from asymptomatic benign course to heart failure (systolic/diastolic dysfunction), atrial fibrillation and sudden cardiac death (SCD) caused by arrhythmias (Nanni et al., 2003; for review, see Maron 2002). The variability of the disease may be influenced by the presence or absence of left ventricular outflow tract obstruction, ventricular cardiac arrhythmias or myocardial ischemia. Whereas most HCM patients are asymptomatic, others may present chest pain during exertion, dyspnoea, vertigo, fainting, fatigue and syncope. Reversal or amelioration of the underlying cardiac hypertrophy could result in an improved morbidity and decrease the risk of SCD in affected patients (for review, see Schlossarek et al., 2011).

1.7.1 Pharmacological and surgical treatments of hypertrophic cardiomyopathy

Current clinical management of HCM is focused on relieving the symptoms mentioned above. Pharmacological treatments such as β -adrenergic blockers, L-type calcium-channel blockers and antiarrhythmic drugs lower heart rate, prolong diastolic filling rates, diminish left ventricular outflow tract gradients and improve HCM symptoms such as dyspnoea, chest pain and fainting (Wang L. et al., 2010). In the case of clinical manifestation of heart failure diuretics and ACE inhibitors are indicated (Schulte et al., 1999) and further impairments require heart transplantation. In patients with outflow tract obstruction a surgical septal myectomy or percutaneous alcohol ablation improve symptoms (Wang L. et al., 2010). Particularly in younger patients with syncope or tachyarrhythmias or who have survived a cardiac arrest, the implantation of a cardioverter defibrillator may be necessary as secondary prevention (Schulte et al., 1999; DiMarco 2003).

1.7.2 Innovative therapies for hypertrophic cardiomyopathy

Although the mentioned drug-based therapies are effective in reducing symptoms, they cannot reverse cardiac hypertrophy. Therefore innovative HCM therapy targets underlying mechanisms of the disease (for review, see Schlossarek et al., 2011; Wang L. et al., 2010). About 5-15% of patients with monogenetic disorders, including patients with *MYBPC3*

mutations, carry frameshift or nonsense mutations, which result in PTCs and therefore C-terminal truncated proteins (Hirawat et al., 2007). These proteins could either act as “poison peptides” interfering with the normal protein function or, if degraded, act as “null alleles” and cause haploinsufficiency. One therapeutic option would be to increase the level of a mutant protein in the case that it has normal or near-normal function. This could theoretically be done with inhibitors of NMD or the UPS. An alternative would be to use molecules that detect, target and enforce read-through of PTCs. Other strategies aim at the replacement of mutant proteins by wild-type forms by gene therapy or RNA-based therapy.

1.7.2.1 Targeting the NMD or UPS?

Selective inhibition of NMD or the UPS may provide a strategy to rescue the phenotype in the cases in which the mutant protein shows no dominant-negative effect and has a near-normal function. The NMD inhibitor wortmannin inhibits the PI3-kinase-related protein SMG-1 that phosphorylates UPF1 during NMD (Rehwinkel et al., 2006). However, wortmannin is cytotoxic and therefore unacceptable as a therapeutic agent in humans, but siRNA-mediated knockdown of SMG-1 or UPF1 restored the level of PTC-bearing collagen VI-2 mRNA and rescued the phenotype in fibroblasts of a patient with Ullrich’s (Usuki et al., 2006). This approach has not been yet tested in cardiac genetic disease.

The theoretical alternative is to prevent the degradation of truncated proteins by proteasome inhibitors. Although this may also stabilize unwanted proteins in different cell types, previous studies have shown that low doses of the proteasome inhibitors MG132, MG262 or Velcade® prevented hypertrophy in neonatal rat cardiomyocytes and reduced hypertrophic heart growth in hypertensive rats, respectively (Meiners et al., 2008). The mechanism of this unexpected antihypertrophic effect of UPS-inhibition is unclear, but cannot involve stabilization of mutant proteins in these models. Cardiomyopathic adverse effects were reported in patients treated with the proteasome-inhibitor bortezomib over a longer period of time, challenging its therapeutic application (Hacihanefioglu et al., 2008).

1.7.2.2 Targeting nonsense mRNA?

An alternative is to use drugs that detect and target PTCs within the mRNA. By enforcing reading through PTCs, these therapies can induce the synthesis of full-length proteins. This can be achieved by aminoglycoside antibiotics (e.g. gentamycin; Hirawat et al., 2007) and was shown e.g. for patients with cystic fibrosis (Wilschanski et al., 2003). While application of gentamicin was associated with severe adverse effects, these were found to be uncommon and usually mild using the non-aminoglycoside PTC124, which allows ribosomal readthrough of PTCs in mRNA (Mingeot-Leclercq et al., 1999; Fischel-Ghodsian 2005; Wilschanski et al., 2011). Both substances were already applied in clinical trials to treat patients with cystic fibrosis (Wilschanski et al., 2003; Wilschanski et al., 2011). However, whereas PTC readthrough is applicable for nonsense mutations, it is not useful for frameshift mutations that result in a PTC, as mainly found in *MYBPC3*, since the newly formed amino acids after the PTC are expected to be non-functional.

1.7.2.3 Targeting mutant pre-mRNA?

The first straight-forward therapy would consist in the addition of a therapeutic wild-type protein by gene therapy. A potential major drawback of this type of gene therapy for HCM would be that mutant proteins, which are still expressed at low levels, might continue to act as poison peptides. More recently, alternative approaches targeting mutant pre-mRNA have been developed, which present a unique potential for native mRNA modification within the endogenous regulatory environment (for review, see Le Roy et al., 2009). Although no RNA-based therapy has yet been tested for HCM, these therapies were developed over the last decade for neuromuscular diseases such as duchenne muscular dystrophy (DMD), spinal muscular atrophy, myotonic dystrophy type 1 and Ullrich disease (for review, see Le Roy et al., 2009). The applied molecular tools include spliceosome-mediated pre-mRNA trans-splicing molecules (SMaRT™) or modified antisense oligonucleotides (AON). These tools have been successfully used in patients' cells or animal disease models to modulate pre-mRNA splicing, mRNA stability or mRNA translation (for review, see Le Roy et al. 2009). Modified AONs are already successfully applied in clinical trials to induce exon skipping and restoration of the open reading frame in DMD patients (van Deutekom et al., 2007; Kinali et al., 2009; Goemans et al., 2011).

1.8 Objectives

The main goal of this thesis was to investigate new molecular strategies to regulate the expression of *MYBPC3* mutations and therefore to treat HCM. Two aims were defined:

(1) To establish a cell-based screening system in human embryonic kidney (HEK293) cells to evaluate the relative contribution of mechanisms controlling the expression of *MYBPC3* mutations.

(2) To evaluate an exon-skipping strategy in neonatal mouse cardiac myocytes derived from a *Mybpc3* knock-in (KI) mouse model.

(1) Previous data in humans support the view that cMyBP-C haploinsufficiency is the major molecular mechanism of HCM. Additional findings in mice bearing a *Mybpc3* mutation suggest that haploinsufficiency results from regulation by NMD, UPS, or both. Therefore NMD and UPS inhibitors could be used as therapeutic options to reduce haploinsufficiency in the case that mutant cMyBP-C has normal or near-normal function. The goal of the first part of my thesis was therefore to establish a cell-based system to analyse i) the expression of human *MYBPC3* mutations and ii) the relative contribution of NMD and UPS in regulating their expression. The main experimental procedure was to construct human minigenes containing mutations located at the C-terminus of *MYBPC3* and to investigate short-term or long-term mRNA and protein levels in HEK293 cells. I focused on mutations that result in truncated proteins, which, when stabilized by drugs, still contain the important functional domains required to be integrated into the sarcomere. The relative contribution of NMD and the UPS was investigated using specific inhibitors.

(2) HCM is the most common inherited cardiac disease and lacks effective treatment. In this project I focused on a mouse model of HCM, which carries a *Mybpc3* point mutation (KI) and developed left ventricular hypertrophy and diastolic dysfunction. This mouse model was therefore adapted for testing therapeutic interventions. The goal of the study was to evaluate the feasibility and efficacy of antisense oligoribonucleotides to remove the mutated exon in KI cardiac myocytes. The strategy was to skip two vicinal exons and to create a shortened, but in-frame protein lacking the mutation. The resultant protein was expected to be functional. To achieve the skipping of both exons, modified antisense oligoribonucleotides (AONs), complementary to exonic splicing enhancer sequences in

both exons were used and transfected in neonatal mouse cardiac myocytes (NMCM). The skipping efficiency of the AONs was investigated at the levels of both mRNA and protein.

2 Material and Methods

2.1 Material

All used antibodies, adeno-associated viruses, bacterial strains, chemicals, consumable materials, kits, laboratory equipment, oligonucleotides, restriction enzymes and vectors are, if not mentioned explicit, listed in the appendix.

2.1.1 Cell lines and neonatal mouse cardiac myocytes

Cell line	Origin	Culture condition
HEK293	Human embryonic kidney cells, transformed with adenovirus type 5	D-MEM containing 4.5 mg/ml glucose (Gibco), 10% heat inactivated FCS (Gibco), 1% penicillin/streptomycin (Gibco); 37 °C, 5% CO ₂
Flp-In TM -293	HEK293 cells transfected with pFRT/lacZeo	D-MEM containing 4.5 mg/ml glucose (Gibco), 10% heat inactivated FCS (Gibco), 1% penicillin/streptomycin (Gibco); 100 µg/ml Zeocin TM (Invitrogen); 37 °C, 5% CO ₂
Flp-In TM -293 WT, Mut-1, Mut-2	Stable transfected Flp-In TM -293 cells expressing the minigene constructs (WT, Mut-1, Mut-2)	D-MEM containing 4.5 mg/ml glucose (Gibco), 10% heat inactivated FCS (Gibco), 1% penicillin/streptomycin (Gibco); 25 µg/ml hygromycin; 37 °C, 5% CO ₂
NMCM	Neonatal mouse cardiac myocytes	Gibco®: DMEM:M199 3:1, 10% horse serum, 5% FCS, 100 U/ml penicillin-streptomycin; 1 mM HEPES, pH 7.4; 37 °C, 10% CO ₂

2.1.2 Targeted *Mybpc3*-knock-in mouse model

The *Mybpc3*-knock-in mouse model (KI) was developed by Nicolas Vignier (Vignier et al., 2009). The mouse model carries a G>A transition on the last nucleotide of exon 6, which was introduced by gene targeting using the Cre/lox system (Figure 2.1). The targeting vector contained a 12.5 kb-insert and was obtained in several steps. In brief, a genomic

DNA fragment ranging from 1747 bp upstream of exon 1 to exon 15 was amplified by long-range PCR and cloning from a FIX II genomic library derived from a 129/Svj mouse strain (wild-type). The amplicon was cloned into the pBluescript® II KS+ vector (Stratagene). To introduce the G>A transition into the *Mybpc3*-insert the site directed mutagenesis kit was used. Beside the mutation the vector contained two selection markers, a neomycin resistance (NEO) and a thymidine kinase gene (HSVtk) flanked by two *loxP* sites. AT1 embryonic stem cells were transfected with the linearized vector by electroporation and screened for homologous recombination by long-range PCR. Positive clones containing the right recombination event were used to obtain germ-line transmitting chimeras. One chimeric mouse was then crossed with a Black-swiss wild-type mouse and analysed for germline transmission. Heterozygous female mice were crossed with a CD1 Sycp1-Cre transgenic male expressing the recombinase Cre under the control of the Sycp1 promoter. After Cre-mediated recombination, the targeted floxed-out knock-in allele was obtained (KI).

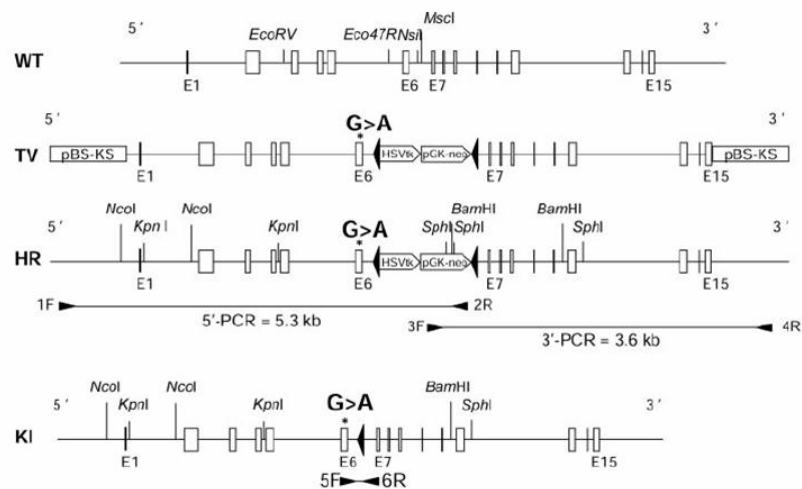


Figure 2.1. Targeting strategy of the *Mybpc3*-knock-in mouse model.

The upper picture represents the wild-type (WT) structure of the *Mybpc3* gene from exon 1 (E1) to exon 15 (E15). Subsequently, the targeting vector (TV) pBluescript® II KS+ (pBS-KS) containing the G>A transition and the selection cassettes (HSVtk, pGK-neo), which are flanked by two *loxP* sites (black arrowheads) is shown. After homologous recombination (HR) in embryonic stem cells the obtained germline transmitting chimeras were crossed with Cre-mice, resulting in the targeted floxed-out knock-in (KI) allele(s) (picture from Vignier et al., 2009).

2.1.3 Treatments applied to HEK293 cells and neonatal mouse cardiac myocytes

Substance	Applied concentration	Time of treatment	Dissolvent
Emetine	1-3-10-30-100-300 µg/ml	4 h	Aqua dest.
Cycloheximide	30-100 µg/ml	3 h; 24-96 h	DMSO (0.1%)
Wortmannin	300-1000 nM	8 h	DMSO (0.1%)
MG132	0.1-0.3-1-3-10-30-100 µM; 50 µM	24-48 h; 2 h	DMSO (0.1%)
MG262	4 µM	2 h	DMSO (0.1%)

2.2 Methods

2.2.1 Molecular biological methods

2.2.1.1 Generation of minigenes by directional TOPO® cloning

To generate a human minigene ranging from exon 29 to exon 34 of the *MYBPC3* gene (“wild-type”, WT; Figure 2.2) the pEF5/FRT/V5 directional TOPO® Expression Kit was used following the instructions of the producer. The kit combines the Flp-In™ System (2.2.2.1.2) with the TOPO cloning method to directionally clone a blunt-end PCR product into a mammalian expression vector compatible with Flp-In cell lines.

The minigene construct includes a Kozak translation initiation sequence (CACCATGG; Kozak 1987) followed in-frame by a N-terminal myc-tag sequence and the C-terminal part of the *MYBPC3* gene (start: position +6 of exon 29 to exon 34; Figure 2.2). Both the Kozak and myc-tag sequences were introduced by the forward primer. The reverse primer was located after the endogenous stop codon in exon 34.

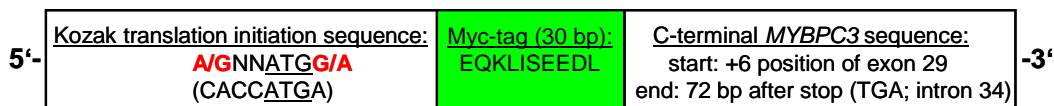


Figure 2.2. Minigene construct generated by PCR.

The Kozak translation initiation sequence, the myc-tag and a small part of the genomic human *MYBPC3* sequence starting in-frame at the position +6 of exon 29 were introduced with the forward primer. The reverse primer was located 72 bp after the normal stop codon in exon 34.

The directed cloning of the PCR product was facilitated by adding an overhang of four bases to the 5'-end of the forward primer (CACC) used for generation of the minigene by PCR. The vector pEF5/FRT/V5-D-TOPO contains the homologous sequence overhang and invades during ligation reaction the 5'-end of the double-stranded PCR product annealing with the added nucleotides (Figure 2.3).

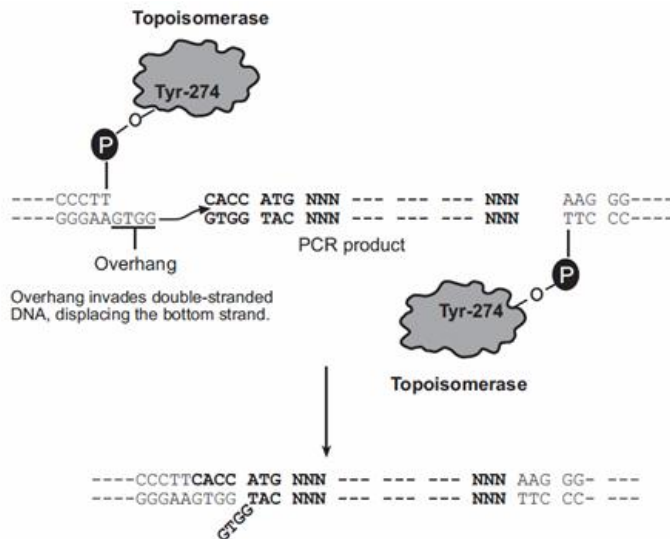


Figure 2.3. TOPO® cloning.

An overhang of four bases (GTGG) is located in the Flp-In vector. By annexing the complementary sequence (CACC) in the forward primer used for PCR amplification, PCR amplicons will be cloned in the proper direction, after the vector overhang displaces the 5'-end of the PCR amplicons. Figure from the pEF5/FRT/V5 directional TOPO® Expression Kit manual.

2.2.1.1.1 Amplification of genomic DNA for directional TOPO® cloning

In order to clone the *MYBPC3* minigene construct into the pEF5/FRT/V5 expression vector, 20 ng DNA derived from a purified blood sample of a healthy human being was used as template for PCR amplification with the PrimeSTAR® HS DNA polymerase according to the instructions of the manufacturer. This polymerase has a matchless proof reading activity and produces blunt-end PCR products. For the PCR reaction 0.2 µM primers were used in a total volume of 20 µl. For amplification the following PCR condition was used (denaturation, annealing, elongation): 98 °C 10 sec, 64 °C 5 sec, 72 °C 2 min 15 sec (1 kb/min) for 33 cycles. The PCR product was analysed by agarose gel electrophoresis (0.8%), followed by excision and gel extraction of the expected DNA fragment (2.2.3.2). The extracted DNA was further analysed by restriction digestion and sequencing (2.2.1.3 and 2.2.3.3). After confirmation of the correct sequence the insert was cloned into pEF5/FRT/V5-D-TOPO vector according to the instructions of the producer. For transformation 1 µl ligation product was added into the supplied “One Shot® TOP10

chemically competent *E. coli*” cells. Subsequently the small-scale and large-scale clones of the generated wild-type minigene were analysed by restriction digestion and sequencing.

2.2.1.1.2 Site-directed mutagenesis

The wild-type minigene plasmid was used as a template for the insertion of two mutations. To introduce a point mutation in intron 31 (IVS31+1G>A; Mut-1) and a four nucleotide insertion in exon 31 (c.3335_3336insAGTG; Mut-2) the QuickChange Site-Directed Mutagenesis Kit was used following the instructions of the kit manual. The mutation-containing primers were designed and used in the PCR reaction (Mut-1 F: 5'-CTT TAT CCC CAG ACC Aga TG-3'; Mut-1 R: 5'- TGA GGG TAC AGC AtC TGG TC-3' and Mut-2 F: 5'-CAG GAG TGa gtg GTT CAC CGT CTT-3'; Mut-2 R: 5'-CAA GAC GGT GAA Cca ctC ACT CC-3'). Both the PCR conditions and the subsequent digestion of the parental DNA with DpnI to select for mutation-containing DNAs were conducted according to the instructions of the manufacturer. For transformation into the supplied Epicurian Coli® XL1-Blue supercompetent cells 1 µl of attempt was added. To proof whether the mutations were inserted small-scale and large-scale clones were analysed by restriction digestion and sequencing (2.2.1.3 and 2.2.3.3). Subsequently Flp-In293 cells were stably transfected with the three minigene plasmids (wild-type, Mut-1 and Mut-2) (Invitrogen; see 2.2.2.1.2).

2.2.1.2 Preparation of plasmid DNA

A small-scale preparation of plasmid DNA was conducted using the “NucleoSpin® plasmid kit” following the instructions of the manufacturer. After screening for proper inserts by restriction digestion and sequencing a large-scale preparation was assessed and plasmids were extracted using the NucleoBond® or PureLink™ HiPure Plasmid Filter Purification.

2.2.1.3 Restriction digestion

Plasmid DNA or PCR amplicons were digested with restriction enzymes from NEB or FastDigest® enzymes from Fermentas in the supplied buffers according to the instructions of the manufacturers. All enzymes used in this work are listed in the appendix (5.1.8). For double digestion the recommendations of the “double digest finder” program from NEB or Fermentas (free available) were followed. Plasmid-DNA or PCR amplicons were digested for 3 h to 4 h with NEB enzymes or for 10 min to 30 min with FastDigest® enzymes at 37 °C.

For analytical analysis 0.2 µg DNA was digested with 5 - 10 U enzyme in a final volume of 10 or 20 µl. For a preparative DNA digestion between 0.5 - 5 µg DNA was digested with 10 - 40 U enzyme in 25 or 50 µl. To avoid religation of the digested vector 10 U calf intestinal alkaline phosphatase was added 1 h prior the end of incubation (CIP, NEB) or 1 U alkaline phosphatase directly (FastAP™, Fermentas).

For analysis or preparative purposes the attempts were loaded on 1% to 2% agarose gels after digestion. To subsequently ligate vector and insert both digested fragments were excised and purified using the QIAquick Gel Extraction Kit.

2.2.2 Cell biology, transfections, treatments and microscopy

2.2.2.1 HEK293 cell line

The HEK293 cell line is derived from human embryonic kidney cells, originated from a healthy aborted fetus, which were grown in tissue culture. The cell line was established by transformation of normal HEK cells with sheared adenovirus 5 DNA, resulting in the integration of about 4.5 kilobases viral genome into the human chromosome 19 of the HEK cells culture (Graham et al., 1977). However, a previous study suggests that HEK293 cells are rather derived from neuronal cells or other type of cells (Shaw et al., 2002).

2.2.2.1.1 Transient transfection of HEK293 cells

For transient transfections HEK293 cells were plated at a density of 1×10^5 up to 3×10^5 cells in 12-well dishes and incubated at 37 °C with 5% CO₂ until a confluency of 50-70% was reached. Transfection was conducted using TurboFect®, following the instructions of the manual.

2.2.2.1.2 Stable transfection of Flp-In™-293 cells and the Flp-In system

In order to establish cell lines stably expressing *MYBPC3* mutations the Flp-In™ System was used and the Flp-In™-293 cell line, purchased from Invitrogen and designed for the use with the Flp-In system. In this cell line a single integrated recognition site (Flp Recombination Target site; FRT) for the enzyme Flp-recombinase is stably integrated into a transcriptionally active genomic locus. The recognition site is integrated directly after the start codon within the coding sequence for a *lacZ*-Zeocin resistance fusion protein. Therefore non-transfected Flp-In™-293 cells show β-galactosidase activity and are resistant against the antibiotic Zeocin®.

To generate stable Flp-In cell lines a co-transfection of a FRT-site enclosing expression vector with the Flp-In recombinase expression plasmid pOG44 (Figure 2.4b) are needed (O'Gorman et al., 1991). Therefore the PCR-generated minigenes (2.2.1.1.1) encoding myc-tagged wild-type or mutated genomic *MYBPC3* sequences were cloned into the expression vector pEF5/FRT/V5-D-TOPO® (Figure 2.4a) and co-transfected with pOG44 into the cell line (Figure 2.4c). The pOG44 mediates a site-specific DNA recombination between the FRT sites of the interacting DNA molecules (Figure 2.4d and e; O'Gorman et al. 1991; Sauer 1994).

The effect resulting from the integration of the pEF5/FRT/V5-D-TOPO® plasmid into the cell line is described as follows (Figure 2.4): The hygromycin resistance gene located in the expression vector lacks a promoter and the start codon (ATG; Figure 2.4a). However both SV40 promoter and ATG initiation codon are integrated into the Flp-In cell line genome upstream of the expression cassette (Figure 2.4c). After homologous recombination the hygromycin resistance gene-containing vector cassette displaces the expression cassette located in the cell line and is then located upstream of the SV40 promoter and ATG initiation site (Figure 2.4e). As a result, the cell line containing the

fusion protein *lacZ*-Zeocin cannot be transcribed anymore and cells become Zeocin® sensitive, hygromycin resistant and lose their β -galactosidase activity.

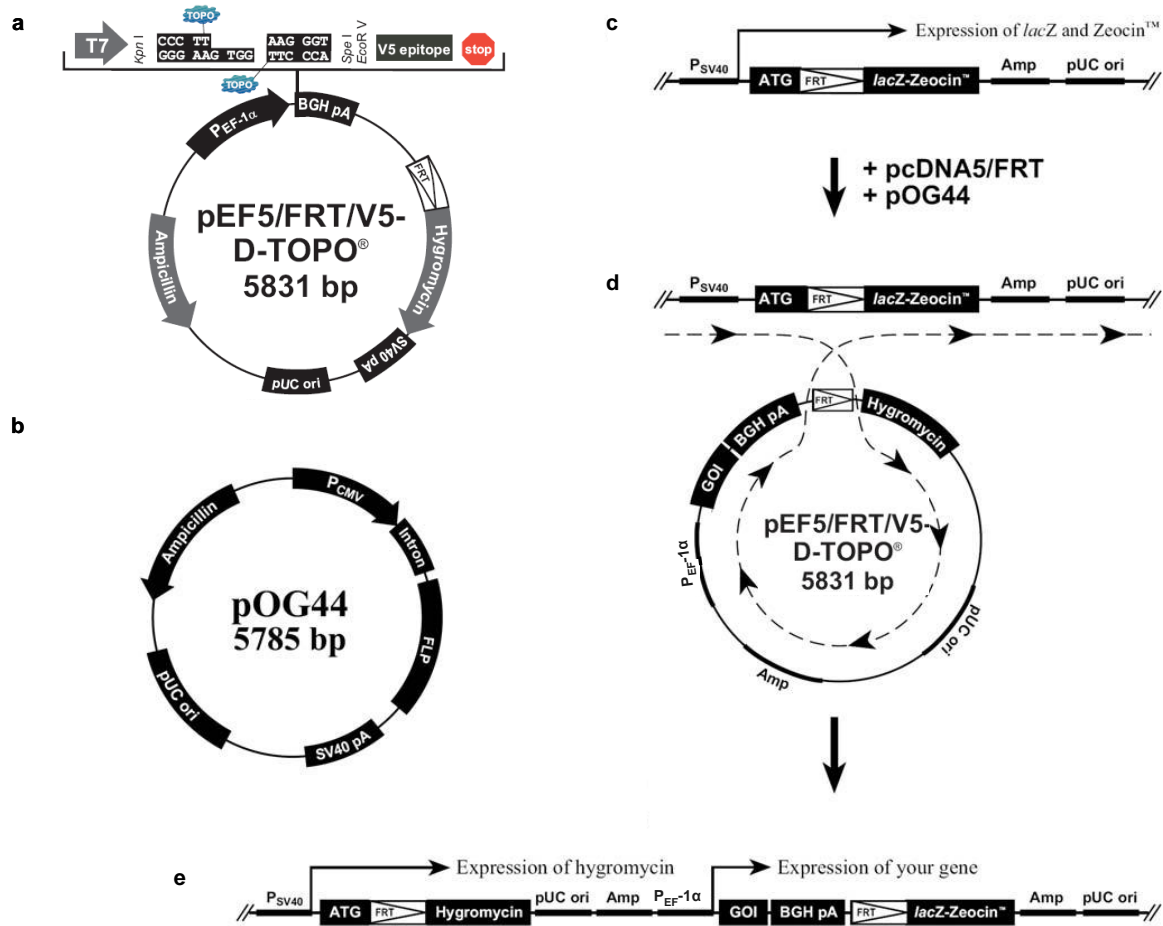


Figure 2.4. The Flp-In™ System.

(a) Vector map of the expression vector pEF5/FRT/V5-D-TOPO. (b) Vector map of the Flp-recombinase encoding plasmid. (c) Flp-In™-cell line containing a stable integrated FRT site and the fusion protein *lacZ*-Zeocin. (d) Schematic representation of the Flp-recombinase mediated site-specific DNA recombination. (e) Stably integrated gene of interest after homologous recombination. (FRT, Flp Recombination Target; GOI, gene of interest (here, myc-tagged *MYBPC3* minigenes)). The figures are modified from the manual of the Flp-In™-system.

After co-transfection of pOG44 with the modified pEF5/FRT/V5-D-TOPO® plasmids (1:9; W/W) using TurboFect®, positive transfected cells were selected in the presence of 25 μ g/ml hygromycin in DMEM. This concentration was determined in a pre-experiment, where various hygromycin concentrations were tested ranging between 10 and 400 μ g/ml hygromycin. The presence of stable cell lines was confirmed by the β -galactosidase activity (*lacZ*-staining).

2.2.2.1.3 *lacZ*-staining of Flp-InTM-293 cells

Isogenic Flp-In cell lines (WT, Mut-1 and Mut-2), were obtained after expanding cell colonies (1 to 10 cell clones per each line), which were grown on the selective antibiotic hygromycin for at least four weeks.

To generate isogenic cell lines, cell colonies were separated at first by adding varying amounts of cell suspensions (pure: 10 - 5 - 2.5 - 1 μ l; 1:10 dil.: 10 - 5 - 2.5 - 1 μ l; 1:20 dil.: 10 - 5 - 2.5 - 1 μ l) derived from confluent cells of a 24-well plate (from WT, Mut-1, Mut-2 and Flp-In293 cells as a positive control) in 100 μ l (total) growing medium of a 96-well-microtiter plate. Subsequently the lowest grown cell colony amount (WT: 1:20 dil. 5 μ l, Mut-1: 1:20 dil. 5 μ l, Mut-2: 1:10 dil. 2.5 μ l and Flp-In293: 2.5 μ l pure) was expanded in a 24-well format. The expanded cells were tested for β -galactosidase activity in a 96-well format (6 wells/cell line). Therefore confluent cells were treated with X-gal (5-bromo-4-chloro-3-indolyl- β -D-galactopyranoside) dissolved in DMSO at a final concentration of 0.12 mg/ml. The activity for each cell line was determined in triplicates, whereby the remaining 3 wells served for subsequent expansion of the cells after confirmation that they were *lacZ*-negative. After an incubation time of ~30 minutes at 37 °C light microscopical pictures were performed (Figure 2.5).

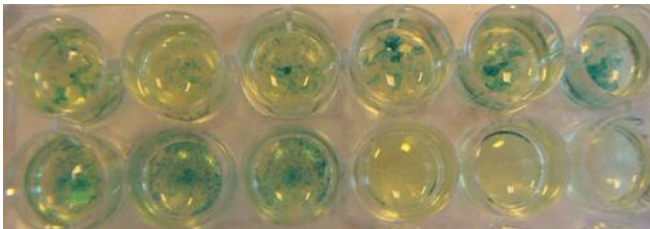


Figure 2.5. Example of screening of Flp-InTM cell lines transfected with different minigene plasmids after *lacZ*-staining.

2.2.2.1.4 The GFP-based reporter system and treatment of HEK293 cells

The GFP-based reporter system used to monitor nonsense-mediated mRNA decay (NMD) in mammalian cells was described in detail previously (Paillusson et al., 2005). The NMD reporter and control NMD reporter plasmid were kindly given by Oliver Mühlemann (Bern, Switzerland). After propagating both plasmids they were analysed by restriction digestion and sequencing.

To investigate NMD or the UPS specific inhibitors of both systems were used. The NMD system was inhibited by substances like cycloheximide (in 0.1% DMSO) and

emetine, which are inhibitors of the protein synthesis in eukaryotic cells by binding to the 60S or 40S ribosomal subunit, respectively. Furthermore the NMD inhibitor wortmannin (in 0.1% DMSO), which inhibits the SMG-1 kinase and plays a key role in mRNA surveillance, was used.

To inhibit the proteasome-mediated degradation of ubiquitin-conjugated proteins the peptide aldehyde MG132 was used. MG132 is a reversible inhibitor of the chymotrypsin-like activity of the 20S proteasome.

All used substances, supplied concentrations and the time of treatment are listed under 2.1.3. As a negative control for each used substance the appropriate dissolvent was added (see 2.1.3).

2.2.2.1.5 Transfection of the NMD reporter in Flp-In cells

Clonal Flp-In293 cells were transiently transfected for up to 72 h with the NMD reporter or the control NMD reporter plasmid. In a pre-test 1 and 2 µg plasmid DNA were used. Whereas 2 µg of each plasmid was toxic for the cells, 1 µg plasmid had no adverse effects. Transiently transfected cells were observed under UV light to estimate GFP expression.

To test whether NMD inhibition results in a higher GFP level, the transiently transfected cells were treated with various amounts of emetine (1-10-30-100-300 µg/ml) or cycloheximide (1-10-30-100 µg/ml). After 24 h of transfection treated cells were analysed qualitatively (microscope; UV light) and quantitatively (RT-qPCR).

2.2.2.2 Isolation and culture of neonatal mouse cardiac myocytes

Wild-type- (WT) or homozygous *Mybpc3*-KI neonatal mouse cardiac myocytes (NMCMs) derived from the targeted *Mybpc3*-KI mouse model were prepared from at least 25 hearts of 0 - 4 days old pups as described by Laugwitz et al. (2005). Neonatal mice were sacrificed by decapitation. Mouse ventricles were removed aseptically, kept in Ca²⁺/Mg²⁺-free HBSS on ice and predigested overnight in 0.5 mg/ml trypsin-HBSS solution at 4 °C under gentle agitation. Trypsin predigestion was followed by five rounds of digestion with 240 U/ml collagenase type II in HBSS at 37 °C for 9 min. All supernatants were collected and spun twice at 600 rpm for 8 or 5 min at room temperature. Cells were resuspended in pre-warmed dark medium (DMEM:M199 3:1, 10% horse serum, 5% FCS, 100 U/ml

penicillin-streptomycin; 1 mM HEPES, pH 7.4) followed by two rounds of pre-plating (75 min at 37 °C, 10% CO₂) in T-75 flasks to exclude non-cardiac myocytes from culture. NMCMs were plated on laminin-coated (0.01 mg/ml) dishes in dark medium at a density of 10⁵ cells/cm² and incubated at 37 °C, 10% CO₂ for 24 h to 5 weeks.

Cytosine arabinoside (Ara-C) was added (25 µM) to block proliferation of remaining fibroblast cells.

2.2.2.2.1 Design of antisense oligoribonucleotides and transfection of neonatal mouse cardiac myocytes

Antisense oligoribonucleotides (AONs) were used to target exonic splicing enhancer (ESE) motifs, which were identified by the ESE prediction program “ESE finder 3.0” (Cartegni et al., 2003; Smith et al., 2006). All AONs were synthesized by Eurogentec and are full-length modified with 2'-*O*-methyl substituted ribose and phosphorothioate backbones (2OMePS). The used AON sequences are listed in the appendix (5.1.9). The sequence for the scrambled AON was obtained using the “siRNA Wizard™” program (from Invivo Gen, online free available). The given sequences were subsequently proven by NCBI blast for hits in the mouse genome.

Four to five day cultured cardiac myocytes from WT or KI-NMCMs were transfected with either 5 µg Cy3-AON-5, scrambled-AON-5, AON-5, AON-6 or both AON-5 plus AON-6, respectively. TurboFect™ was used for all transfections according to the manufacturer instructions. The quantity and transfection reagent for AON transfections were determined in a pre-test. Non-transfected, but transfection reagent-containing (mock) or scrambled-AON-5-transfected NMCMs served as controls. As a control for transfection efficiency and to identify the localization of the AONs in NMCMs the Cy-3-tagged AON-5 was used (Cy3-AON-5). This AON contains the identical sequence designed for AON-5, but additionally a Cy3-tag. Transfection efficiencies were evaluated by counting the number of fluorescent nuclei.

2.2.2.2.2 Treatment of neonatal mouse cardiac myocytes

To inhibit the proteasome-mediated degradation of ubiquitin-conjugated proteins the peptide boronate MG262 (Proteasome Inhibitor III, Z-Leu-Leu-Leu-B(OH)₂; 4 µM 2 h)

was applied in dark medium. MG262 is a specific, but reversible inhibitor of the chymotrypsin-like activity of the 20S proteasome.

In order to determine the half-lives of both WT and KI proteins, NMCs were treated with 30 µg/ml cycloheximide (CHX) in 0.1% dimethylsulfoxide (DMSO) applied in dark medium. As a control NMCs treated with DMSO 0.1% for 6 h to 96 h were used.

2.2.2.2.3 Fluorescence analysis of NMCs

Coverslips (diameter: 12 mm) with cultured NMCs (24 h to 2 weeks) were washed twice in 1x D-PBS for 5 min, fixed in 4% paraformaldehyde for 10 min at 4 °C followed by three times washing in 1x D-PBS. NMCs were incubated with the nuclear dye TO-PRO-3 (1 µM) in the presence of triton X-100 (0.5%) in 1x D-PBS for 15 min at room temperature. After a final wash step (three times 5 min) in 1x D-PBS, cells were fixed with Mowiol and analysed by confocal microscopy using a Zeiss confocal inverted microscope.

2.2.3 Purification, analysis and sequencing of DNA and RNA

2.2.3.1 Agarose gel electrophoresis

For separation, analysis and purification of cDNA and (plasmid) DNA samples the agarose gel electrophoresis was used (Sugden et al., 1975). After mixing the samples with 6x loading dye they were separated on 0.8% - 2% agarose gels (in TAE: 40 mM Tris base, 20 mM acetic acid, 1 mM EDTA, pH 8.0) containing DNA intercalating ethidium bromide (0.8 µM). Electrophoresis was conducted in 1x TAE running buffer at 80 V to 110 V clamping. To determine the size of the migrated fragments the molecular weight (MW) marker Gene Ruler™ 100 bp or 1 kb DNA Ladder were used (see Appendix 5.2). The gels were visualized in ultraviolet light using the Chemie Genius² Bio imaging system.

2.2.3.2 Preparative agarose gels

DNA or cDNA fragments were extracted from the agarose gel using a sterile scalpel. DNA was then extracted using the QIAquick Gel Extraction Kit according to the instructions of the manufacturer. The DNA was eluted in 30 µl aqua ad iniectabilia and concentration determined using the NanoDrop Spectrometer.

2.2.3.3 Sequencing of DNA

Sequencing was done by MWG Biotech AG.

2.2.3.4 RNA isolation

WT and KI-NMCMs (see 2.1.2) or transient and stable transfected HEK293 cells (see 2.2.2.1.1 and 2.2.2.1.2) were harvested on ice after washing the cells once with ice-cold PBS. Total RNAs were then extracted using the SV Total RNA kit according to the manufacturer's instructions. The RNA was eluted in 50 µl diethylpyrocarbonate (DEPC)-treated aqua ad iniectabilia and its concentration determined using the NanoDrop Spectrometer.

2.2.3.5 Determination of the RNA and DNA concentration

The absorbances of RNA or DNA samples were measured at 260 nm. For both RNA and DNA samples it was assumed that 1 unit of absorbance corresponds to 40 µg/ml and 50 µg/ml, respectively. The RNA and DNA purity was determined by the ratio between 260 nm and 280 nm. While for RNA samples a ratio of about 2.0 generally counts for "pure" RNA, a ratio of about 1.8 counts for "pure" DNA. In addition, the ratio between 260 and 230 nm is used to proof DNA purity and accounts for "pure" DNA within the range of 1.8 and 2.2. For both RNA and DNA samples a lower ratio indicates a contamination with proteins or phenol, which are detected at 280 nm.

2.2.3.6 Reverse transcription

The cDNA synthesis was performed according to the instructions of the manual of the SuperScript™ III kit. For reverse transcription oligo-dT primer supplied with the Kit and 50 ng or 100 ng RNA (100 ng from HEK293 cell preparations and 50 or 100 ng from NMCM preparations) were used. As a control for genomic contamination a reaction without reverse transcriptase was performed in parallel. The quality and quantity of the cDNAs was validated by polymerase chain reaction (PCR) according to Mullis (Mullis et al., 1987). For amplification AmpliTaq Gold® polymerase and 200 nM human or murine GAPDH primers were used (see Appendix 5.1.9). The used touch-down PCR program (65 °C to 60 °C) is listed in Table 2.3. The PCR products were analysed on 2% agarose gels.

2.2.3.7 Polymerase chain reaction (PCR)

For thermal cycling 200 µl-PCR tubes were used in a Thermal PCR cycler. The applied PCR program was adapted to the used polymerase and annealing temperatures of the primers (indicated in the supplied data sheet from MWG). The elongation time was conformed to the length of the expected DNA fragment, whereby the synthesis rate was supposed to be 1 kb/min, unless noted otherwise by the manufacturer. The amount of template was between 20 ng to 40 ng for genomic or plasmid DNA and 1 or 2 µl cDNA. All used primers and probes are listed in the Appendix (5.1.9).

For mRNA analysis of transient or stable transfected HEK293 cells either the AmpliTaq Gold® polymerase or PrimeSTAR® HS DNA polymerase were used according to the instructions of the appropriate manual. For the PCR reaction 1 or 2 µl cDNA template and 0.2 - 0.4 µM primers were applied in a total volume of 20 µl. For thermal cycling the AmpliTaq Gold® polymerase was used for touch-down PCRs and PrimeSTAR® HS DNA polymerase for classical PCRs or to test the specificity of primers before application in RT-qPCR analyses (programs are listed in Table 2.1, Table 2.2 and Table 2.3). The determination of *Mybpc3* mRNAs derived from WT- or KI-NMCMs transfected with different AONs was performed during a 35-cycles touchdown PCR using the AmpliTaq Gold® polymerase with a forward primer located in exon 4 and a reverse primer located in exon 9 (primers are listed in the Appendix 5.1.9). For the PCR

reaction 1 or 2 μl cDNA template and 0.2 μM primers were applied in a total volume of 20 μl . To identify the *Mybpc3* isoforms cDNA derived from WT-NMCMs was used as a template for two rounds of touch-down PCR (Table 2.3; 35 and 31 cycles, respectively) with the AmpliTaq Gold® polymerase. For amplification a forward primer located in exon 4 and a reverse primer located in exon 7 were applied in a total reaction volume of 50 μl (Appendix 5.1.9). After the first round of PCR 0.5 μl PCR product were used as template for the second round of PCR in a total volume of 50 μl . Subsequently the amplicon at the correct size was excised and gel extracted using the QIAquick Gel Extraction Kit according to the instructions of the manufacturer. For sequencing analysis the amount of extracted mRNA fragment was increased again by another round of PCR (35 cycles) with the same primers. Consecutively the PCR product was purified using the QIAquick PCR Purification Kit. All PCR products were separated on agarose gels (0.8 – 2%).

Table 2.1. Standard PCR program used for PrimeSTAR® HS DNA polymerase.

PCR step	Temperature (°C)	Time	
Denaturation	98	10 sec	} 30 cycles
Annealing	65 to 60	5 sec	
Elongation	72	1 kb/min	
Cooling	4	∞	

Table 2.2. PCR program adapted to RT-qPCR conditions for use with PrimeSTAR® HS DNA polymerase.

PCR step	Temperature (°C)	Time	
Initial denaturation	50	2 min	
Denaturation	98	15 sec	} 40 cycles
Annealing	60	5 sec	
Elongation	72	20 sec	
Cooling	4	∞	

Table 2.3. Standard PCR program (touch-down) used for AmpliTaq Gold® polymerase.

PCR step	Temperature (°C)	Time	
Initial denaturation	98	3 min	
Denaturation	98	30 sec	} 11 cycles (0.5 °C/cycle)
Annealing	Touch down* (range: 5 °C)	30 sec	
Elongation	68	1 kb/min	
Denaturation	98	30 sec	} 24 cycles
Annealing	65; 60; 55	30 sec	
Elongation	68	1 kb/min	
Final primer extension	68	10 min	
Cooling	4	∞	

*70 °C - 65 °C, 65 °C - 60 °C, 60 °C - 55 °C

2.2.3.8 Determination of mRNA level by quantitative PCR

The mRNA level was determined by quantitative PCR using either cDNA-based probes (TaqMan®) or SYBR® green. Both chemistries TaqMan® probes and SYBR® green enable the detection of PCR products by generating a fluorescent signal. The generation of the signal in TaqMan® probes is based upon the Förster Resonance Energy Transfer (FRET) via the coupling of the fluorescent reporter (at 5'-end, here FAM) and a quencher (at 3'-end, here TAMRA) to the same oligonucleotide. In contrast SYBR® green is a fluorogenic dye emitting a strong fluorescent signal, when bound to double-stranded DNA. In unhybridized TaqMan probes the detection of the fluorescent signal from the probe is suppressed by the proximity of the reporter and quencher molecules (Figure 2.6a, left-hand side). During PCR reaction, the 5'→3' nuclease activity of the DNA polymerase cleaves the probe, which is bound to the complementary sequence of the template. As a result both dyes are decoupled and finally FRET does not take place any longer (Figure 2.6b to d, left-hand side). Therefore, the fluorescence signal of the reporter dye increases in each cycle with the amount of the cleaved probe. By monitoring the increase in fluorescence signal the accumulation of PCR products is directly detected.

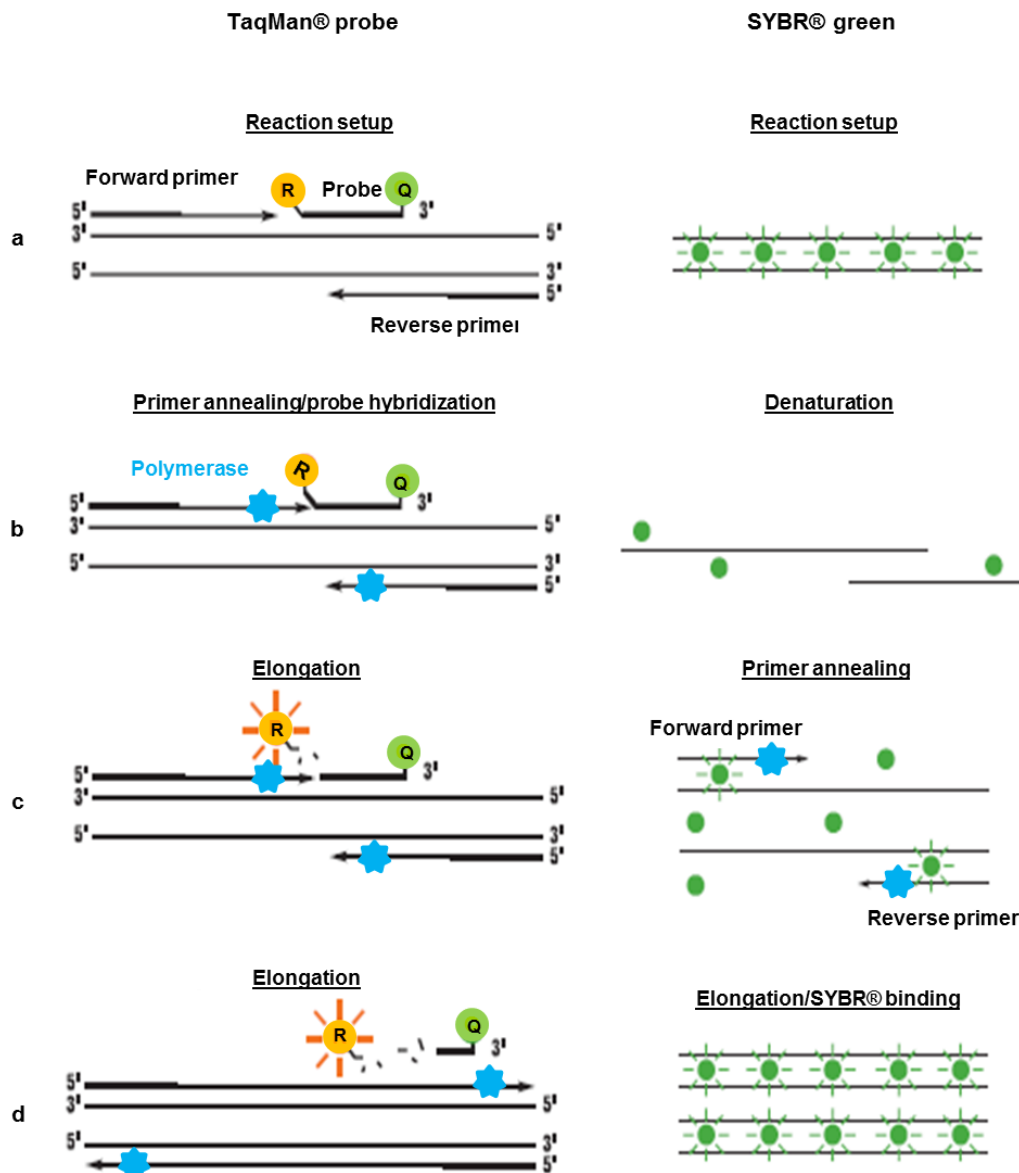


Figure 2.6. TaqMan® probe and SYBR® green chemistries for RT-qPCR analysis.

Left-hand side: The TaqMan® probe contains a reporter (R, 5'-end) and a quencher (Q, 3'-end) dye, which are held in adjacent positions. (b) During the PCR reaction the primers and probe hybridize to the complementary DNA strand and the DNA polymerase extends the primer in 5'-3' direction forming a new strand. (c), (d) During this process the intact hybridized probe is cleaved by the exonuclease activity of the DNA polymerase and the fluorescence signal released. Right-hand side: (a) SYBR green intercalates with the double-stranded DNA of the sample. (b) During the denaturation step of the PCR SYBR® green is released and the fluorescence signal reduced. (c), (d) As the PCR progresses the target DNA is amplified and SYBR® green bound to each new copy of double-stranded DNA. As a result the fluorescence signal intensity increases with to the increased amount of PCR product. Picture modified from the Applied Biosystems website.

On the other hand, SYBR® green binds directly to double-stranded DNAs (Figure 2.6a, right-hand side). During the denaturation step SYBR® green is released resulting in a drastically reduction of the fluorescence signal (Figure 2.6b, right-hand side). While thermal cycling the polymerase amplifies the target DNA and SYBR® green dye binds to

each new copy of double-stranded DNA. Thus, during each PCR cycle the fluorescence intensity increases with the increased amount of amplified PCR product (Figure 2.6c and d, right-hand side).

During the exponential phase of qPCR amplification (Figure 2.7) the relative cDNA concentrations are determined by plotting the fluorescence signal against the cycle number on a logarithmic scale. A threshold helps to assign the fluorescence signal above the background. The point at which the fluorescence intensity exceeds the background signal (at the beginning of the exponential phase) is set as the cycle threshold (C_t value). The quantification of the PCR is based on the calculation of the C_t value.

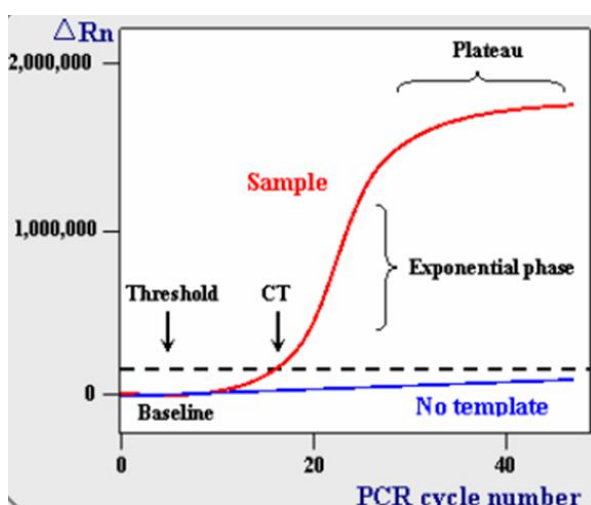


Figure 2.7. Amplification plot.

Representation of a typical amplification curve consisting of the exponential phase and a plateau phase. The vertical axis represents the amount of normalized reporter signal in arbitrary units and is plotted against the cycle number. The threshold line assigns the fluorescence signal above the background. The point at which the fluorescence intensity crosses the threshold is set as the C_t value. Picture from the “rt-pcr” website.

For quantitative analysis of mRNAs (diluted 1:10 for Flp-In293 cell analysis and 1:2 for analysis of NMCMS) the TaqMan® ABI Prism® 7900 HT sequence detection system was used. TaqMan® probes were used in combination with the TaqMan® Universal PCR Master Mix (Applied Biosystems) or the Maxima Probe/ROX qPCR Master Mix (Fermentas). For analysis with SYBR® green the Maxima SYBR green/Rox qPCR Master Mix (Fermentas) was used. The used specific primers and probes (listed in Appendix 5.1.9) were applied at a concentration of 0.3 μ M/each in a total volume of 10 μ l. Each sample was analysed in triplicates. The qPCR programs used for both chemistries are listed in Table 2.4 and Table 2.5.

Table 2.4. PCR program for qPCR analysis with TaqMan probes using the relative quantification method.

PCR stage	Temperature (°C)	Time
Stage 1	50	2 min
Stage 2	95	10 min
Stage 3	95	15 sec
	60	1 min

} 40 cycles

Table 2.5. PCR program for qPCR analysis with SYBR® green using the absolute quantification method.

PCR stage	Temperature (°C)	Time
Stage 1	50	2 min
Stage 2	95	10 min
Stage 3	95	15 sec
	60	1 min
Stage 4	95	15 sec
	60	15 sec
	95	15 sec

} 40 cycles

For quantification of the mRNA amount the $2^{-\Delta\Delta C_t}$ method was used. To calculate the $\Delta\Delta C_t$ value, samples (target) were normalized to the endogenous control (GAPDH or G α S) and related to the calibrator (e.g. mock- or scrambled-treated NMCMs):

$$\Delta C_t = \text{mean } C_t (\text{target}) - \text{mean } C_t (\text{endogenous control})$$

$$\Delta\Delta C_t = \Delta C_t - \Delta C_t (\text{calibrator})$$

The calculated $2^{-\Delta\Delta C_t}$ provides the amount of mRNA in each sample and is expressed in arbitrary unit (AU). All analyses were performed with the software ABI SDS 2.2 or 2.4 and the obtained data plotted as graphs using the software GraphPad Prism 5.

2.2.4 Protein analysis

2.2.4.1 Protein isolation and concentration determination

After transfection/treatment of HEK293 cells (see 2.2.2.1.1), Flp-In293 cells (WT, Mut-1 and Mut-2; see 2.2.2.1.2) or WT- and KI-NMCMs (see 2.1.2), cells were rinsed once with ice-cold 1x D-PBS and lysed in 150 μ l or 200 μ l lysis buffer (30 mM Tris base pH 8.8, 5 mM EDTA, 30 mM NaF, 3% SDS, 10% glycerol). Cells were collected in Eppendorf tubes and stored at -20 °C prior to use for Western blot.

The concentration of the proteins was determined using the **Bradford protein assay** (Bradford 1976), which is a colorimetric assay based on an absorbance shift in the dye Coomassie Brilliant Blue G-250 when bound to arginine or hydrophobic amino acid residues present in proteins. The increase of absorbance at 595 nm is proportional to the amount of bound dye and represents the protein concentration present in the sample. To determine the protein concentration 1 ml Bradford reagent diluted 1:5 in 0.1 M NaOH and 5 μ l of sample was used. Samples were measured in duplicates and incubated for 5 min at room temperature prior measurement with the spectrophotometer. The protein quantity was determined after subtracting the blank from the protein value and comparison of the calculated value with a standard curve obtained with known concentrations of bovine serum albumin.

2.2.4.2 Immunoprecipitation of proteins

For enrichment of proteins derived from Flp-In293 cells the immunoprecipitation method was conducted followed by Western blot. Proteins from Flp-In293 cells (as negative control) and isogenic Flp-In cells (WT and Mut-1) plated in 15 cm dishes, were yielded at a confluency of 90%, lysed in 1 ml high salt RIPA buffer (500 mM NaCl, 1 mM EDTA, 50 mM Tris-HCl pH 7.4, 1% triton X-100 and 1 tablet complete mini-proteases inhibitor cocktail per 10 ml buffer) and incubated for 10 min on ice. Cells were collected in 1.5 ml Eppendorf tubes and sonicated three times for 7 s with 40% power on ice. After centrifugation for 10 min at 13200 rpm and 4 °C the supernatant, containing the solubilized proteins, was transferred into a new tube and diluted up to 1 ml with high salt RIPA buffer. The pellet (P0) was stored for subsequent analysis by Western blot. The primary antibody

(anti-c-myc antibody, 5 µg) was added and cell lysate gently rocked in an orbital shaker overnight at 4 °C. To capture the immune complexes 40 µl of protein A/G PLUS-Agarose beads were added for further incubation at 4 °C (2 h, orbital shaker). Beads were collected by centrifugation at 200x g (2 min, 4 °C) and supernatant (SN1) stored for Western blot. To get rid of unspecific binding beads were washed three times with high salt RIPA buffer, centrifugated (200x g) and washed once with 1x D-PBS. Prior Western blot the beads were resuspended in 20 or 40 µl 1x Laemmli buffer (1x buffer: 0.3% SDS, 1.6% glycerol, 1.6 mM Tris base, pH 6.8; 16.6 mM DTT and 0.002% bromphenol blue) and the samples boiled for 5 min at 95 °C to dissociate the immune complexes from the beads.

2.2.4.3 Western blot

For Western blot analysis 30 µg (HEK293 or Flp-In293 cells) or 50 – 60 µg (NMCMs) proteins were separated by the SDS-polyacrylamide-gel electrophoresis (SDS-PAGE) according to Laemmli (Laemmli 1970). Prior loading, samples were centrifuged for 5 min (13200 rpm at room temperature), mixed with 6x Laemmli buffer (2% SDS, 10% glycerol, 10 mM Tris base, pH 6.8; 100 mM DTT and 0.01% bromphenol blue) and denatured for 5 min at 95 °C.

The polyacrylamide gel consists of a stacking gel (125 mM Tris base pH 6.8, 5% acrylamide/bis acrylamide solution (29:1), 0.1% SDS, 0.1% APS, 0.08% TEMED) and a running gel (375 mM Tris base pH 8.8, 6% to 15% acrylamide/bis solution (29:1), 0.1% SDS, 0.1% APS, 0.03% TEMED). The running gels were composed of 6% - 15% polyacrylamide depending on the expected apparent molecular weight. The gels were inserted into an electrophoresis chamber (BIO-RAD) filled with 1x electrophoresis buffer (25 mM Tris base, 192 mM glycine, 0.1% SDS). The Precision Plus Protein Standard™ was used as a standard molecular weight marker (see Appendix 5.2). Proteins were separated by gel electrophoresis, which was conducted at 80 V for 10 min followed by a voltage between 80 V to 150 V as long as needed.

After electrophoresis, proteins were transferred onto a nitrocellulose membrane and electroblotted at 300 mA for 90 min at 4 °C in a Mini Trans-blot chamber system using transfer buffer (50 mM Tris base, 380 mM glycine, 0.1% SDS, 20% methanol).

To visualize the transferred proteins, membranes were stained with Ponceau S and washed three times with 1x TBS-T 0.1% (100 mM Tris base, pH 7.5, 150 mM NaCl, 0.1% Tween

20). Prior addition of the primary antibody, the membranes were incubated in 5% milk powder solution (in TBS-T buffer) for 1 h at room temperature to block remaining free hydrophobic binding sites. The primary antibody was diluted in TBS-T and added to the membrane for 1 h at room temperature or overnight at 4 °C under gentle agitation. The blot membrane was washed in 1x TBS-T 0.1% (three times, 5 min) before adding the secondary antibody (anti-rabbit IgG or anti-mouse IgG conjugated to horseradish peroxidase) diluted in 5% milk powder solution for 1 h at room temperature. After the final wash (three times 5 min with 1x TBS-T 0.1%), the membrane was incubated with a detection reagent according to manufacturer's instructions (ECL-Plus Kit or SuperSignal® West Dura). The emitted light of the produced chemiluminescent signal (chemiluminescent substrate converts the peroxidase) was detected at different time points (10 sec to 10 min) with the Chemie Genius² Bio Imaging System and quantified with the Gene Tool Software (Syngene, Cambridge). Obtained values were plotted with the software GraphPad Prism 5 (GraphPad Software, Inc.).

2.2.4.4 Determination of the half-lives of cMyBP-C wild-type and knock-in proteins

To determine the half-lives of WT- and KI-proteins NMCs were treated with 30 µg/ml cycloheximide (CHX in 0.1% dimethylsulfoxide, DMSO) in dark medium. Mock-transfected NMCs treated with DMSO 0.1% were used as a control. The calculation of the protein half-lives was based on the obtained densitometric raw data (Gene Tools software) for each point in time. These values were related to the mean of the mock transfected samples (control), expressed as percent of control and plotted against the time of treatment. To obtain the relative half-life (50%) the slope, described as formula ($y = x^2 + px + q$), was converted after the following p-q-formula:

$$x_{1/2} = -\frac{p}{2} \pm \sqrt{\frac{p^2}{4} - q}$$

2.3 Statistical analysis

Data were expressed as mean \pm SEM. Statistical analyses comparing 2 groups were performed using the unpaired Student's t-test. Curve fittings and transformations were performed using the commercial software GraphPad Prism5. A value of $P<0.05$ was considered statistically significant.

3 Results

3.1 Establishment of a cell-based system to analyse the expression of *MYBPC3* mutations

Most of the *MYBPC3* mutations disrupt the reading frame and are expected to result in C-terminal truncated proteins. Nevertheless, the expected aberrant proteins could not be detected by Western blot analysis of myocardial tissue from patients bearing a frameshift mutation in the heterozygous state (Rottbauer et al., 1997; Moolman et al., 2000; van Dijk et al., 2009). The absence of detection suggests regulation at the mRNA level (most likely by NMD) or protein level (by autophagy or the UPS). Finally, the low level of cMyBP-C proteins can result in haploinsufficiency, suggested as the disease mechanism that causes HCM. However, different *MYBPC3* mutations are associated with a wide range of ages of onset and disease penetrance. The molecular mechanisms involved in the progression of HCM are not fully elucidated. Their study is impeded by difficulties in access to human tissue samples and the inherently long time-line needed to create several mouse models. Therefore the idea was to establish a cell-based screening system in HEK293 cells to analyse the expression of *MYBPC3* mutations. This system was further used to study the relative contribution of NMD and/or UPS in controlling the expression of *MYBPC3* mutations using inhibitors of both systems.

3.1.1 Choice of *MYBPC3* mutations

We focused on mutations that result in C-terminal truncated proteins, which, when stabilized by drugs still may contain important functional domains required for sarcomeric incorporation and function. Therefore two mutations in the heterozygous state were selected. The first one is a splicing point mutation in intron 31, which results in a “normal” level of mutant mRNA, suggesting regulation by the UPS (mutant-1, Mut-1; Rottbauer et al., 1997). Mut-1 is a human G>A transition at position +1 of the splice donor site in intron 31 (IVS31+1G>A; NCBI gene assessment no. Y10129), which leads to the skipping of the corresponding exon 31 (Figure 3.1). The expected truncated protein (~125 kDa) with loss of 164 amino acids (aa) was not detected by Western blot.

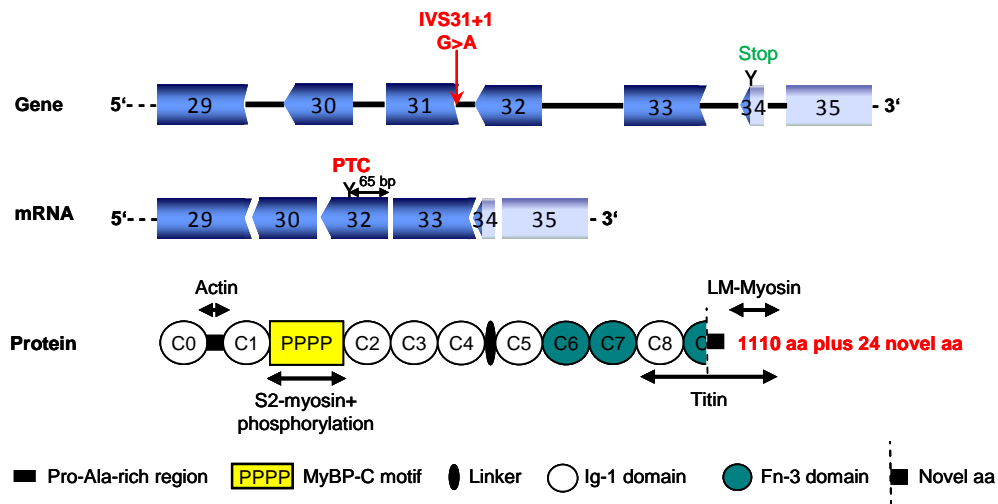


Figure 3.1. Consequences of a splicing mutation in *MYBPC3*.

(a) The consequence of the G>A transition at the splice donor site of intron 31 is shown on the structure of the mutant mRNA and protein. The mutation induces the skipping of exon 31, which results in a frameshift and formation of 24 novel amino acids followed by a premature termination codon (PTC) in exon 32, 65 bp upstream of the 5'-splice site of intron 32. The mutant mRNA is expected to produce a truncated protein of ~125 kDa containing a part of the titin binding site but missing the light meromyosin (LM-myosin) binding site.

The second mutation is a 4-bp-insertion (c.3335_3336insAGTG; NCBI gene accession no. Y10129) at the position +6 in exon 31, which results in a low level of nonsense mRNA, suggesting a regulation by NMD (mutant-2, Mut-2; unpublished data). Mut-2 directly results in a premature termination codon 162 bp upstream of the splice donor site of intron 31 (TGG>TGA; Figure 3.2). The mutant protein contains a part of the titin-binding site but loses the LM-myosin binding site.

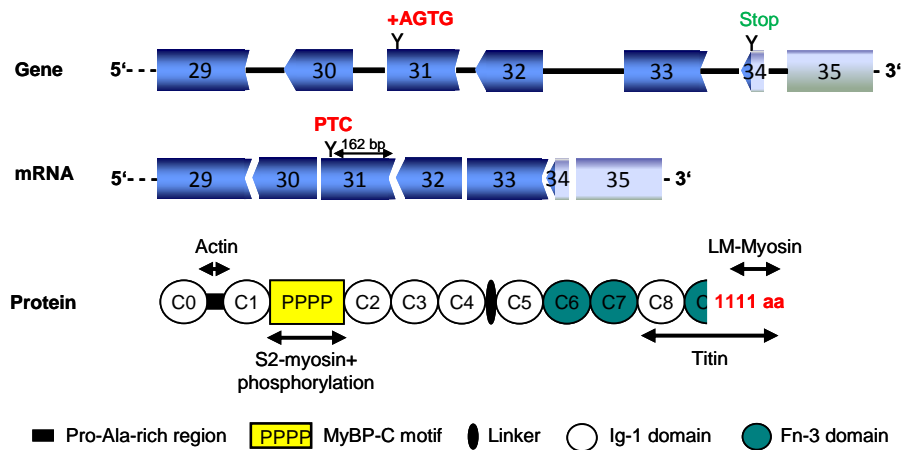


Figure 3.2. Consequences of a 4-bp-insertion in *MYBPC3*.

The consequence of the insertion of AGTG at the position +6 of exon 31 (c.3335_3336ins4) is shown on the structure of the mutant mRNA and protein. The mutation directly results in a premature termination codon (PTC), located 162 bp upstream of the 5'-splice site of intron 31. The normal stop codon (green) is located in exon 34. The mutant mRNA is expected to produce a ~122 kDa truncated protein containing a part of the titin binding site, but losing the light meromyosin (LM-myosin) binding site.

Western blot analysis of left ventricular tissue failed to detect the expected truncated protein of 122 kDa (Figure 3.3a). Quantitative PCR analysis revealed that the total *MYBPC3* mRNA amount was 27% lower in patient than in control samples and that mutant *MYBPC3* mRNAs represented 11% of total, suggesting mRNA instability and degradation by the NMD system (Figure 3.3b).

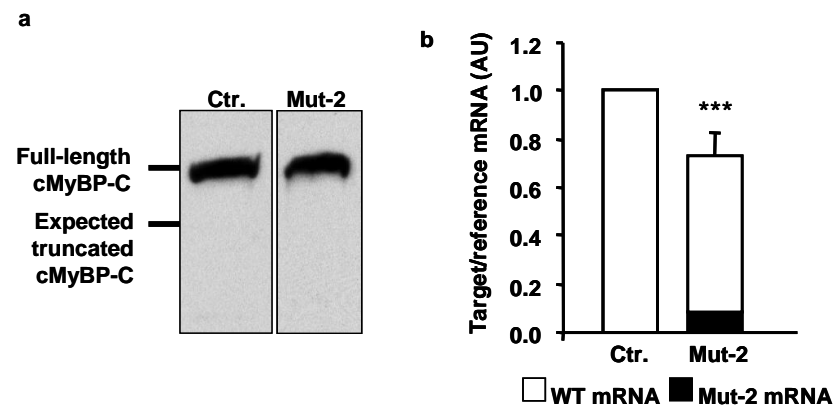


Figure 3.3. Analyses of a 4-bp-insertion in *MYBPC3* at both the mRNA and protein level in patient samples.

(a) Western blot of cardiac tissue samples derived from an unaffected (ctr.) and affected (Mut-2) patient was stained with an anti-cMyBP-C antibody. (b) Total myocardial RNA of an unaffected (ctr.) and affected (Mut-2) patient was analysed by qPCR using specific primers for amplification of total, wild-type (empty boxes) and mutant (black boxes) *MYBPC3*. Data from six independent experiments are expressed as mean \pm SD. *** P <0.001 vs. ctr., unpaired Student's t-test. The experiments were performed by Nicolas Vignier, Paris.

To analyse the expression of *MYBPC3* mutations and to evaluate the relative contribution of NMD or the UPS in lowering the levels of mutant mRNAs or proteins, c-myc-tagged minigenes encoding human WT and mutant cMyBP-Cs were generated. Subsequently, the splicing pattern, as well as the amount of mRNA and protein produced from the minigenes were analysed in HEK293 cells and Flp-In293 cells.

3.1.2 Generation of minigenes encoding human mini-cMyBP-Cs

The WT minigene ranging from exon 29 to exon 34 of *MYBPC3* was generated using the pEF5/FRT/V5 directional TOPO® Expression Kit (Invitrogen). In brief, a blunt end DNA fragment was amplified by PCR from human DNA and cloned into the mammalian expression vector pEF5/FRT/V5. The mutations (Mut-1 and Mut-2) were introduced afterwards by site-directed mutagenesis of the WT clone. The presence of each *MYBPC3* insert (WT, Mut-1 and Mut-2) was verified by restriction digestion using two enzymes, which cut once in the vector and once in the insert. Therefore two fragments at the molecular weight of 5263 bp and 2629 bp were expected for each construct (Figure 3.4a and b). As a control for the restriction enzyme activity, single digestions with each enzyme were conducted (Figure 3.4b). Restriction digestion exhibited the expected restriction pattern. The presence of the introduced mutations was subsequently validated by sequencing. One plasmid was then used for large-scale preparation followed by restriction digestion and sequencing (Figure 3.4b-d). This revealed the successful insertion of the mutations (Mut-1 and Mut-2).

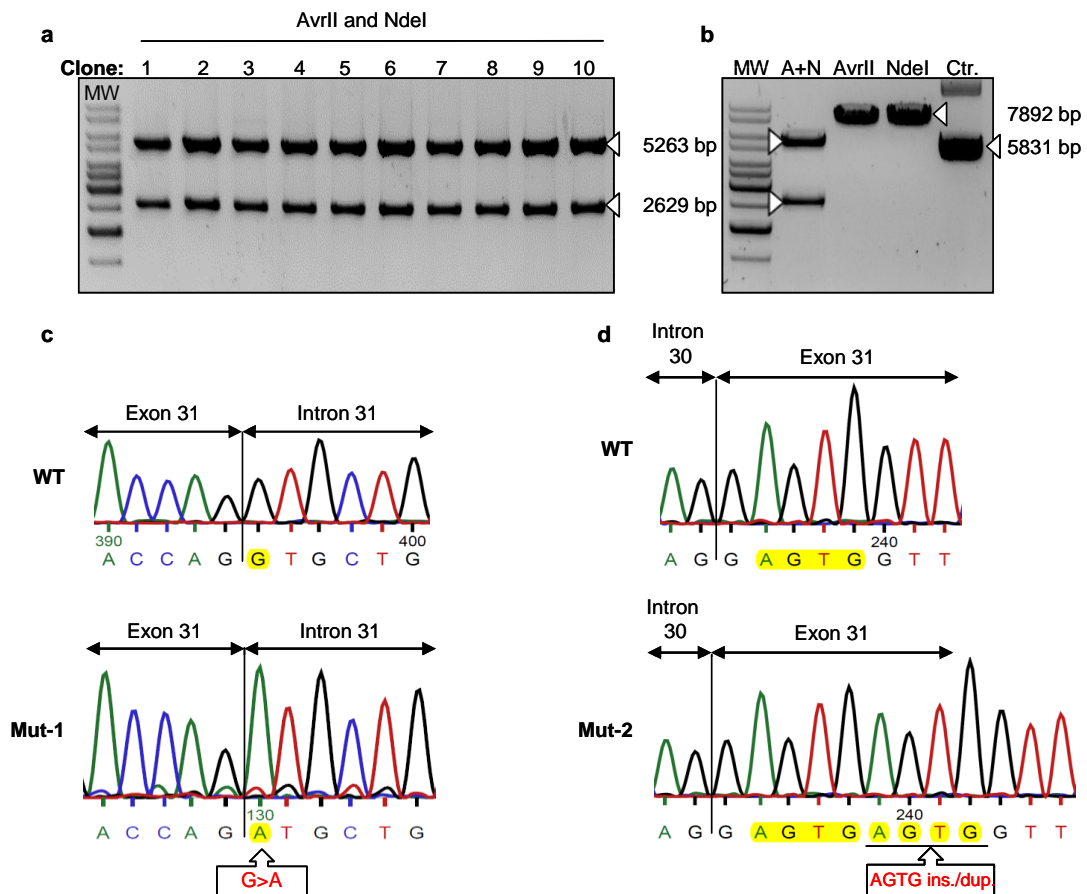


Figure 3.4. Evaluation of generated minigenes by restriction digestion and sequencing.

Representative agarose gel pictures of restriction digestions of minigene plasmids after small-scale (a) and large-scale (b) preparations. Double digest was performed with AvrII and NdeI, which cut once in the vector and once in the insert sequence. As a control for the restriction enzyme activity, single digestions with each enzyme were conducted (ctr., control). In one sample no enzymes were added (ctr., control). All investigated plasmids showed the expected restriction pattern as indicated by the arrowheads. The molecular weight (MW) marker was the Gene Ruler™ 1 kb DNA Ladder. Subsequent sequencing analysis of Mut-1 (c) and Mut-2 (d) revealed the successful inserted mutations.

The presence of the cloned WT, Mut-1 and Mut-2 *MYBPC3*-minigenes in the expression vector pEF5/FRT/V5 was further analysed by PCR. Templates included the generated plasmids and different mutation-specific *MYBPC3* primers, as indicated in the scheme on the right-hand side of Figure 3.5. Amplicons of the expected size were obtained for each minigene: 584 bp/588 bp (WT, Mut-1/Mut-2, respectively; Figure 3.5a), 220 bp (WT), 584 bp (Mut-1) and 358 bp (Mut-2; Figure 3.5b), indicating the presence of genomic *MYBPC3* DNA in the plasmids.

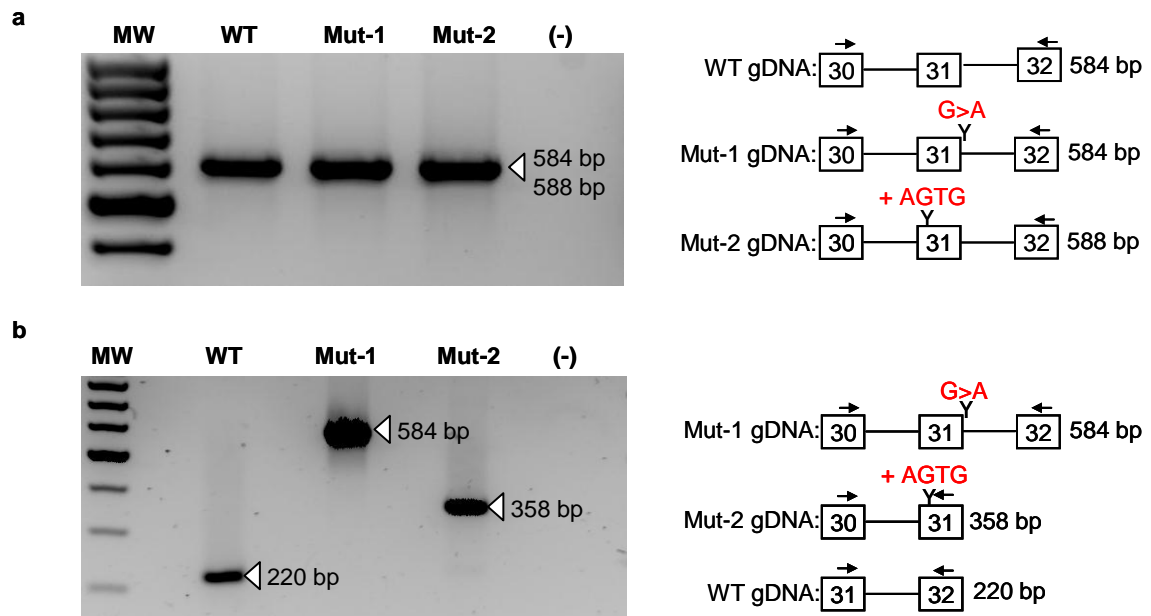


Figure 3.5. Evaluation of generated minigenes by PCR.

Plasmid DNA derived from minigene-containing vectors (WT, Mut-1 and Mut-2) was used as template for PCR amplification with different *MYBPC3* primers. As a negative control (-) water was added instead of DNA. The molecular weight (MW) marker was the Gene Ruler™ 100 bp DNA Ladder. The location of the primers (black arrows) and the expected amplicon sizes (arrowheads) are indicated in the scheme on the right-hand side.

3.1.3 Evaluation of the expression of human minigenes after transient transfection into HEK293 cells

To validate first that unmodified HEK293 cells do not express cMyBP-C, cells were stained with an antibody directed against the MyBP-C motif and analysed by confocal microscopy (Figure 3.6a). The nuclei were stained with TO-PRO-3. As a negative control HEK293 cells were stained exclusively with the secondary antibody (Figure 3.6b). Immunofluorescence revealed that HEK293 cells do not express cMyBP-C, indicating that they can be used to express human minigenes.

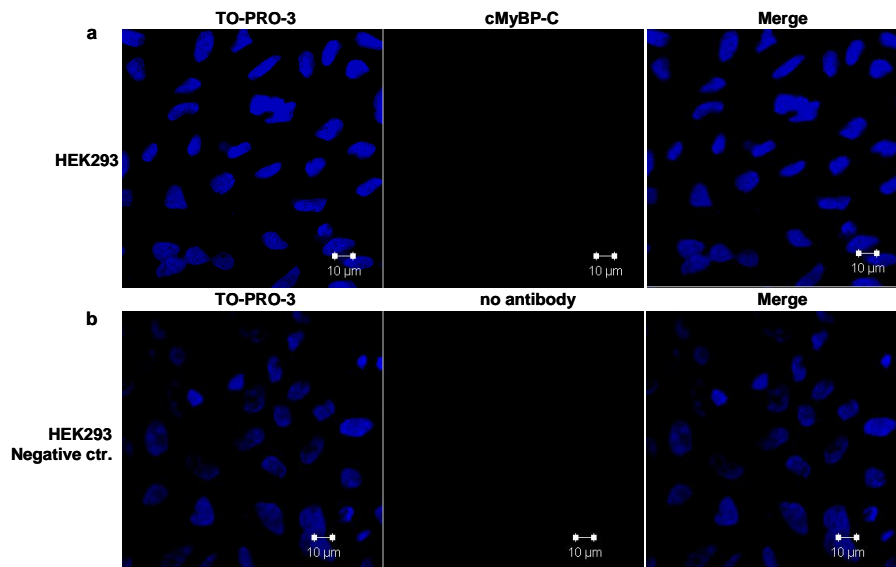


Figure 3.6. cMyBP-C expression in non-transfected HEK293 cells.

(a) HEK293 cells were stained with a cMyBP-C-specific antibody, which is directed against the MyBP-C motif (polyclonal, secondary antibody Alexa Fluor-546). (b) As a negative control cells were stained without the primary antibody. Nuclei were stained with TO-PRO-3 (in blue).

To investigate whether the human minigene constructs (WT, Mut-1, Mut-2) are transcribed into mRNAs, total RNA from transiently-transfected HEK293 cells (24 h) was reverse transcribed (+RT) and used as template for PCR amplification (Figure 3.7). Each sample was also investigated for plasmid contamination in the absence of the reverse transcriptase (-RT, --). As a positive control (++) plasmid DNA was used and expected to exhibit a fragment of 220 bp. HEK293 cells were used as a negative control, since they were not expected to express *MYBPC3*. For PCR analysis specific *MYBPC3* primers located in exons 31 and 32 were applied. While WT and Mut-2 mRNAs were expected to show a fragment of 109 bp, no amplification was expected for Mut-1, which is missing exon 31. Figure 3.7 shows that WT and Mut-2 mRNA fragments, but not the Mut-1 mRNA fragment were amplified (white arrowhead). This suggests that the expression of the mutations works in HEK293 cells. In addition, a 220-bp band was obtained in all conditions, which corresponds to the plasmid DNA. However, both bands of 220 bp and 109 bp were also amplified in the non-transfected HEK293 sample, suggesting contamination during preparation of the RNA or during PCR. Unfortunately, we could not solve this contamination problem by application of either different RNA-purification methods or additional DNase I digestion (data not shown).

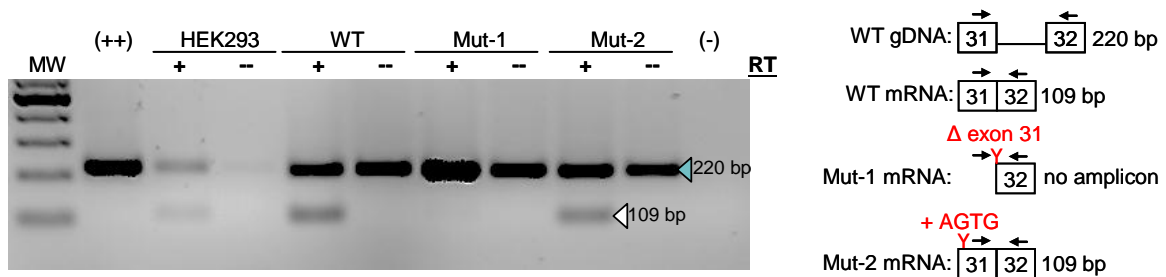


Figure 3.7. Expression of human minigenes after transient transfection.

Total RNA was extracted from HEK293 cells transiently transfected with WT, Mut-1 and Mut-2 plasmids and reverse transcribed (+) into cDNA. As a negative control (-) samples were 'reverse transcribed' without reverse transcriptase. The cDNAs were used as templates for PCR amplification with *MYBPC3* primers located in exons 31 and 32. As a positive control (++) plasmid DNA was used as template. As additional negative controls, HEK293 cell mRNA or water (-) was added instead of cDNA. The molecular weight (MW) marker was the Gene Ruler™ 100 bp-DNA-Ladder. The location of the primers (black arrows) and the expected molecular weights of the amplicons (arrowheads) are indicated in the schemes on the right side.

3.1.4 Evaluation of human mini-cMyBP-C proteins after transient transfection

Despite the problem of contamination revealed by PCR, we evaluated whether transient transfection results in human mini-cMyBP-C proteins. In contrast to the WT minigene (31 kDa), which was expected to be stable, the mutant proteins were not expected to be detected by Western blot (Mut-1, 16 kDa; Mut-2, 13 kDa; Figure 3.8). For transfection two different plasmid quantities (1 μ g and 2 μ g) were used and samples were analysed after 48 h of transfection. In parallel HEK293 cells were transfected with a GFP-encoding plasmid (pEGFP-C3, 26 kDa) to estimate the transfection efficiency. The Western blot membrane was double-stained with antibodies directed against the myc-tag and GFP. Whereas GFP was detected in the control, indicating that the transfection in HEK293 cells worked correctly, the expected myc-positive WT, Mut-1 and Mut-2 proteins were not detected by Western blot (Figure 3.8a). Probing with the anti-myc antibody revealed the same, presumably non-specific, pattern in WT, Mut-1 and Mut-2-transfected cells. These data suggest that all three mini-proteins are either not translated or are degraded after synthesis.

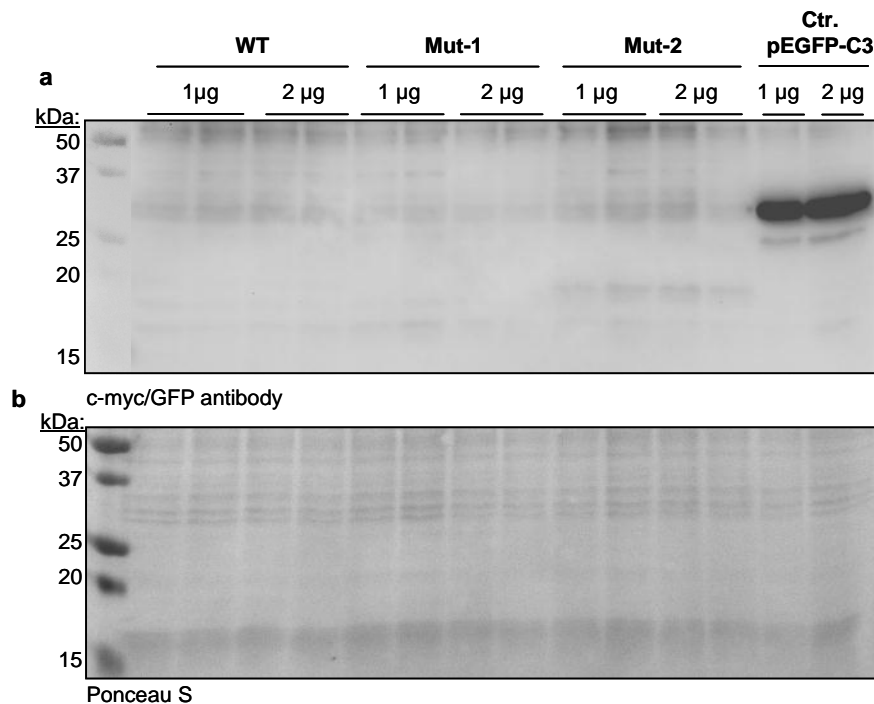


Figure 3.8. Protein expression of human minigenes after transient transfection.

(a) Western blot of protein extracts 48 h after transient transfection in HEK293 cells. The cells were transfected with two quantities of plasmids encoding WT, Mut-1, Mut-2 and GFP. The expected proteins for the WT minigene and GFP were about 31 kDa and 26 kDa, respectively. The membrane was double-stained with an antibody directed against the myc-tag and GFP. (b) The same membrane stained with Ponceau S.

In summary, human minigenes are transcribed into mRNA, but subjected to post-transcriptional regulation that results in undetected proteins. The presence of the marked amount of “contaminated transgene” in the mRNA prompted us to change the approach and therefore to establish stable cell lines.

3.1.5 Establishment of stable cell lines expressing human minigenes

To establish stable cell lines that i) allow continuous expression of the minigenes over a long time period and ii) are isogenic with a single-copy integration of the minigene constructs into the chromosome of the cell genome, the Flp-In™ System was used and Flp-In293 cell lines generated (see Material and Methods, 2.2.2.1.2). In brief, non-transfected Flp-In293 cells encode for a *lacZ*-Zeocin fusion protein and show β -galactosidase activity, zeocin resistance and hygromycin sensitivity. After homologous recombination of the minigene constructs into the Flp-In293 cell line genome, cells become zeocin sensitive, hygromycin resistant and *lacZ* negative. Thus, the growth of the cells in the presence of hygromycin and the determination of the β -galactosidase activity should validate the

presence of isogenic cell lines expressing the mentioned minigenes.

The β -galactosidase activity of the isogenic cell lines (WT, Mut-1, Mut-2) was analysed in confluent cells grown in the presence of hygromycin in a 96-well-microtiter plate using X-Gal (see Material and Methods, 2.2.2.1.3). For each cell line the activity was determined in triplicate and light microscope images were obtained (Figure 3.9). In the positive control for *lacZ*-staining (Flp-In293 cell line) all cells were blue. In contrast, none of the clonal cell lines showed blue cells, indicating that the insertion and isogenic expression of the minigene constructs worked out.

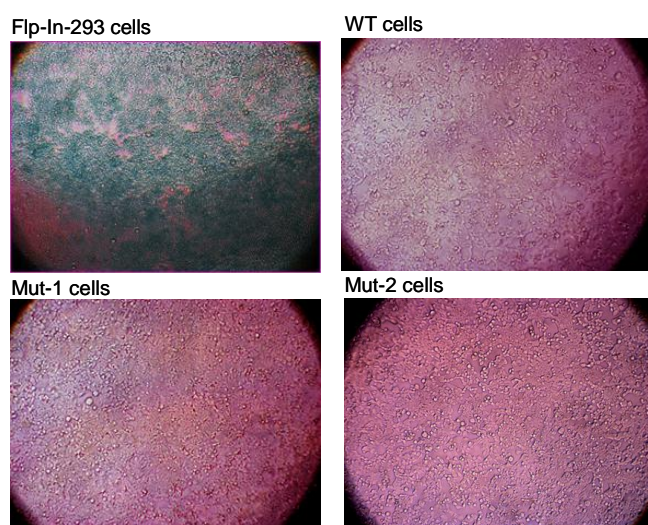


Figure 3.9. β -Galactosidase activity in clonal Flp-InTM cell lines.

Light microscope images of clonal Flp-In293 cell lines stably expressing minigene constructs after X-Gal staining to screen for *lacZ*-positive (not transfected/not isogenic cells; blue cells) and *lacZ*-negative (transfected/isogenic cells; white cells) cells. As a positive control for *lacZ*-staining Flp-In293 cells were stained in parallel.

3.1.5.1 Evaluation of minigenes' expression at the level of mRNA

To investigate whether the clonal cell lines transcribe the expected mutations into mRNAs, total RNA from WT, Mut-1 and Mut-2 cells was extracted, reverse transcribed into cDNA, and used as template for PCR amplification (Figure 3.10). One sample was also investigated for plasmid contamination in the absence of reverse transcriptase (-RT, --; Figure 3.10a). Specific PCR primers located in exons 30 and 32 of *MYBPC3* were used that are expected to amplify fragments at the molecular weight of 253 bp (WT), 93 bp (Mut-1) and 257 bp (Mut-2; Figure 3.10a). cDNA from Flp-In293 cells, which does not express *MYBPC3*, was used as a negative control. To determine whether the expression efficiency of the three minigene constructs is comparable, primers with binding sites in the Flp-In293 cell genome that are located exclusively after the insertion of the minigene construct were used (Figure 3.10b). These primers are complementary to sequences in the

SV40 promoter and in the hygromycin cassette. PCR amplification with primers located in exons 30 and 32 revealed the expected amplicons for WT, Mut-1 and Mut-2 samples (Figure 3.10a). Additional larger fragments of unknown identity were amplified in Mut-1 and Mut-2 samples. In the two control samples (Flp-In293 and -RT) no amplicons were obtained, as expected. Thus, in contrast to transiently-transfected HEK293 cells, which showed a marked “transgene contamination” in the mRNA (Figure 3.7), stable cell lines did not. PCR amplification with primers located in the SV40 promoter and hygromycin cassette revealed amplicons of the expected size of 356 bp (Figure 3.10b). The amount of amplicon did not differ between the groups, suggesting that the expression level of the different minigenes was similar.

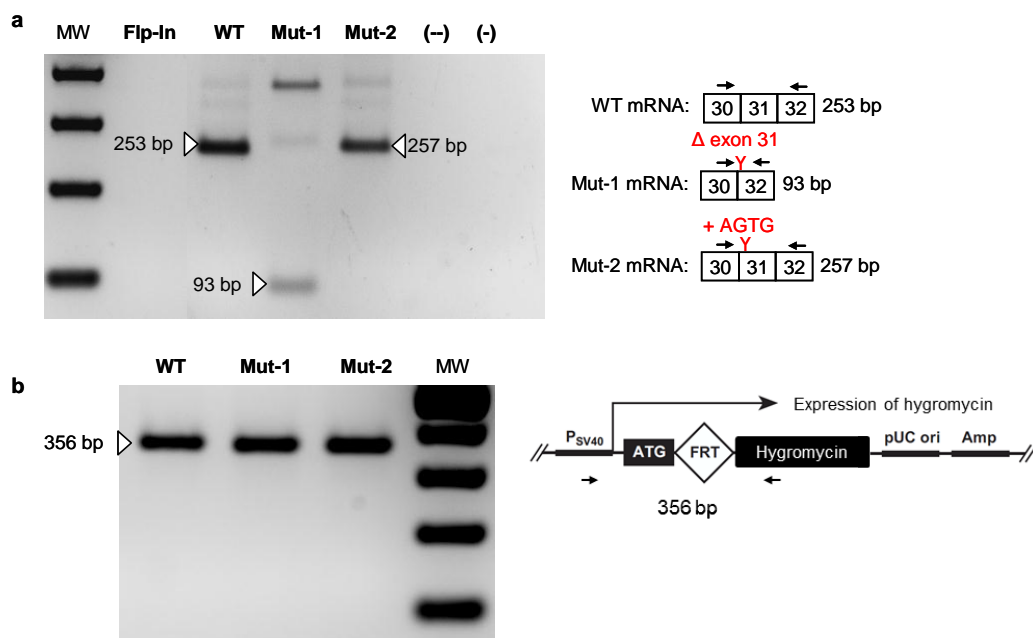


Figure 3.10. Expression of human minigenes in clonal Flp-In293 cell lines.

Total RNA was extracted from clonal Flp-In293 cells (WT, Mut-1 and Mut-2) and reverse transcribed into cDNA. The cDNAs were used as templates for PCR amplification with minigene-specific primers (a). As a negative control (-) one sample was ‘reverse transcribed’ without reverse transcriptase. As a further negative control (-) water was added instead of cDNA. To estimate the expression efficiency of the minigenes, primers binding in the SV40 promoter and hygromycin cassette were used in parallel (b). The molecular weight (MW) marker was the Gene Ruler™ 100 bp DNA Ladder. The location of the primers (black arrows) and the expected sizes of the amplicons (arrowheads) are indicated in the scheme on the right side. The illustration of the vector was adapted from the Flp-In manual (Invitrogen).

To subsequently determine the mRNA level resulting from the expression of the three minigenes a quantitative RT-PCR (RT-qPCR) was conducted using primers and a probe that are similarly present in the three mRNAs. Forward and reverse primers were complementary to exons 32 and 33, respectively, and the probe recognized the boundary

between both exons of *MYBPC3* (Figure 3.11). The expression of WT and Mut-1 minigenes did not differ, whereas the level of Mut-2 mRNA was 2.5-fold lower than WT, suggesting a regulation by the NMD system. Importantly, these data in HEK293 cells were consistent with those in myocardial tissue of HCM patients carrying the same mutations (Rottbauer et al., 1997 for Mut-1 and Figure 3.3 for Mut-2). This validates the feasibility of stable HEK293 cells as a cell-based screening system to analyse the expression of the mutations at the mRNA level.

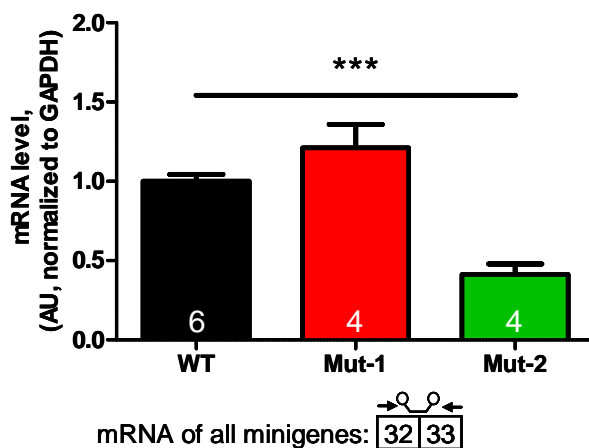


Figure 3.11. Determination of the minigene expression level.

Total RNA was extracted from Flp-In293 cell lines stably expressing WT, Mut-1, Mut-2 and analysed by RT-qPCR. The location of the primers (black arrows) and probe are indicated in the scheme below the plot. All samples were normalized to human GAPDH and values are shown relative to WT. Bars represent the mean \pm SEM. *** P <0.001 vs. WT, unpaired Student's t-test. The number of samples is indicated in the bars.

3.1.5.2 Evaluation of the contribution of NMD in the regulation of gene mutation expression

To investigate the involvement of NMD in the degradation of mutation-containing mRNAs, a GFP-based reporter system was used to monitor NMD in mammalian cells (Paillusson et al. 2005). The NMD reporter gene is based on a T-cell receptor- β (TCR- β) minigene construct in which the stop codon of the GFP-ORF is inserted such that it is recognized as a PTC (Figure 3.12). In general, NMD only occurs when the PTC is located at least 50-55 bp upstream of the last exon-exon junction (Maquat 1995). In mammals, NMD requires a pioneer round of translation and can be prevented by translation inhibitors such as emetine or cycloheximide. In the TCR- β -GFP PTC+ NMD reporter plasmid the general NMD rule is fulfilled, and therefore the resulting aberrant mRNA is susceptible for NMD-mediated degradation, resulting in low steady-state mRNA level and, in turn in a low level of GFP. By inhibiting NMD the NMD reporter mRNA level is expected to be stabilized, leading to an increase in the GFP signal, which can be evaluated by

fluorescence microscopy or RT-qPCR. A control plasmid (TCR- β -GFP Δ JCin) is used in parallel and is deleted of the intron present in the TCR- β -GFP PTC⁺ plasmid. The resulting mRNA is hence not expected to be degraded via NMD. It was expected that the GFP level of the control NMD reporter would not change after NMD inhibition.



Figure 3.12. NMD reporter genes.

Schematic depiction of the NMD reporter genes: The open reading frame of the enhanced GFP (green) was inserted in-frame into the middle exon of the human T-cell receptor β -minigene (yellow) more than 50 nt upstream of the last exon-exon junction. Thus, in the presence of the intron (JCin) the stop codon of GFP is recognized as a premature termination codon (PTC) and subjected for degradation by the NMD system. In the absence of the intron (Δ JCin) the PTC is located in the last exon and is not expected to be a substrate for NMD-mediated degradation (control NMD reporter). The NMD reporter gene expression is driven by the human β -actin promoter (hu β -act). Picture from Paillusson et al. (2005).

For proof of principle, clonal WT cells were transiently transfected with the NMD reporter or the control NMD reporter plasmid. Subsequently, cells were treated with various concentrations of emetine (1-10-30-100-300 μ g/ml) or cycloheximide (1-10-30-100 μ g/ml) for 4 h or 3 h, respectively. The GFP levels of the treated cells were analysed 24 h post-transfection under UV light and by RT-qPCR (Figure 3.13). Under UV light a very low number of GFP-positive cells transfected with either the control or the NMD reporter plasmid was observed (Figure 3.13b, e). At 72 h post-transfection no increase in the number of GFP-positive cells was detected in both conditions (data not shown). The GFP mRNA level of NMD reporter-transfected cells was 1.4-fold and 1.3-fold higher after treatment with 100 μ g/ml and 300 μ g/ml emetine, respectively (Figure 3.13f), suggesting that emetine stabilized the mRNA at high concentrations. The level of WT-Flp-In293 mRNA did not differ under any of the conditions (Figure 3.13c, f). In contrast, cells transfected with the control NMD reporter showed a negative effect after treatment with emetine (Figure 3.13c). Treatment with CHX did not result in accumulation of the GFP-NMD reporter (data not shown). Hence a subsequent analysis by RT-qPCR was not performed.

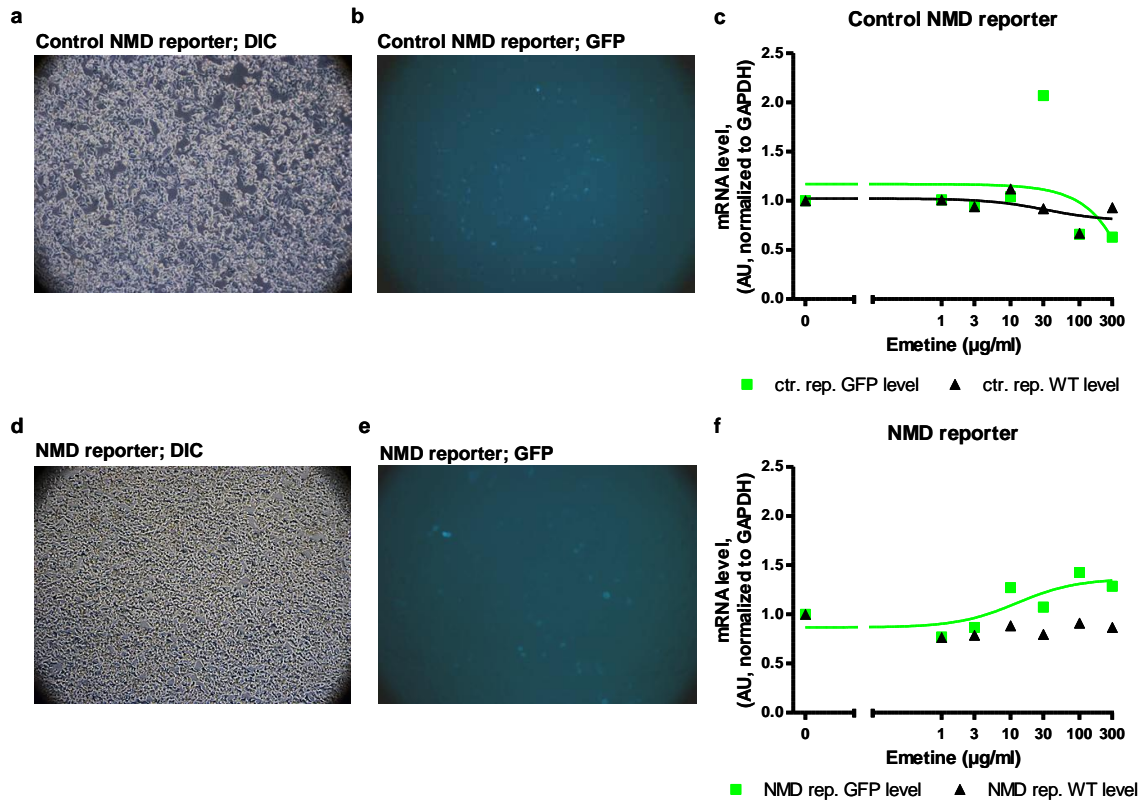


Figure 3.13. NMD-inhibition by emetine in clonal WT-Flp-In293 cells transfected with NMD reporter plasmids.

(a) - (e) Light microscope pictures (differential interference contrast microscopy, DIC and UV light) of clonal WT cells transfected with the control NMD reporter (24 h; upper part) or the NMD reporter plasmid (24 h; lower part). Total RNA was extracted and reverse transcribed from control NMD reporter ((c), ctr. rep.) or NMD reporter ((f), NMD rep.) transfected clonal WT cells, treated for 4 h with different concentrations of emetine. Analysis of the samples was conducted by RT-qPCR using specific probes for the minigene mRNA (WT) or for GFP. All data were normalised to GAPDH and plotted as logarithmic curves.

In summary, the data showed that the NMD reporter system principally works in HEK293 cells, but only exhibits a small regulatory range.

3.1.5.3 Evaluation of NMD inhibition in clonal Flp-In293 cells

Based on the previous result the three minigene-expressing Flp-In293 cell lines were similarly treated with emetine and analysed by RT-qPCR. The expectation was a stabilization, especially in the case of the Mut-2 mRNA, by the NMD inhibitor. A concentration-response curve was created whereby the drug response was plotted against the logarithm of drug concentration (Figure 3.14). In non-treated cells the mRNA levels of WT and Mut-1 did not differ, whereas the level of Mut-2 mRNA was 2.5-fold lower than WT. The WT cell line showed no sensitivity to the treatment with emetine at all tested

concentrations. However, for Mut-1 cells a negative effect of the drug on the cells was revealed, suggesting that emetine is toxic for these cells. In Mut-2 cells increasing concentrations of emetine did not significantly increase the mRNA levels, although a trend to a higher mRNA level was observed with 300 $\mu\text{g/ml}$. Similar results were obtained after treatment with different concentrations of cycloheximide and wortmannin (data not shown).

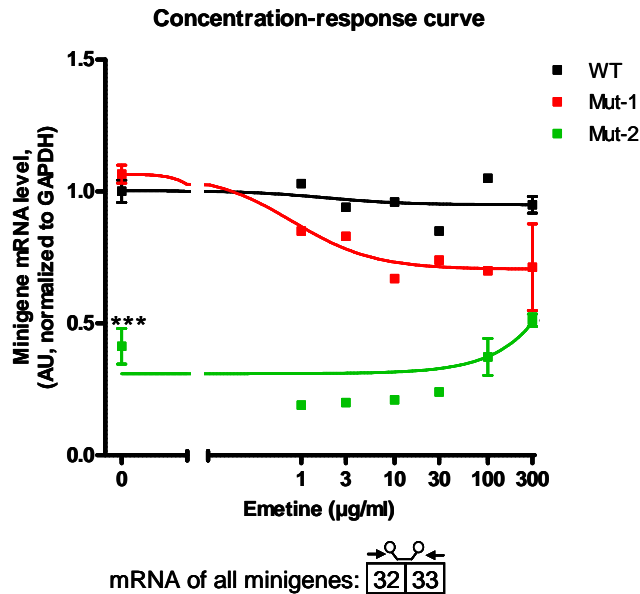


Figure 3.14. Effect of NMD inhibition in Flp-In293 cells.

Total RNA was extracted from Flp-In293 cell lines stably expressing WT, Mut-1 and Mut-2 after treatment with various concentrations of emetine for 4 h. The analysis was done by RT-qPCR. The location of the primers (black arrows) and probe are indicated in the scheme below the plot. All samples were normalized to GAPDH and values are shown relative to WT. Bars represent the mean \pm SEM. *** P <0.001 vs. WT emetine 0 $\mu\text{g/ml}$, unpaired Student's t-test. Numbers (n) of analysed samples: n=6 (WT control), n=4 (Mut-1 and Mut-2 control), n=5 (WT 300 $\mu\text{g/ml}$), n=2 (Mut-1 300 $\mu\text{g/ml}$, Mut-2 100, 300 $\mu\text{g/ml}$), n=1 (WT, Mut-1, Mut-2 1 $\mu\text{g/ml}$ to 100 $\mu\text{g/ml}$).

In summary, mRNA levels of WT and Mut-1 minigenes were comparable, whereas the level of Mut-2 mRNA was ~60% lower. Treating cells with protein translation inhibitors, which have been shown to block NMD, did not significantly stabilize Mut-2 mRNA levels. This suggests that NMD may not be the primary regulatory system controlling expression of the mutations in the Flp-In293 cells, at least at the investigated concentrations and times.

3.1.5.4 Evaluation of minigenes' expression at the protein level

The expression of the clonal WT minigene, expected to be translated into protein (31 kDa), was analysed by Western blot using an anti-c-myc antibody (Figure 3.15a). In parallel, proteins from Mut-1 cells (16 kDa), not expected to be detected, as well as a non-cardiac sample (-, negative control) and a positive control (+) for myc-tagged proteins (34 kDa) were analysed. Whereas myc-staining worked for the positive controls (+), myc-WT and myc-Mut-1 were not detected (Figure 3.15a). In contrast, a distinct band of about 80 kDa of unknown identity was detected in WT, Mut-1 and non-transfected samples.

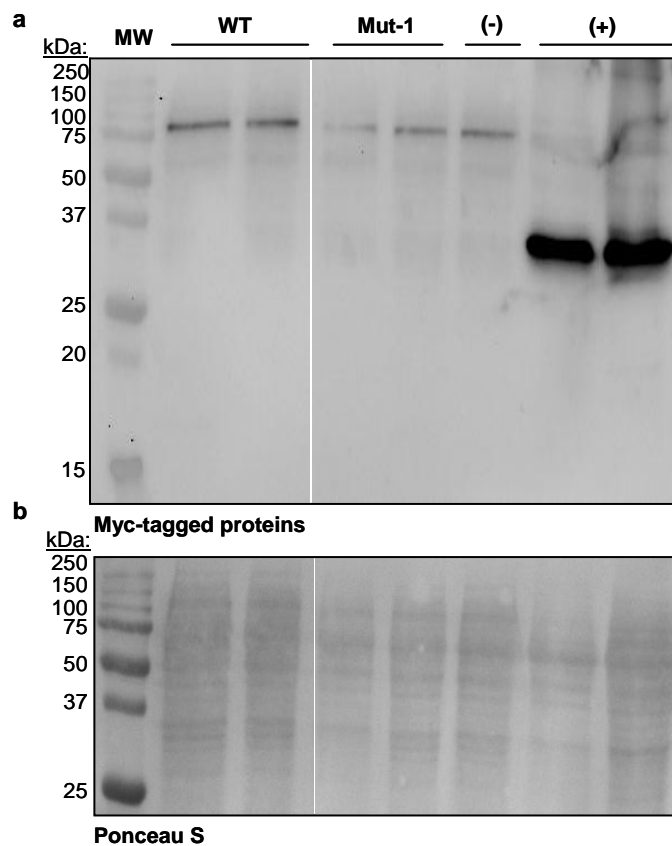


Figure 3.15. Evaluation of protein levels in Flp-In293 cells.

Proteins derived from clonal Flp-In293 cells (WT and Mut-1) were analysed by Western blot using a specific antibody directed against the myc-tag (a). As a negative control (-) a non-cardiac protein sample was used. As a positive control (+) for the myc signal, HEK293 cells transfected with a truncated cMyBP-C-encoding plasmid in the presence of the proteasome inhibitor MG132 (M7t, 34 kDa) was used. (b) The same membrane stained with Ponceau S.

Since the expected myc-WT protein was not detected by Western blot an immunoprecipitation (IP) was conducted on WT and Mut-1 cells using an anti-c-myc antibody. Analysis was performed by Western blot using the same antibody (Figure 3.16). Detection revealed 4 to 5 bands between 25 kDa and 37 kDa in either IP sample. In WT, a

specific 31-kDa extra band, not present in Mut-1 or Flp-In293 cells, was detected after IP (Figure 3.16a; indicated by the arrowhead). Similarly, a specific extra band of about 16 kDa was detected only in the Mut-1-pellet (Figure 3.16a; indicated by the arrowhead). These data suggest that i) at least a low level of myc-WT mini-protein is translated, and ii) a low level of myc-Mut-1 mini-proteins is also translated, but remains in the insoluble fraction.

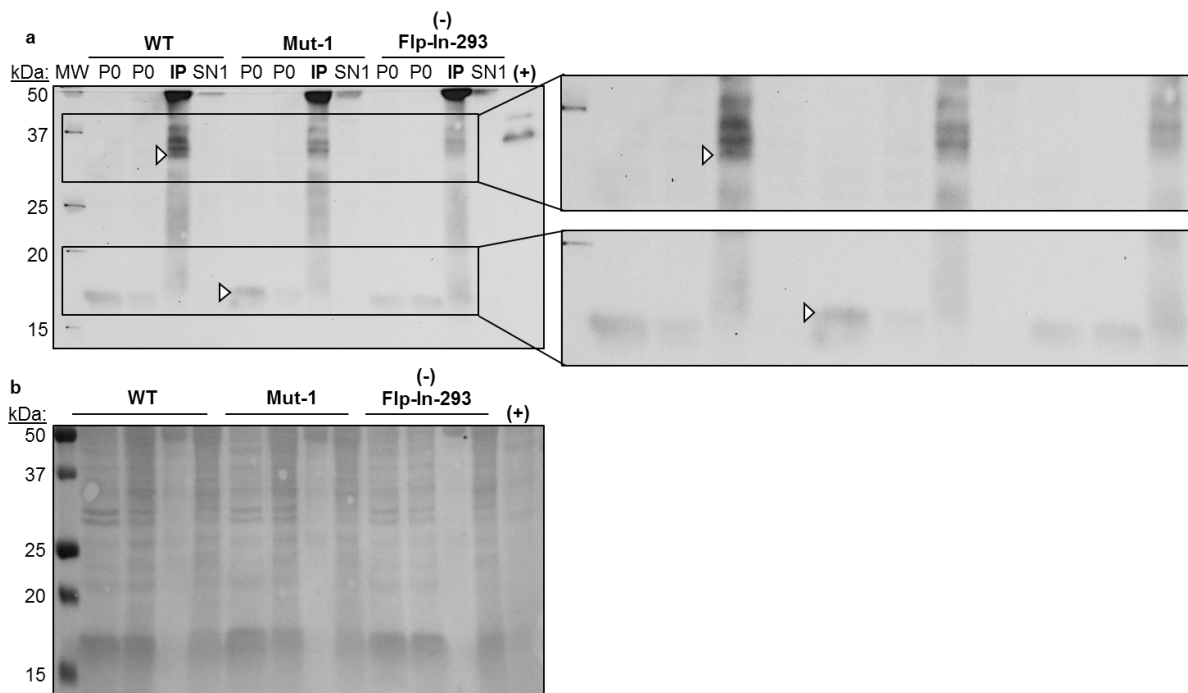


Figure 3.16. Validation of protein expression in Flp-In293 cells after immunoprecipitation.

(a, left-hand side) Western blot of clonal WT and Mut-1 cells after immunoprecipitation. Different fractions obtained during the process of immunoprecipitation were loaded: pellet after the first centrifugation (P0), supernatant after the first wash of the beads (SN1) and finally the immunoprecipitated proteins (IP). The membrane was stained with an antibody directed against the myc-tag and the upper part cut. As a negative control (-) Flp-In293 cells were immunoprecipitated. (a, right-hand side) Parts of the Western blot membrane (indicated by the rectangles) were zoomed in to show that in WT cells a band at the size of about 31 kDa, not present in Mut-1 or Flp-In293 cells, was detected in IP samples (upper part, indicated by the arrowhead). In the insoluble pellet fraction of Mut-1 cells a protein at the size of about 16 kDa was detected, which was not present in WT or Flp-In293 cells at this size (lower part; indicated by the arrowhead). As a positive control (+) for the myc signal, HEK293 cells transfected with a truncated cMyBP-C encoding plasmid (M7t, 34 kDa) were used. (b) The same membrane stained with Ponceau S.

To investigate whether the low level of the WT protein, even after IP, results from degradation by the UPS, concentration-response curves of the UPS inhibitor MG132 were performed. After treatment with various concentrations of MG132 for 24 h, cells were analysed by Western blot using specific antibodies directed against the myc-tag (Figure 3.17) or ubiquitinated proteins (Figure 3.18). Mut-1 proteins, which were expected to be degraded via the UPS were investigated in parallel, as well as Flp-In293 cells as a negative control. The analysis revealed two distinct bands of about 35 kDa in all samples (Figure

3.17a, b), but the expected myc-WT (31 kDa; Figure 3.17a) and myc-Mut-1 proteins (16 kDa, Figure 3.17b) were not detected.

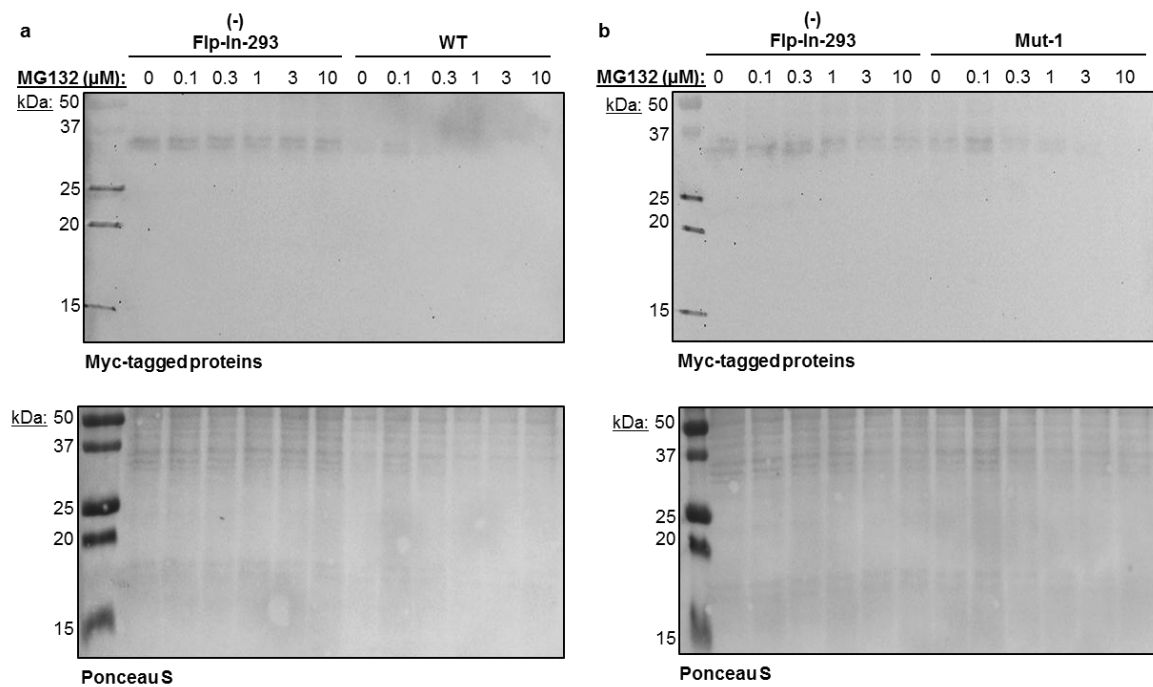


Figure 3.17. Evaluation of protein levels in Flp-In293 cells after proteasome inhibition.

Proteins derived from Flp-In293, clonal WT (a) and clonal Mut-1 (b) cells were treated with various concentrations of the UPS inhibitor MG132 for 24 h. The membranes were stained with an antibody directed against the myc-tag (upper part). Lower part: The same membranes stained with Ponceau S.

To investigate whether inhibition of the proteasome by MG132 indeed worked, the steady-state levels of ubiquitinated proteins were determined. The assumption was that the levels of ubiquitinated proteins increase with increasing concentrations of MG132. Therefore the same Western blot membranes were stained with an antibody directed against both mono- and poly-ubiquitinated proteins. Western blots were subsequently quantified and data normalized to ponceau (Figure 3.18). For quantification the whole lane was included. Whereas raising MG132 concentrations increased the steady-state levels of ubiquitinated proteins in Flp-In293 cells, it had no effect in WT and Mut-1 cells. This suggests that i) the experiment did not work for WT and Mut-1 cells or ii) WT and Mut-1 cells are much less sensitive to proteasome inhibition than Flp-In293 cells.

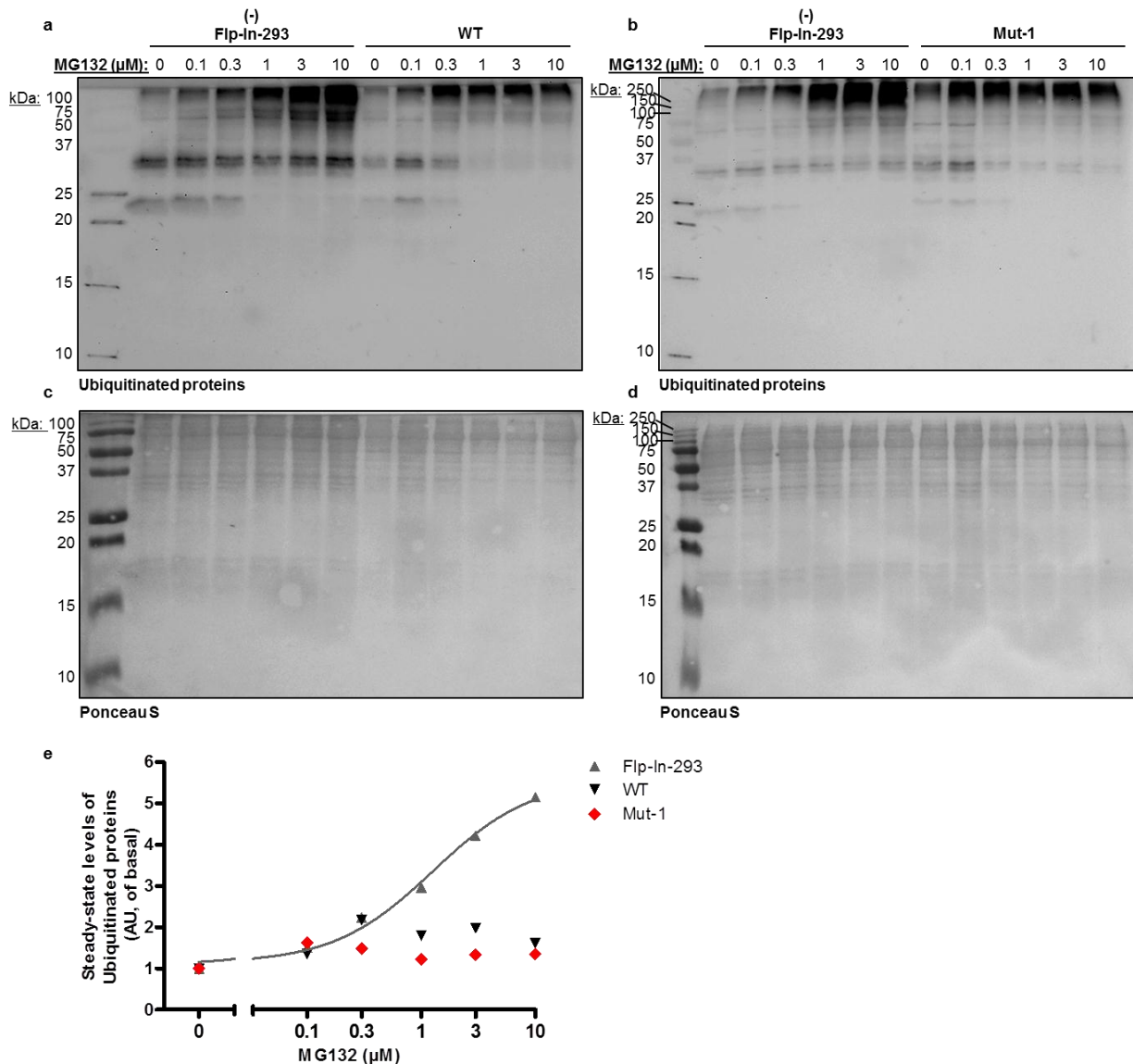


Figure 3.18. Determination of the steady-state levels of ubiquitinated proteins.

Proteins derived from Flp-In293 and clonal Flp-In293 cells (WT and Mut-1) were treated with various concentrations of the UPS inhibitor MG132 for 24 h (a, b). Membranes were stained with an antibody directed against mono- and poly-ubiquitinated proteins. (c, d) The same membranes stained with Ponceau S. (e) Densitometric quantification of ubiquitinated proteins. Data were normalized to Ponceau S.

In order to investigate whether higher concentrations of MG132 may increase/stabilize ubiquitinated- and myc-tagged proteins, different concentrations were tested in WT, Mut-1 and Mut-2 cells. The analysis was conducted by Western blot using antibodies directed against ubiquitinated or myc-tagged proteins (Figure 3.19). High concentrations of MG132 resulted in marked accumulation of ubiquitinated proteins in all groups (Figure 3.19a). This validated proteasome inhibition. However, whereas the myc-positive control was detected by Western blot, myc-WT, myc-Mut-1 and myc-Mut-2 proteins were not (Figure 3.19b). This suggests that the proteins are either i) not translated or ii) degraded via another system, such as autophagy.

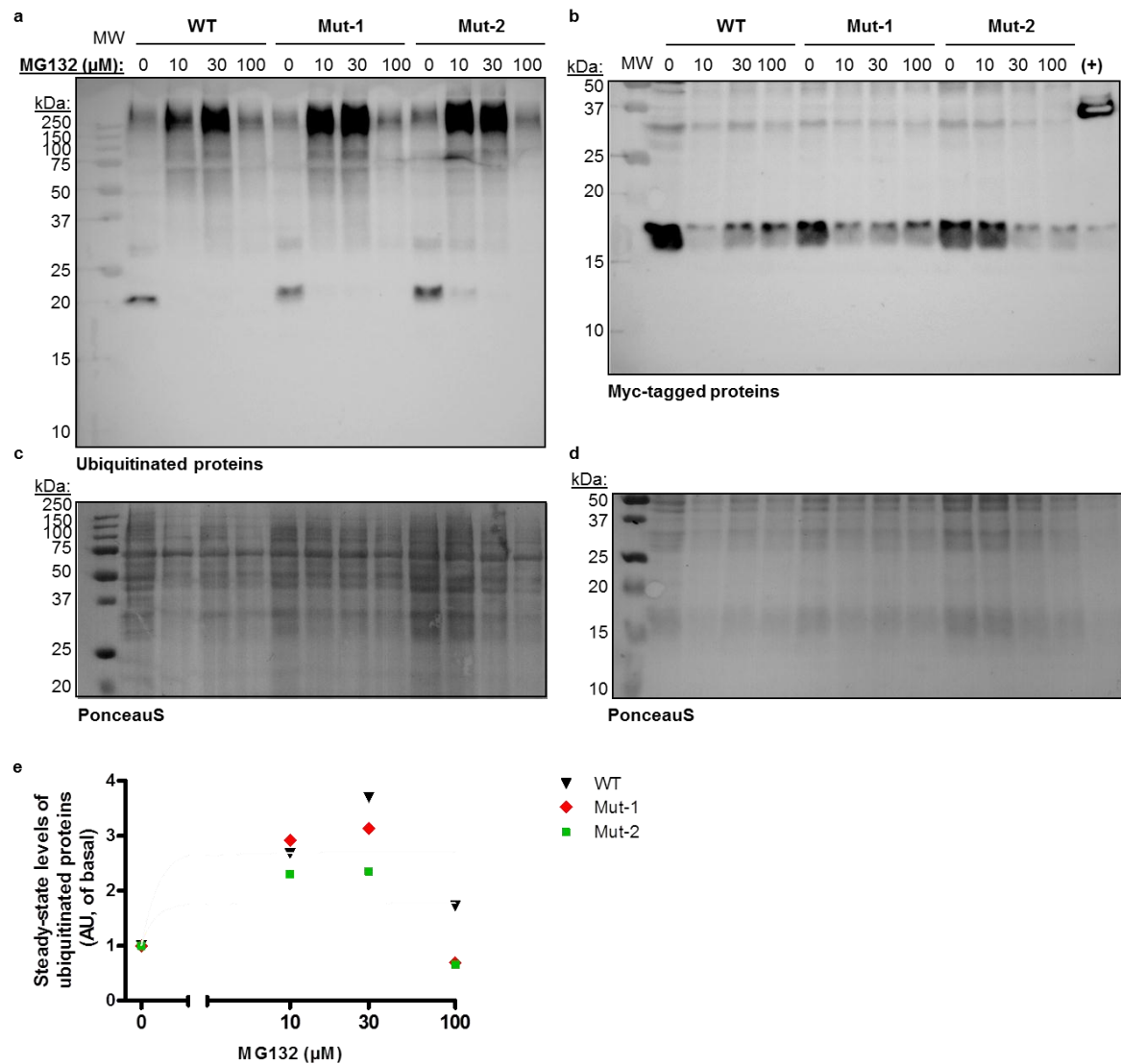


Figure 3.19. Validation of protein expression in Flp-In293 cells after proteasome inhibition.

Proteins derived from clonal Flp-In cells (WT, Mut-1 and Mut-2) were treated with different concentrations of the proteasome inhibitor MG132 for 24 h. Membranes were stained with antibodies directed against mono- and poly-ubiquitinated (a) or against myc-tagged proteins (b). As a positive control (+) for the myc signal, HEK293 cells transfected with a truncated cMyBP-C encoding plasmid in the presence of MG132 (M7t, 34 kDa) was used. (d, e) The same membranes stained with Ponceau S. (e) Densitometric quantification of ubiquitinated proteins. Data were normalized to ponceau and are presented relative to non-treated cells.

3.1.6 Summary of the chapter

The major findings of this chapter were:

- Transient transfection of HEK293 cells with human *MYBPC3* minigenes resulted in mRNAs, but not in proteins. Marked contamination of transgenes in RNA preparations impeded further analysis.
- Establishment of stable cell lines expressing human myc-tagged minigenes resolved the problem of contamination and showed that mRNA levels of WT and Mut-1 were similar, whereas the level of Mut-2 mRNA was 2.5-fold lower than WT. This suggests i) a lower transcription rate or ii) a lower mRNA stability.
- Transfection of clonal WT cells with a control- or NMD reporter plasmid encoding GFP resulted in a very low number of GFP-positive cells. Inhibition of the NMD pathway with the protein translation inhibitor emetine revealed, as expected, a stabilization of GFP-positive mRNA in NMD reporter-treated cells. However, the effect was very small. Emetine did not significantly stabilize Mut-1 and Mut-2 mRNA levels, which was expected in the case of Mut-1, but surprising in the case of Mut-2. This suggests that NMD is not the main system involved in the regulation of the expression of the mutations. Western blot analysis of stably transfected cells failed to detect the expected protein(s). However, immunoprecipitation of WT and Mut-1 proteins revealed the appearance of a protein band at the expected size for WT cells only, whereas the expected protein for Mut-1 was likely detected in the insoluble fraction. Inhibition of the proteasome did not result in stabilization of the expected proteins (WT, Mut-1), but stabilized the ubiquitinated proteins in both Flp-In293 cells and clonal Flp-In cells (WT, Mut-1 and Mut-2) at high concentrations.
- In conclusion, modified HEK293 cells stably expressing human *MYBPC3* minigenes allowed to study the expression of *MYBPC3* mutations and reproduced data obtained in humans at the level of mRNA. However, this system appears not to be suitable to investigate the relative contribution of NMD or the UPS.

3.2 Evaluation of an RNA-based approach to remove the mutated exon in cardiac myocytes from *Mybpc3* knock-in mice

The goal of the second part of my thesis was to evaluate the feasibility and efficacy of antisense oligoribonucleotides to remove the mutated exon in cardiac myocytes from KI mice. The used RNA-based approach modifies the pre-mRNA splicing and results in the skipping of the targeted exon(s).

The KI mouse model was developed as described in detail in Vignier et al., 2009. It carries a G>A transition at the last nucleotide of exon 6, which is located in the consensus sequence for donor splice sites. The introduced mutation is associated with a severe phenotype and poor prognosis in humans in the heterozygous state (Niimura et al., 1998; Nanni et al., 2003; Richard et al., 2003; Marston et al., 2009). The homozygous mice exhibited left ventricular hypertrophy (Figure 3.20a), increased heart weight/body weight ratio (HW/BW; Figure 3.20b), a lower fractional shortening and diastolic dysfunction (Birgit Geertz and Florian Weinberger; data not shown). In the present study we focussed on homozygous KI mice.

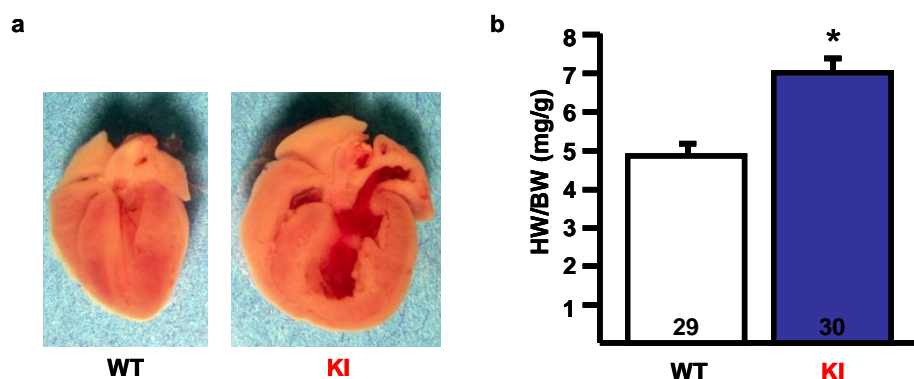
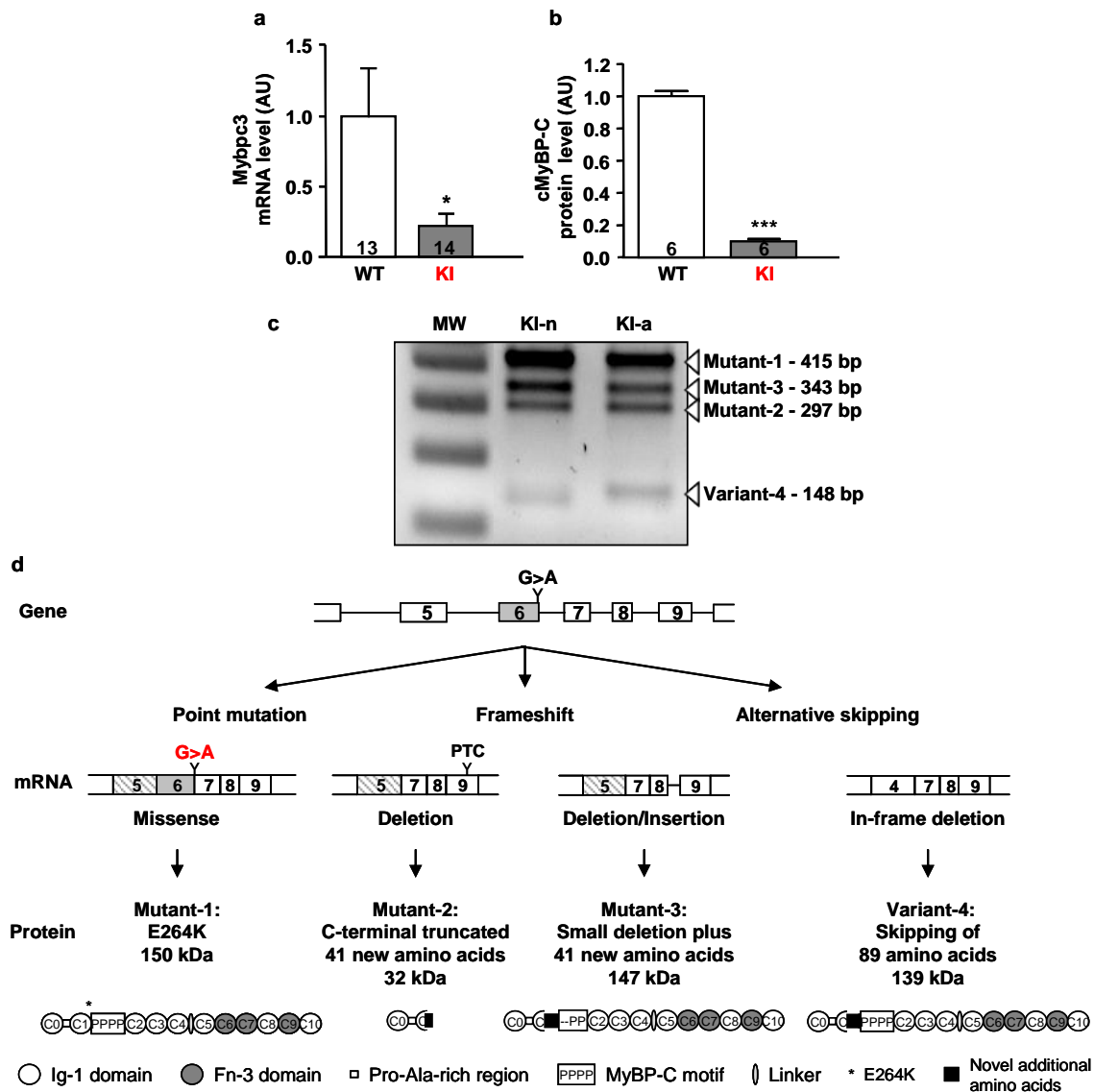


Figure 3.20. Cardiac phenotype of cMyBP-C knock-in mice.

(a) Longitudinal myocardial sections of 3-month-old mice reveal a left ventricular hypertrophy in KI mice vs. WT littermates. (b) The heart weight to body weight ratio (HW/BW) is significantly increased in KI vs. WT mice (figure modified according to Vignier, 2009).

The molecular phenotype of KI mice is characterized by 80% lower total *Mybpc3* mRNA levels and 90% lower mutant cMyBP-C protein levels (Figure 3.21a, b; Vignier et al., 2009). Furthermore the mutation results in three different mutant mRNAs and one splicing variant: a missense mRNA (mutant-1) resulting in a E264K protein (150 kDa), an mRNA lacking exon 6 (mutant-2), which leads to a premature termination codon (PTC) in exon 9 and should produce a truncated protein (32 kDa) including 41 novel amino acids, and an mRNA lacking exon 6 with a partial retention of intron 8, which restores the open

reading frame (mutant-3) and results in a 147-kDa-protein including 41 novel amino acids. The spliced isoform (variant-4) is an in-frame deletion of exons 5 and 6, whereby the open reading frame (ORF) and functionally important domains are maintained. The expected size of the variant-4 protein is 139 kDa. Variant-4 was detected recently using primers located in exons 4 and 9 of the *Mybpc3* (Figure 3.21c).



3.2.1 Validation of an alternative spliced isoform in WT mice

To investigate whether variant-4 is a naturally occurring alternative spliced isoform, mRNA from non-transfected WT-NMCMs was used for two rounds of PCR amplification with primers complementary to exons 4 and 7 (Figure 3.22).

In the first round of PCR only the expected fragment for WT-*Mybpc3* mRNA (406 bp) was obtained. Interestingly, the second round of PCR revealed not only the WT-fragment, but also an additional ~139 bp fragment which shows the same gel migration pattern as the variant-4 fragment detected in KI-NMCMs. This suggests that variant-4 is an alternative spliced isoform in WT mice. Sequencing analysis of variant-4 revealed the fusion of exon 4 with exon 7.

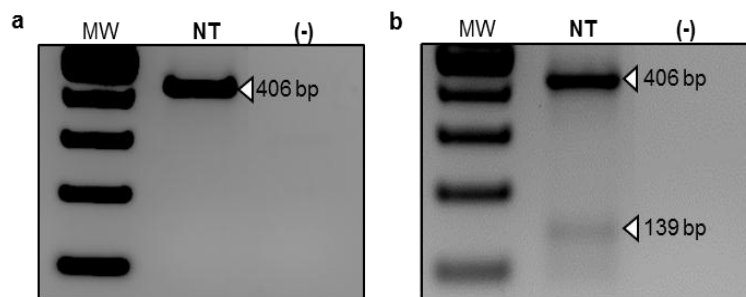


Figure 3.22. Validation of an alternative spliced isoform.

Representative PCR result using a cDNA derived from non-transfected (NT) WT-NMCMs. (a) First round of PCR amplification using primers located in exons 4 and 7 of *Mybpc3*. (b) The PCR product of the first PCR was used as template for a second round of PCR. As a negative control (-) water was added instead of cDNA. The molecular weight (MW) marker was the Gene Ruler™ 100 bp DNA Ladder. The expected fragment sizes are indicated by arrowheads.

3.2.2 Stability and localisation of spliced variant-4

To investigate the stability of the four proteins (mutant-1, mutant-2, mutant-3, variant-4) HEK293 cells were transiently transfected (48 h) with plasmids encoding each protein. The cells were additionally treated with or without the proteasome inhibitor MG132 (Figure 3.23). While the proteins of mutant-1 (150 kDa), mutant-3 (147 kDa) and variant-4 (139 kDa) were detected in both the presence and absence of the proteasome inhibitor MG132 at roughly similar levels, mutant-2 was exclusively detected in the presence of MG132, indicating that this protein is very unstable. Inhibition with MG132 also resulted in the stabilization (~ +50%) of mutant-3 and variant -4 proteins, suggesting regulation of these variants via the UPS.

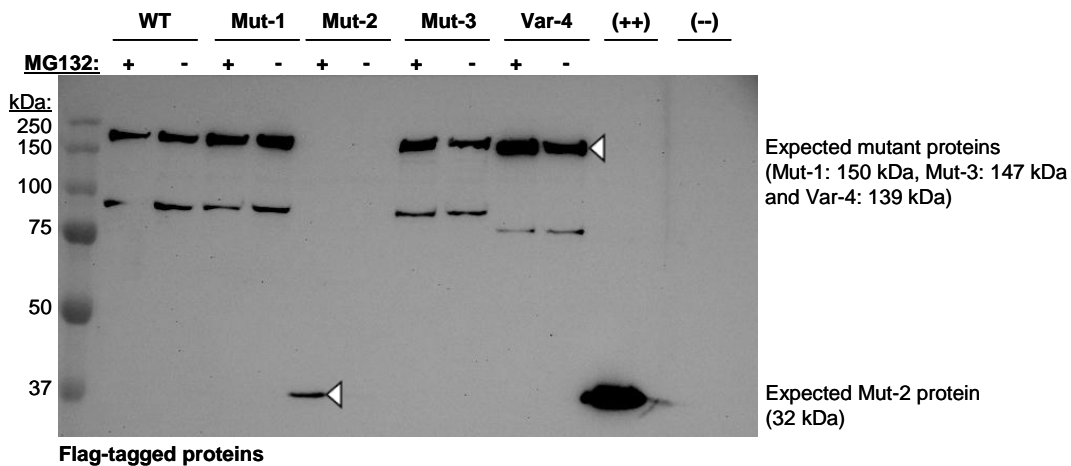


Figure 3.23. Evaluation of the stability of aberrant cMyBP-C proteins in HEK cells.

HEK293 cells were transiently transfected for 48 h with plasmids encoding the flag-tagged WT and mutant proteins (mut-1 to mut-3, var-4). The cells were additionally treated with (+) or without (-) the proteasome inhibitor MG132 (50 μ M, 2 h). The membrane was stained with an antibody directed against the flag-tag. The expected protein molecular weights are indicated by the arrowheads. As a positive control (++) for the flag signal HEK293 cells transfected with a plasmid encoding a flag-truncated cMyBP-C was used (30 kDa). As a negative control (-) untransfected HEK293 cells were loaded. The polyacrylamide gel concentration was 10%. The entire experiment was done by Doreen Khajetoorians.

To investigate whether the stable protein spliced variant-4 is incorporated into the sarcomere of KI-NMCMs, the cells were infected with an adeno-associated virus (AAV) encoding the flag-tagged variant-4 and analysed by confocal microscopy using specific antibodies directed against cMyBP-C, the flag-tag and titin (Z-band; Figure 3.24). The flag-variant-4 cMyBP-C protein exhibited i) a striation pattern ii) a co-localization with cMyBP-C (Figure 3.24a) and iii) an alternation pattern with the titin-Z-band (Figure 3.24b). This suggests that variant-4 is incorporated in the C-zones of the A-band of the sarcomere.

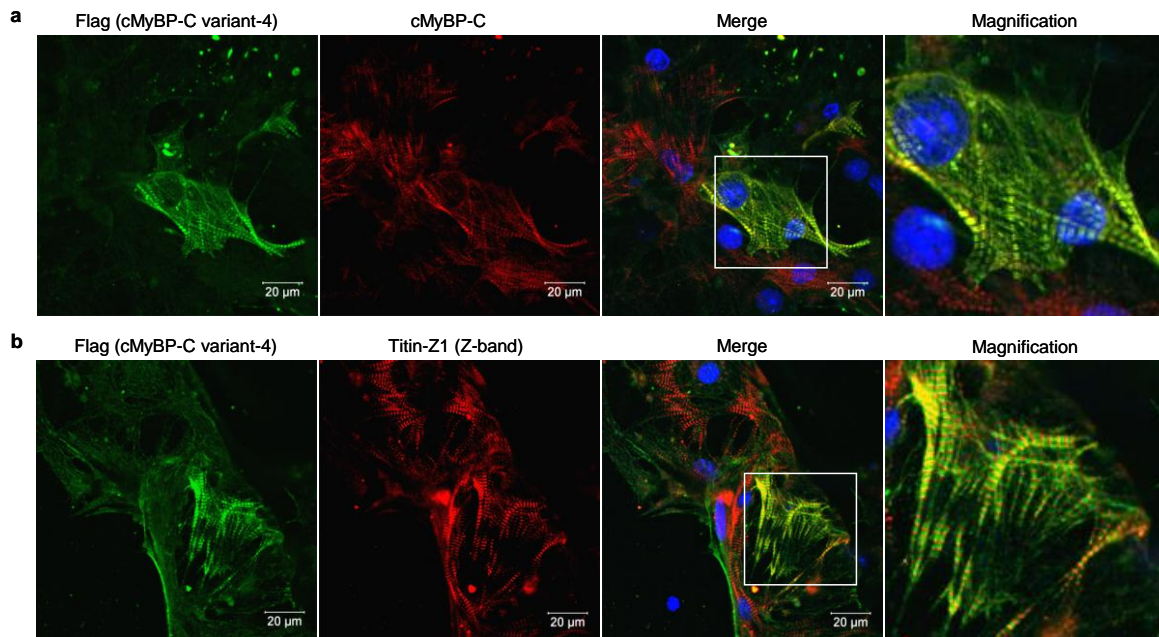


Figure 3.24. Intracellular localisation of the variant-4 protein in KI-NMCMs.

KI-NMCMs were infected with an AAV encoding the flag-tagged variant-4 (48 h) at a MOI of 5000. Cells were double-stained with antibodies directed against (a) the flag-tag and cMyBP-C or (b) the flag-tag and titin (Z1-domain). Nuclei were stained with TO-PRO-3 (in blue in the merge). A representative region was zoomed in (white rectangle) to show the staining at a higher magnification. This experiment was performed by Doreen Khajetoorians and Verena Behrens.

3.2.3 The exon-skipping strategy and choice of the target

To rescue the molecular and cardiac phenotype of the homozygous KI mice, three different RNA-based strategies are currently tested in our group for their efficiency to remove the mutation (exon skipping, exon inclusion and spliceosome-mediated RNA trans-splicing). This work focused on the exon-skipping strategy with the goal to increase the expression of variant-4 mRNA, deleted of exons 5 and 6. The expected resultant variant-4 protein contains all important interacting domains and intact phosphorylation sites, located in the MyBP-C motif (Figure 3.27). Therefore the protein is expected to be functional. In contrast to variant-4, stabilization of mutant-2 or mutant-3 would affect the cMyBP-C phosphorylation since mutant-2 loses four and mutant-3 two of the four phosphorylation sites due to the skipping of exon 6 (Figure 3.25). cMyBP-C phosphorylation was found to be essential for normal cardiac function *in vivo* and cardioprotective (Barefield et al., 2010; Sadayappan et al., 2006).

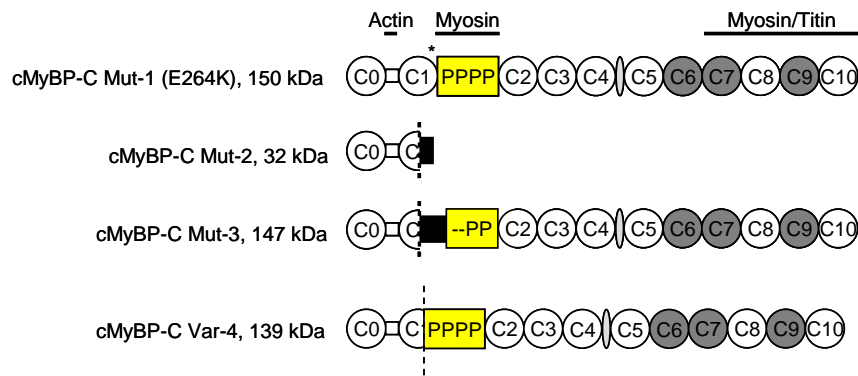


Figure 3.25. Protein structures resulting from the G>A transition in *Mybpc3*-KI mice.

In this illustration the three detected mutants as well as the spliced variant-4 resulting from the cMyBP-C E264K mutation are illustrated on the structure of protein. Mutant-1 protein (missense) contains the G>A transition and intact phosphorylation sites (yellow), mutant-2 (nonsense) and mutant-3 (deletion/insertion) are deleted of exon 6, which results either in a frameshift and a truncated protein with loss of the MyBP-C motif (mutant-2) or in a partial retention of intron 8, which restores the ORF and produces a 147-kDa-protein (mutant-3). In the latter two phosphorylation sites are also destroyed. Variant-4 contains an in-frame deletion of exons 5 and 6 and is therefore expected to produce a shortened protein containing all important domains.

3.2.4 Design of antisense oligoribonucleotides

In order to enhance the expression of variant-4, antisense oligoribonucleotides were designed to target exonic splicing enhancer (ESE) motifs in exons 5 and 6 of *Mybpc3* (AON-5 and AON-6, respectively). These motifs are normally recognized by serine/arginine-rich (SR) proteins, which induce the inclusion of an exon during the splicing process. Targeting the ESEs results therefore in exon exclusion. The ESEs were identified by the ESE prediction program “ESE finder 3.0” (Figure 3.26; Cartegni et al., 2003; Smith et al., 2006).

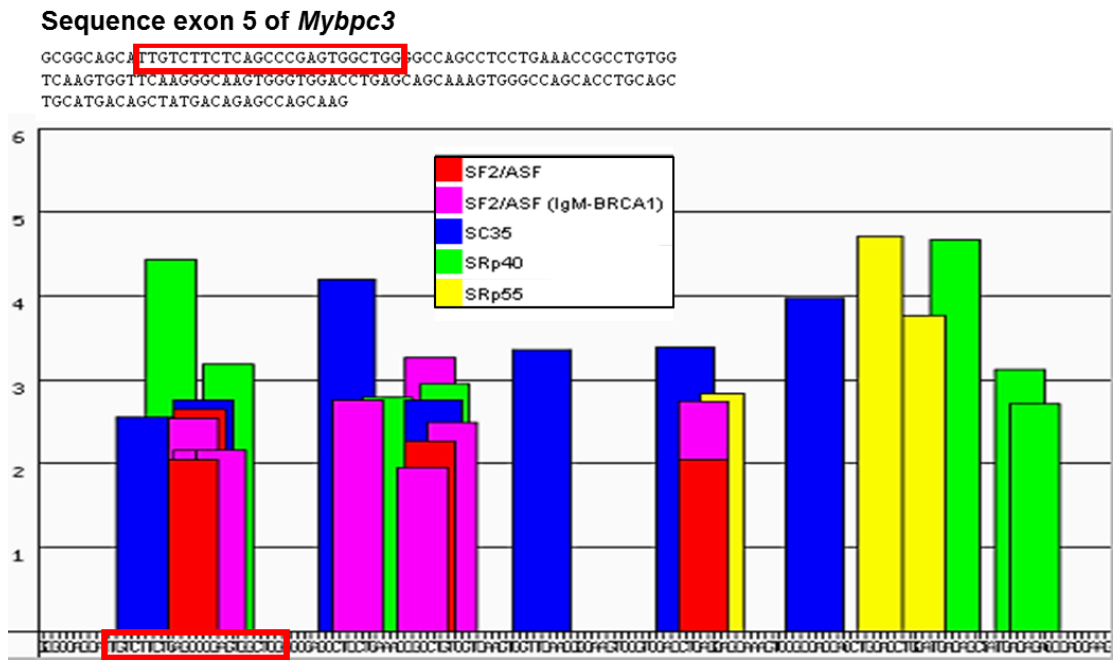


Figure 3.26. Predicted ESE sequences of *Mybpc3*-exon 5.

The ESE finder program predicts exonic splicing enhancer (ESE) sequences, which are assumed to be recognized by specific serine/arginine-rich (SR) proteins (given in the legend). In the present figure the graphical result of the *Mybpc3*-exon 5-sequence is shown. The height of the bars represents the scores of the motifs and thus the binding possibility of the different SR proteins, which are represented in different colors in turn. The width of the bars represents the length of the motifs (6 to 8 nucleotides). The red rectangle indicates the sequence (25 nucleotides) selected for AON-5.

In addition to AON-5 and AON-6, two further AONs were designed: a 5'-Cy3-tagged AON-5 (Cy3-AON-5) and a scrambled-AON-5, which contains the same nucleotide composition as AON-5, but is not complementary to the *Mybpc3* pre-mRNA (Figure 3.27). The synthesized AONs were full-length modified with 2'-*O*-methyl substituted ribose and phosphorothioate backbones (2OMePS) to minimize their degradation and subsequently transfected in neonatal mouse cardiac myocytes (NMCM) derived from WT and KI mice.

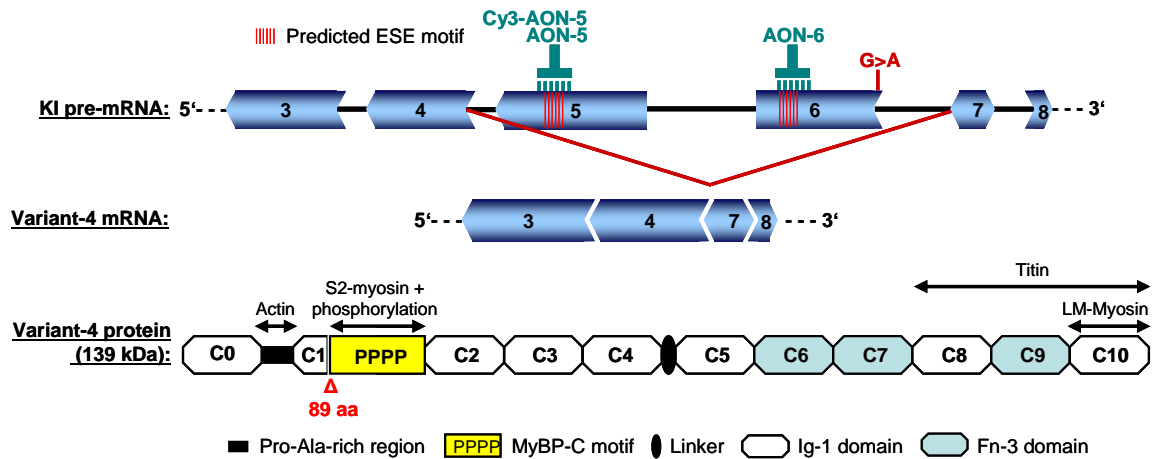


Figure 3.27. Exon-skipping strategy.

Illustration of the exon-skipping strategy with the goal to exclude exons 5 and 6 from the mRNA. The exclusion of both exons can be achieved using antisense oligoribonucleotides (AONs), which interfere with the naturally pre-mRNA splicing process (upper drawing). The AONs are complementary to exonic splicing enhancer (ESE) motifs in exon 5 and/or exon 6, resulting in the skipping of the targeted exons (middle drawing). The resultant protein is shortened in the C1 domain, with a loss of 89 amino acids, but contains all important interacting domains and the four intact phosphorylation sites, located in the MyBPC-motif (lower drawing).

3.2.5 Intracellular localisation of antisense oligoribonucleotides

Antisense oligoribonucleotides (AONs) interfere with the natural pre-mRNA splicing process, which is exclusively active in the nucleus of eukaryotes and results in the skipping or inclusion of exons in the mRNA (for review, see Le Roy et al., 2009). Hence the transport of AONs into the nucleus is of high importance for their functionality. To estimate the cell delivery and localisation of the AONs, WT- and KI-NMCMs were transfected with 5 μ g of a Cy3-tagged AON-5 (Cy3-AON-5) for different time points (here 8 days and 2 weeks). Analysis was performed by confocal microscopy after fixation of the cells and staining the nuclei with TO-PRO-3 (Figure 3.28). About 80% Cy-3 positive cells were observed in WT- and KI-NMCMs. The Cy3-AON-5 positive dots were localized in both the cytosol and the nucleus (merge, Figure 3.28), suggesting that AONs enter the cells and may target the pre-mRNAs.

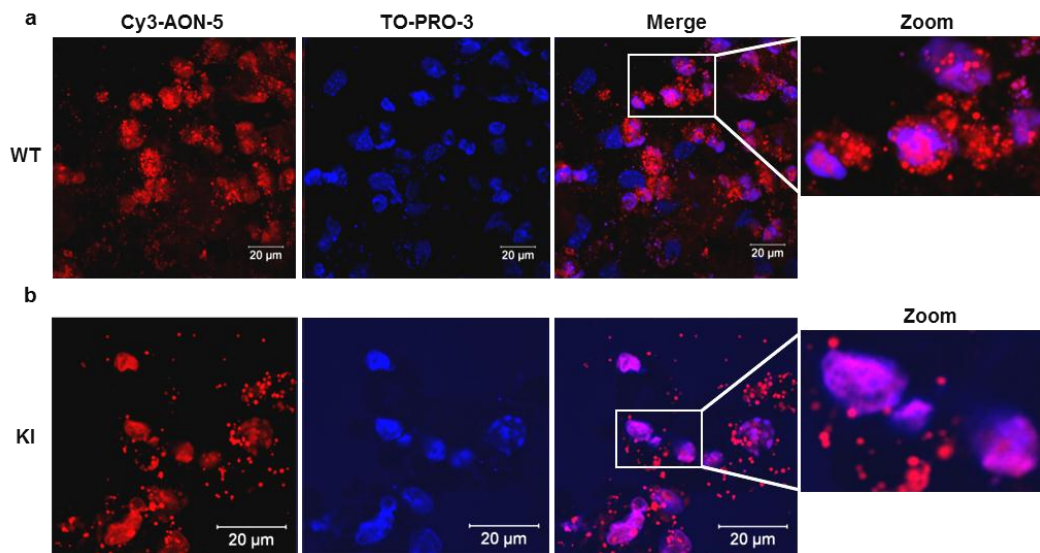


Figure 3.28. Fluorescence analysis of AON-5-treated NMCs by confocal microscopy.

(a) WT- and (b) KI-NMCs were treated with 5 µg Cy3-AON-5 for 8 days or 2 weeks, respectively. After fixation, nuclei were stained with TO-PRO-3. A representative region was zoomed in (white rectangle) to show cells with a higher magnification.

3.2.6 Evaluation of the skipping efficiency in AON-treated NMCs

For proof of principle the targeting specificity of the designed AONs was investigated. Total RNA from WT-NMCs transfected for 24 h with 5 µg of AON-5, AON-6 or AON-5 plus AON-6 was subjected to RT-PCR analysis using primers located in exon 4 and exon 9 of *Mybpc3* (Figure 3.29). AON-treatment of WT-NMCs resulted in the appearance of additional bands that indicate skipping of the corresponding exons (exon 5, 266 bp; exon 6, 297 bp; exon 5+6, 148 bp) as indicated by the colored arrows. This was accompanied by reduced amounts of the amplicon for endogenous WT mRNA (415 bp).

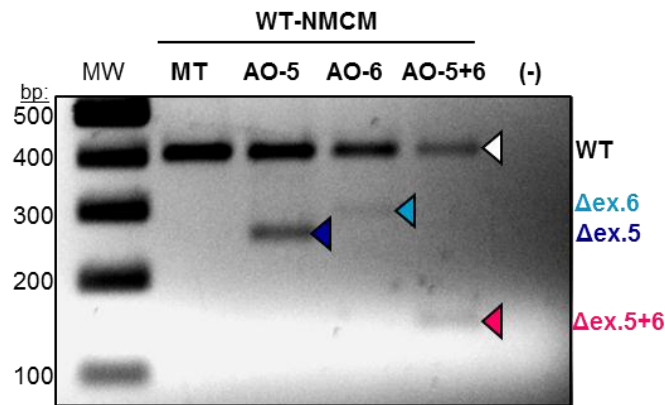


Figure 3.29. Targeting specificity of AONs in WT-NMCMs.

Total RNA was extracted from WT-NMCMs mock-transfected (MT) or treated with AON-5 (AO-5), AON-6 (AO-6) or AON5+6 (AO-5+6) for 24 h, and reverse transcribed into cDNA. The cDNAs were used as templates for PCR amplification with primers located in exons 4 and 9 of *Mybpc3*. As a negative control (-) water was added instead of cDNA. The molecular weight (MW) marker was the Gene Ruler™ 100 bp DNA Ladder. The expected amplicons are indicated by the colored arrowheads.

It was next evaluated which amount of AON is needed to achieve a high skipping efficiency of exons 5 and 6. Since AON-5 and AON-6 contain the same number of RNA bases and have similar molarities, only one AON was tested. Different quantities of AON-5 were applied in a 24 h pre-test in KI-NMCMs (Figure 3.30).

Mock-transfected NMCM showed four bands corresponding to the four mRNAs (mutant-1, mutant-2, mutant-3, variant-4). Interestingly, in KI-NMCMs, in contrast to WT, treatment with AON-5 only was sufficient to skip both exons 5 and 6 efficiently, suggesting that the mutation weakened the inclusion of exon 6. Besides the skipping of both exons additionally the single skipping of exon 5 was detected (indicated as Δ ex. 5). The most efficient skipping was obtained with 5 or 10 μ g AON. The skipping efficiency was estimated to be 40% of total KI mRNA variants. Thus, for all subsequent experiments 5 μ g per AON were used.

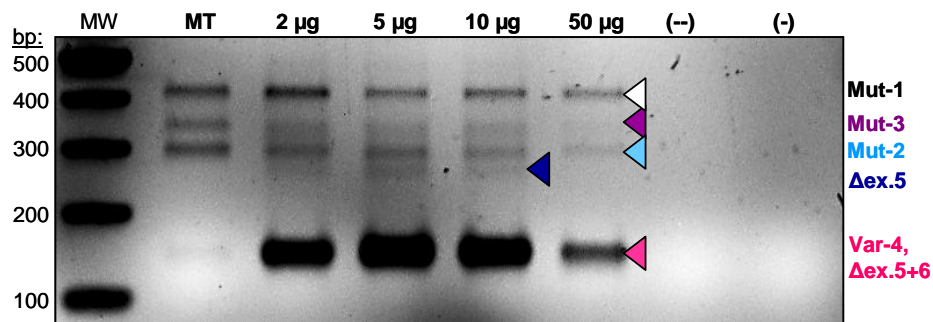


Figure 3.30. Identification of the required AON amount to induce exon skipping in KI-NMCMs.

Total RNA was extracted from KI-NMCMs mock-transfected (MT) or transfected with different quantities of AON-5 (2-5-10-50 μg) and reverse transcribed into cDNA. As a negative control one sample was reverse transcribed without reverse transcriptase (--). The cDNAs were used as template for PCR amplification with primers located in exons 4 and 9 of *Mybpc3*. As a negative control (-) water was added instead of cDNA. The molecular weight (MW) marker was the Gene Ruler™ 100 bp DNA Ladder. The expected amplicons for mutant-1, -2 and -3 (Mut-1 to Mut-3) as well as variant-4 (Var-4) are indicated by the colored arrowheads.

3.2.7 Half-lives of WT- and KI-cMyBP-C proteins

To estimate the time required for onset of the effect of AONs after transfection, the half-lives of WT- and KI-cMyBP-C proteins were determined. Therefore, cultured WT- and KI-NMCMs were treated with cycloheximide (30 $\mu\text{g}/\text{ml}$) for different time points (24 h, 48 h, 72 h, 96 h) and analysed by immunoblotting and densitometric quantifications (Figure 3.31). For KI proteins the sum of both protein bands (150 kDa and 139 kDa) was calculated and expressed as percent of control. The obtained values were plotted against the time and the protein half-lives determined (indicated as 50%). The calculated half-life (50% of control sample) was approximately 53 h (2.2 d) for the WT-cMyBP-C protein and about 30 h (1.25 d) for the KI proteins, suggesting the AON effect begins at these time points, respectively.

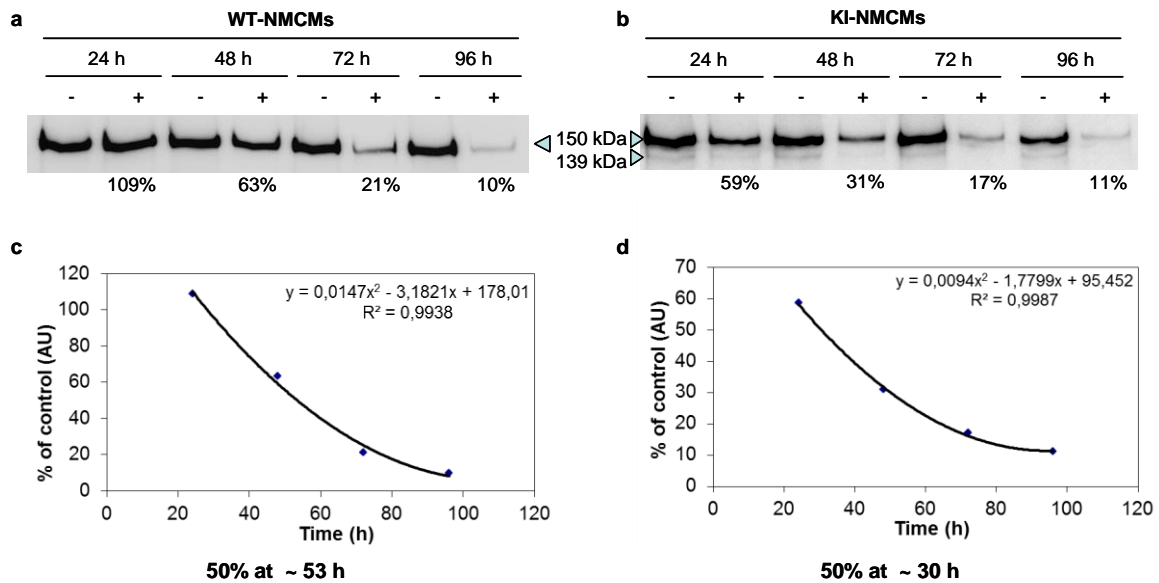


Figure 3.31. Determination of the protein half-life of WT- and KI-cMyBP-C proteins.

(a) WT- and (b) KI-NMCMs were treated with (+) or without (-) the translation inhibitor cycloheximide (30 μ g/ml) for different time points and analysed by Western blot using an anti-cMyBP-C antibody. The detected protein bands were quantified and expressed as percent of control (-). For KI proteins the sum of both bands (150 kDa and 139 kDa) was calculated and expressed as percent of control. The obtained values were plotted against the time and the protein half-lives determined (indicated as 50%).

3.2.8 Determination of the mRNA levels in AON-treated NMCMs

Based on the calculated half-lives and on the fact that the variant-4 protein was present at the earliest 6-days post-transfection (data not shown), subsequent analyses were performed at least 8 days after AON-transfection of WT- and KI-NMCMs (Figure 3.32b). It was assumed that AON-treatment results in a higher level of variant-4 mRNA, associated with reduced levels of WT or mutant mRNAs. As a control a scrambled AON (Scram) was investigated in parallel for evaluating potential adverse effects of AONs/AON-chemistries on NMCMs. This AON contains a random distribution of nucleotides of AON-5 and should not affect *Mybpc3* pre-mRNA. The cells were transfected in the presence of 5 μ g scram-AON or in its absence (mock-transfected, MT) for 8 days (Figure 3.32a). RT-PCR was performed using primers located in exons 4 and 9 of *Mybpc3*. The pattern of amplified *Mybpc3* mRNA did not differ between scram-AON and mock-transfection in both WT and KI-NMCMs, suggesting that scram-AON had no obvious adverse effects (Figure 3.32a). Nevertheless, the presence of a low level of an amplicon at the expected size of mRNA deleted of exons 5 and 6 in scram-AON-treated WT-NMCM suggests that scram-AON may stimulate the expression of variant-4. Treatment of WT-NMCMs with AON-5

resulted in the skipping of exon 5, whereas treatment with AON-5+6 resulted in the skipping of both exons, as well as the single skipping of exon 5 or exon 6 (Figure 3.32b, left-hand side). In mock-transfected KI-NMCMs four bands corresponding to the four mRNAs (mutant-1, mutant-2, mutant-3, variant-4) were detected, with the mutant-2 amplicon seeming to be more abundant than the others (Figure 3.32b, right-hand side). Treatment of the cells with AON-5 or AON-5+6 resulted in a higher level of the variant-4 band than mock-transfected cells, as expected. This was accompanied by reduced amounts of amplicons for mutant-1, mutant-2 and mutant-3. The total level of amplified mRNA did not differ between AON-5+6-treated and mock-transfected-cells, whereas a lower level was observed in AON-5-treated KI-NMCM. However, we cannot rule out that a lower cDNA amount was used.

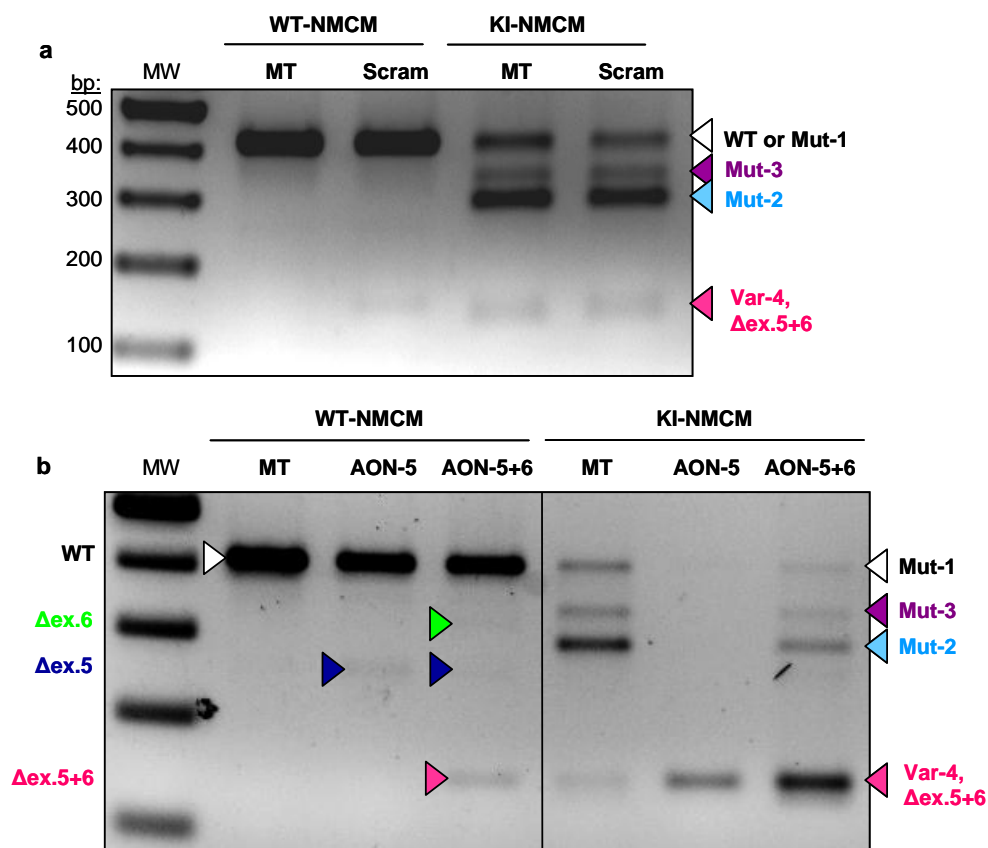


Figure 3.32. AON-induced exon skipping in WT- and KI-NMCMs.

(a, b) Total RNA was extracted from WT-NMCMs and KI-NMCMs mock-transfected (MT) or transfected with the scrambled AON (Scram), AON-5 (AON-5), AON-6 (AON-6) or AON5+6 (AON-5+6), and reverse transcribed into cDNA. The cDNAs were used as template for PCR amplification with primers located in exons 4 and 9 of *Mybp3*. The molecular weight (MW) marker was the Gene Ruler™ 100 bp DNA Ladder. The expected fragments are indicated by the colored arrowheads.

To estimate the time course of the effect of AONs, AON-treated KI-NMCMs were analysed for 2 to 5 weeks after transfection. In addition, the skipping efficiency of Cy3-

AON-5 was investigated, assuming that it has a similar effect on pre-mRNA splicing to that seen with AON-5 (Figure 3.33). The band corresponding to variant-4 was detected after 2 weeks, 3 weeks, 4 weeks and even after 5 weeks of transfection of KI-NMCMs with AON-5 or AON-5+6 (Figure 3.33a and b). This was associated with no visible adverse effects on the cells, like e.g. on the beating behaviour (not shown). Although RT-PCR is not quantitative, one can notice that the level of the variant-4 mRNA amplicon seemed higher in AON-treated cells than in mock-transfected-cells in all conditions. In addition, treatment of KI-NMCMs with the Cy3-tagged AON-5 for 3 weeks increased the variant-4 mRNA band as well (Figure 3.33a). Due to the lifespan of the NMCMs in cell culture a longer analysis of AON-treatment was not possible. After 5 weeks the number of beating cells became lower, but was still comparable to mock-transfected cells. This was associated with reduced amounts of amplicons for *Mybpc3* mRNA in mock-transfected and AON-5+6-treated cells relative to the 2-week time point (Figure 3.33b).

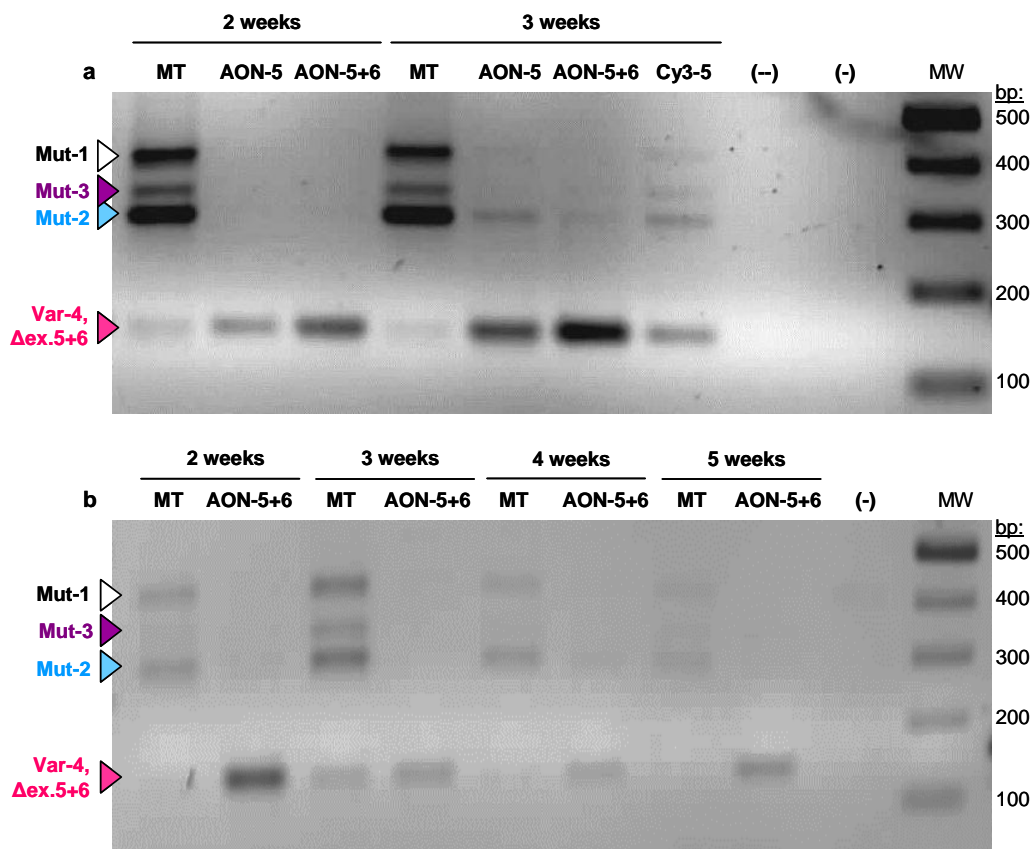


Figure 3.33. RT-PCR of KI-NMCMs after AON-treatment.

Total RNA was extracted from KI-NMCMs mock-transfected (MT) or treated with AON-5 (AON-5), AON-5+6 (AON-5+6) or Cy3-AON-5 (Cy3-5) for 2 to 5 weeks, and reverse transcribed into cDNA (a, b). A sample without reverse transcriptase is indicated as (-). The cDNAs were used as templates for PCR amplification with primers located in exons 4 and 9 of *Mybpc3*. As a negative control (-) water was added instead of cDNA. The molecular weight (MW) marker was the Gene Ruler™ 100 bp DNA Ladder. The expected amplicons are indicated by the colored arrows.

Based on the standard RT-PCR results, it was assumed that the AON-induced skipping of exons 5 and 6 in KI-NMCMs leads to a higher level of variant-4 mRNA and a lower level of mutant-1 mRNA (missense). To quantify the expression of mutant-1 and variant-4 mRNA in mock- and AON-treated KI-NMCMs mutant-specific primers and probes were used. The level of total *Mybpc3* transcripts was determined using SYBR® green and primers located in exons 2 and 3 of *Mybpc3* (Figure 3.34). The analysis first revealed that the levels of total mutant mRNAs, as well as variant-4 and mutant-1 mRNAs were significantly lower in cells treated with scram-AON than mock-transfected cells (data not shown). This suggests a toxicity of the AONs, which was not visible by standard RT-PCR (Figure 3.32a). On the other hand, the level of total mutant mRNAs did not differ between scram-AON-, AON-5- and AON-5+6-treated KI-NMCMs (Figure 3.34), and the results are therefore presented relative to scram-AON-treated samples. Variant-4 mRNA levels were higher in cells treated with AON-5 than in scram-treated KI-NMCMs (Figure 3.34b). This was not associated with the expected lower mutant-1 mRNA level (Figure 3.34c), in contrast to what was observed in standard RT-PCR (Figures 3.32 and 3.33). Variant-4 and mutant-1 mRNA levels appeared higher in AON-5+6- than scram-AON-treated cells, but the difference was not statistically significant.

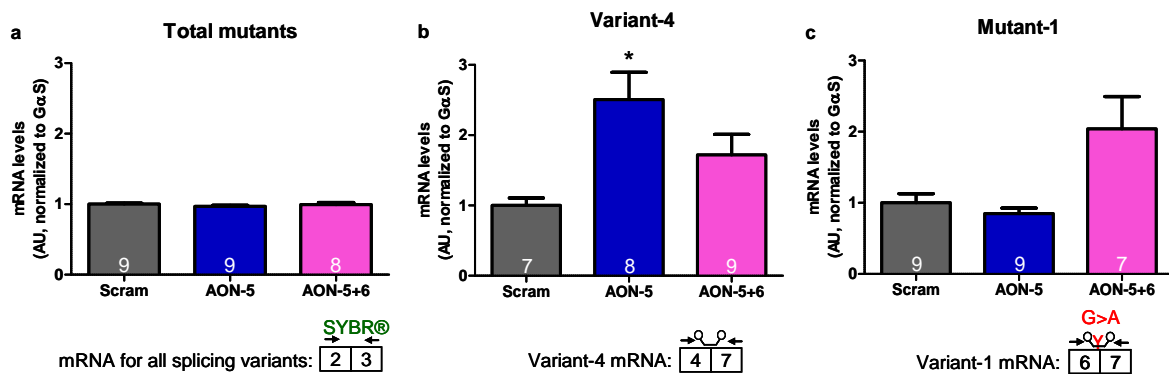


Figure 3.34. RT-qPCR analysis of KI-NMCMs after AON-treatment.

Total RNA was extracted from KI-NMCMs, which were transfected with scrambled AON (Scram), AON-5 (AON-5) or AON-5+6 (AON-5+6) for 8 days, and reverse transcribed into cDNA. The cDNAs were used as templates for qPCR analysis. To determine the total *Mybpc3*-mutant mRNA level SYBR® green and primers located in exons 2 and 3 were used (a). For amplification of variant-4 (b) and variant -1 (c) specific primers and probes, indicated below the figures, were used. All samples were normalized to GαS and values are presented relative to scrambled-AON treated cells. Bars represent the mean ± SEM. * $P < 0.05$ vs. scram, unpaired Student's t-test. The number of analysed samples is indicated in the bars.

Taken together, this mRNA analysis revealed different results using either standard or quantitative PCR. One possibility could be attributed to the PCR conditions, which are not exactly the same, e.g. different polymerases, touchdown PCR in the standard PCR vs.

fixed temperatures in the qPCR. The other possibility is a competition between the different mutant mRNAs for the primers during the RT-PCR. However, although the specific TaqMan probes revealed the mRNA of interest, different mRNAs are also amplified in the qPCR, indicating that competition may also exist. Finally, we cannot rule out that the Taqman probes may not be fully specific and may bind to other mutant mRNAs. This will be further evaluated.

3.2.9 Evaluation of the cMyBP-C protein levels in AON-treated NMCMs

To investigate whether the (induced) spliced variant-4 mRNA is translated into a stable protein, protein extracts from 8-day mock-transfected and AON-transfected KI-NMCMs were analysed by Western blot (Figure 3.35). As positive controls HEK293 cells transiently transfected with plasmids encoding mutant-1, mutant-3 and variant-4 were investigated in parallel. Proteins were detected using an antibody, which recognizes the N-terminus (first 14 amino acid) of cMyBP-C protein. After 8 days of transfection two protein bands were detected in KI-NMCMs (Figure 3.35a). The first one of ~150 kDa should correspond to mutant-1/mutant-3 cMyBP-C and the second band of ~139 kDa should correspond to the variant-4 protein. Interestingly, mock-transfected myocytes also showed both protein bands, suggesting that the natural spliced isoform results in a stable protein in KI-NMCMs. The mutant-1 (150 kDa) and mutant-3 (147 kDa) proteins, resulting from transfected HEK293 cells did not differ in apparent molecular weight and were thus not distinguishable in samples of KI-NMCMs expressing both proteins (Vignier et al., 2009). This was also shown by loading both protein extracts, mutant-1 together with mutant-3 (Figure 3.35a, last lane). The HEK293 cell derived variant-4 protein was detected at a similar apparent molecular weight as the second protein fragment detected in KI-NMCMs and a co-loading of HEK cell derived mutant-1 with variant-4 protein revealed a similar pattern as in KI-NMCMs. As for the mRNA level variant-4 protein level was significantly higher in KI-NMCMs treated with AON-5 than in mock-transfected cells (Figure 3.35c). However, it did not differ between cells treated with AON-5+6 or mock-transfected.

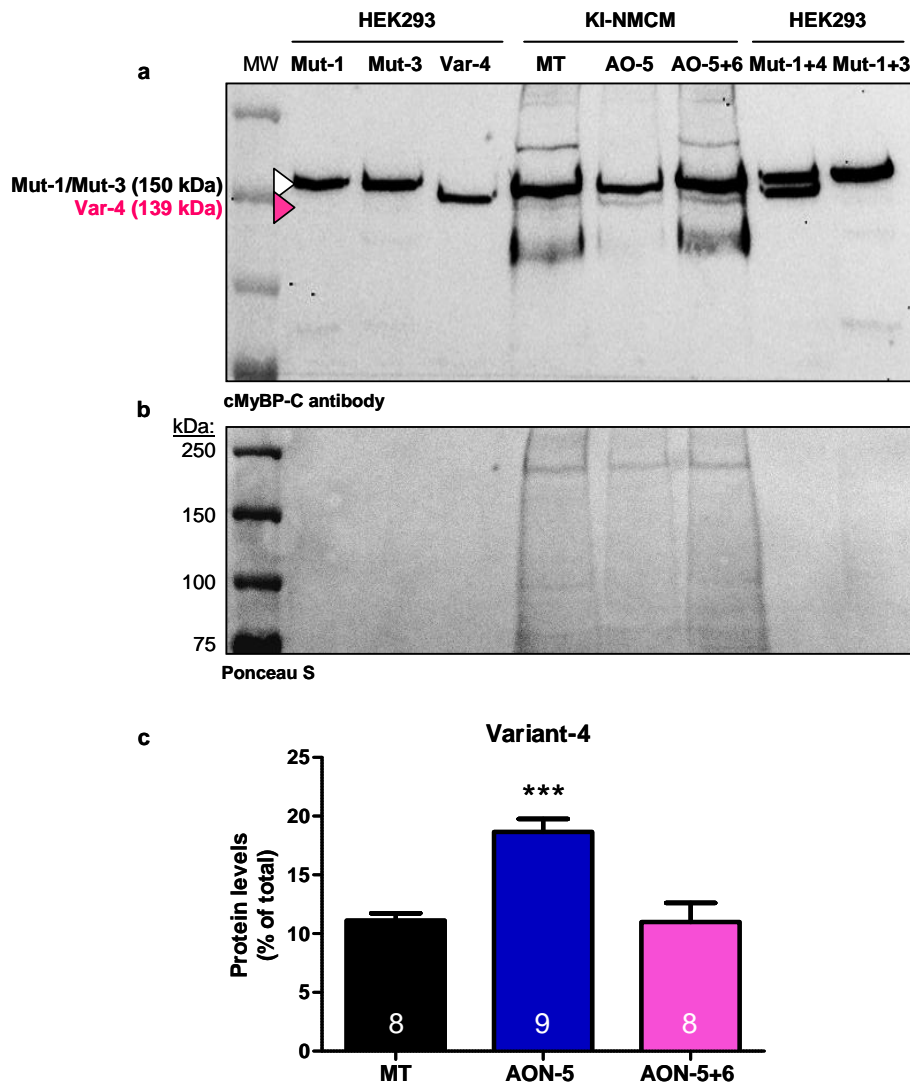


Figure 3.35. Protein expression of cMyBP-C variants.

(a) Representative Western blot of proteins derived from HEK293 cells and KI-NMCMs. HEK293 cells were transiently transfected for 24 h with plasmids encoding mutant-1 (Mut-1), Mut-3 and variant-4 (Var-4). KI-NMCMs were treated for 8 days with AON-5 (AO-5) and AON-5+6 (AO-5+6). As a control mock-transfected (MT) NMCMs were loaded. Western blot was stained with an antibody directed against the N-terminus of the mouse cMyBP-C protein (1st 14 amino acids). The expected protein fragments are indicated by the colored arrowheads. (b) The same membrane stained with Ponceau S. (c) Quantitative determination of variant-4 protein levels (expressed as percent of total) from Western blot analyses. Bars represent the mean \pm SEM. *** P <0.001 vs. MT, unpaired Student's t-test. The number of samples is indicated in the bars.

To further identify the detected protein fragment at the molecular weight of ~139 kDa, the corresponding band was excised after SDS-PAGE, stained with coomassie (PageBlue™, Fermentas) and analysed by mass spectrometry. However, this analysis failed to detect the 139-kDa-cMyBP-C protein, probably due to its marginal amount.

To quantify the level of total cMyBP-C protein, Western blot analysis was performed in 8-day mock-transfected and scram-AON, AON-5 or AON-5+6 transfected KI-NMCMs (Figure 3.36). For immunoblotting an anti-cMyBP-C antibody, recognizing

the first 14 amino acids, and an antibody directed against calsequestrin (CSQ) were used. The level of total cMyBP-C protein was 3.5-fold lower in scram-AON-treated than in mock-transfected myocytes (statistical data not shown). Since the 2OMePS chemistry of the AONs seems to have a toxic effect on the cells, the values were normalized to CSQ and are presented relative to Scram. The level of total cMyBP-C was higher in AON-5+6- than in scram-treated cells, but it did not differ between AON-5- and scram-treated NMCMs (Figure 3.36c, left plot). Variant-4 protein level was higher in AON-5- and AON-5+6- than in scram-treated cells, suggesting stabilization of this variant using these approaches (Figure 3.36c, middle plot). Mutant-1/3 levels did not differ between AON-5 and scram-treated cells, whereas they were markedly higher in AON-5+6- than in scram-AON-treated NMCMs (Figure 3.36c, right plot). This suggests that AON-6 may be beneficial for stabilization of one or both mutants.

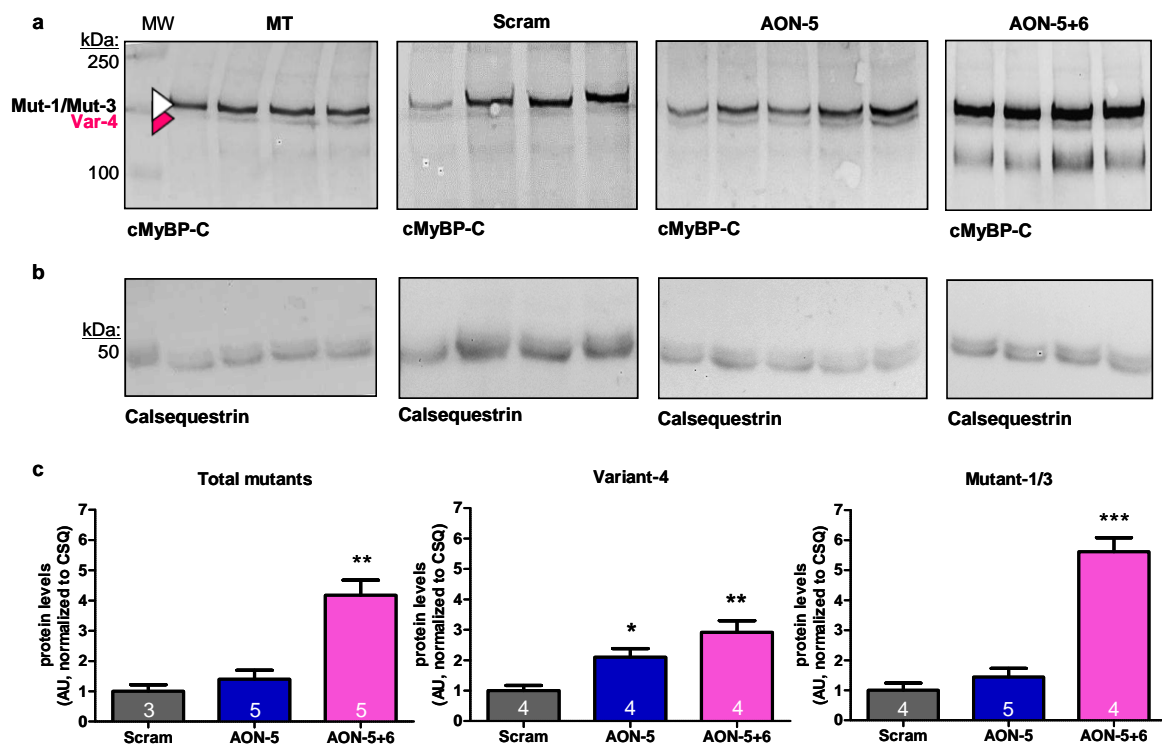


Figure 3.36. Determination of the level of total cMyBP-C of KI-cMyBP-C mutants.

(a) Representative Western blots of proteins derived from KI-NMCMs, which were mock-transfected (MT) or treated with different AONs (AON-5, AON-5+6, scrambled AON) for 8 days. The upper part of the Western blots was stained with an antibody directed against the 1st 14 amino acids of cMyBP-C and the lower part with an anti-calsequestrin antibody (b). The expected protein fragments are indicated by the colored arrowheads. (c) Densitometric quantifications of the total cMyBP-C protein level (left plot) and variant-4 (middle plot) or mutant-1/3 (right plot) protein level. All values were normalized to CSQ and values are presented relative to scrambled-AON treated samples. Bars represent the mean±SEM. ****P*<0.001, ***P*<0.01, **P*<0.05 vs. scram; unpaired Student's t-test. The number of samples is indicated in the bars.

3.2.10 Summary of the chapter

The major findings of this chapter were:

- Overexpression of variant-4 in KI-NMCMs revealed integration of the protein into the sarcomeric A-band and its co-localisation with endogenous mutant cMyBP-C. This suggests that variant-4 is likely functional and may be stabilized as a therapeutic tool.
- The Cy3-tagged 2'-*O*-methyl phosphorothioate antisense oligoribonucleotide, complementary to ESE-sequences in exon 5, was detected in both the nucleus and cytosol after transfection of neonatal WT and KI cardiac myocytes (NMCMs). This suggests that the AONs enter the cells and may target the pre-mRNA.
- Transfection with AONs directed against ESEs in exon 5, exon 6, or both induced the skipping of the corresponding exons in WT- and KI-NMCMs. Furthermore, AON-5 alone was sufficient to skip both exons 5 and 6 together in KI-NMCMs. This indicates that the exon-skipping method worked.
- The mRNA level of variant-4, deleted of exons 5 and 6, was higher in AON-treated than in scram-AON-treated KI-NMCMs. In contrast, the mRNA levels of mutant-1 and total mutant-*Mybpc3* did not differ from those in scram-AON-treated myocytes.
- Skipping of exons 5 and 6 was associated with the appearance of a cMyBP-C protein band at the molecular weight of ~139 kDa in KI-NMCMs. Protein level of this putative variant-4 was higher in AON-5- than in scram-AON-treated KI-NMCMs. However, this was not enough to increase the amount of total cMyBP-C. On the other hand, the levels of total and mutant-1/3 protein were markedly higher in AON-5+6- than in scram-AON-treated KI-NMCMs, suggesting that it was beneficial for the cells.

4 Discussion

The aim of the first part of this study was to establish a cell-based screening system in HEK293 cells expressing *MYBPC3* minigenes to analyse the regulation of the expression of *MYBPC3* mutations. The aim of the second part was to evaluate the feasibility and efficacy of antisense oligoribonucleotides to skip specific exons in cardiac myocytes isolated from *Mybpc3*-targeted KI mice in order to rescue the molecular phenotype. The two major findings of this study were: i) HEK293 cells stably expressing human *MYBPC3* minigenes allow study of the expression of *MYBPC3* mutations and reproduce data obtained in humans at the mRNA level, and ii) antisense oligoribonucleotides (AONs) targeting exonic splicing enhancer sequences (ESEs) in mouse *Mybpc3* induce the skipping of the corresponding exons. This study provides first proof-of-concept that human *MYBPC3* mutations can be evaluated in a cell-based system and that the exon-skipping strategy can be envisioned to remove mutated exons in the context of HCM.

4.1 Flp-In293 cells stably expressing human *MYBPC3* minigenes are suitable for analysis of the expression of *MYBPC3* mutations

About 61% of *MYBPC3* mutations are frameshift or nonsense mutations that should result in C-terminal truncated proteins (for review, see Schlossarek et al. 2011). In addition, missense mutations that are expected to produce full-length mutant proteins may also have an influence on sequences to which proteins bind during the process of splicing, and thus could also potentially result in a frameshift due to altered splicing. Despite the high number of *MYBPC3* mutations identified so far (n=185; for review, see Schlossarek et al., 2011), only few myectomy samples of patients carrying frameshift mutations have been investigated. Truncated proteins were never detected by Western blot analysis, suggesting that mutant mRNAs and/or proteins are highly unstable (Rottbauer et al., 1997; Moolman et al., 2000; van Dijk et al., 2009). As shown by our group and others, at least part of the instability can be explained by accelerated degradation by NMD and/or the UPS (Sarikas et al., 2005; Bahrudin et al., 2008; Vignier et al., 2009). In the majority of cases, however, evaluation of the expression of these mutations and of the contribution of quality control systems in their regulation have not been conducted, primarily because it is difficult to access human myocardial tissue or time consuming to develop mouse models. Therefore,

the need to develop a simple cell-based screening system to analyse the expression of *MYBPC3* mutations was obvious. In addition, it was assumed that if the expression levels of investigated mutations were increased by NMD or UPS inhibitors in cultured cells, then these mutations may also be targeted in mice to evaluate therapies *in vivo*. We therefore focused on mutations that should result in C-terminal truncated proteins, which still contain important domains required for sarcomeric incorporation and function. Two human *MYBPC3* mutations were selected, both resulting in C-terminal truncated proteins, which were not detected in myocardial tissue of patients by Western blot. The first one is a point mutation in the donor splice site of intron 31 (IVS31+1G>A, Mut-1; Rottbauer et al. 1997), which results in a “normal” level of mutant mRNA, suggesting regulation by the UPS. The second one is an insertion in exon 31 (+AGTG; Mut-2), which results in a low level of nonsense mRNA (unpublished data, this study), suggesting regulation by the NMD pathway.

Minigenes are commonly used to evaluate the functional effects of splicing mutations (Baralle et al., 2003; Maciolek et al., 2006; Dujardin et al., 2011). It has been shown that cells transiently transfected with minigenes gave rise to mRNAs and proteins in several cell lines including HEK293 cells (Maciolek et al., 2006; Olsen et al., 1991; Gong et al., 2007). Therefore in the first part of this study a human WT-*MYBPC3* minigene was constructed encompassing exons 29-34, from which Mut-1 and Mut-2 minigenes were then produced by *in vitro* mutagenesis. Transient transfection of HEK293 cells with each minigene resulted in the expected WT and mutant mRNAs after RT-PCR, demonstrating that human *MYBPC3* minigenes are expressed at the mRNA level. However, this analysis also revealed a high amount of contaminating plasmid DNA in each condition, as well as WT mRNA in untransfected HEK293 cells. The presence of contaminating plasmid DNA in RNA preparation is a well-known problem after transient transfections and corresponds to the non-integrated episomal DNA (Lottspeich and Engels, 2006). This is mainly due to insufficient DNase I digestion during RNA extraction. Although other RNA extraction methods as well as additional DNaseI digestion steps were tried, the problem could not be solved. For this reason stable HEK293 cell lines expressing each of the three minigenes were generated, which also had the advantage to analyse minigene expressions over a long period of time.

In general, stable cell lines are generated by transfecting a transcriptional unit containing the gene of interest along with a selection marker (Liu et al., 2006). Cells that have stably incorporated the plasmid into their genome are selected with an antibiotic for

1 to 2 weeks. Subsequently positive cells are picked and expanded. It was shown that stable transformants of mammalian cells often reveal large variability in the amount of expression of the integrated plasmid (Fukushige et al., 1992). This was likely due to a variable number of copies introduced into the genome as well as position effects on gene expression due to random integration (Fukushige et al., 1992). To circumvent these problems the Flp-In™ system was developed, which allows integration of minigenes as single-copies at a specific genomic locus in Flp-In293 cells (the FRT site is stably integrated into the cell line). A proof-of-principle study confirmed the site-specific recombination event at the FRT site by Southern blot analysis (Liu et al., 2006). This group showed that the majority of Flp-In293 clones contained single integrants, while only few contained multiple integration events or less frequently random integration events. In addition, most of the isolated clones maintained the initial homogenous transgene expression over a long period of time under selective conditions (Liu et al., 2006). Therefore, in the present study, the Flp-In™ system was used to generate cell lines stably expressing human WT, Mut-1 and Mut-2 *MYBPC3* minigenes. Isogenic cell lines were positively selected with hygromycin, and the correct insertion and isogenic expression of the minigenes was validated by the loss of *lacZ*-activity. Using a common Taqman probe and primers, which are complementary to the three minigenes, it was validated that all stable cell lines transcribe minigenes into mRNAs. Furthermore, whereas mRNA levels of WT and Mut-1 cells did not differ, Mut-2 mRNA was ~60% lower than the WT. This suggests stability of Mut-1 mRNA and instability of Mut-2 mRNA. These data also support findings obtained in human myocardial tissue showing that the level of Mut-1 and WT mRNAs did not differ (Rottbauer et al., 1997), whereas the level of Mut-2 mRNA was >80% lower than the WT mRNA (present unpublished data; Figure 3.3). Therefore, these data suggest that stable modified HEK293 cells (Flp-In293) can be used as a simple cell-based system to evaluate the expression of human *MYBPC3* mutations.

Nonsense-mediated mRNA decay (NMD) is an mRNA surveillance mechanism found in all eukaryotes. NMD secures mRNA quality by selectively targeting mRNAs that contain a premature termination codon (PTC) for degradation (Maquat 1995; Hentze et al., 1999). PTCs are only recognized and regulated by NMD when they are located at least 50 nucleotides upstream of the last exon-exon junction (Nagy et al., 1998). To investigate whether the low Mut-2 mRNA level results from partial degradation by NMD, different NMD inhibitors (emetine, cycloheximide, wortmannin) were tested at various concentrations. Unexpectedly, treatment with these inhibitors at the tested concentrations

did not significantly stabilize the mRNA level of Mut-2, although a tendency was observed with 300 µg/ml emetine. At this point, the exact reasons for the small effect are unknown. But it is noteworthy that emetine also had only a minor effect, even at high concentrations (100 and 300 µg/ml), on WT cells transiently transfected with a NMD reporter plasmid encoding GFP. This indicates on the one hand, that the reporter system worked in principle, but that on the other hand, NMD may play only a minor role in (modified) HEK293 cells. Another explanation could be that emetine simply did not reach its intracellular targets, but the toxicity seen at high concentrations makes this explanation unlikely. It is also possible that NMD may behave differently in HEK293 cells compared to e.g. cardiac myocytes from which the drug concentrations were adapted (Vignier et al., 2009). These cells likely respond to higher concentrations of the drugs or to longer periods of treatment. Therefore both conditions should be tested in further analyses. In summary, these data suggest that NMD may not be significantly involved in the regulation of the expression of these mutations in cultured modified HEK293 cells. Accordingly, they suggest that another mRNA degradation mechanism (e.g. micro-RNAs) may be involved (Valencia-Sanchez et al., 2006). On the other hand, the obtained data suggest that NMD is not well testable in these cells.

Despite the presence of mini-mRNAs, mini-proteins resulting from the expression of *MYBPC3* minigenes were never detected in either transient transfections or after stable transfections of HEK293 or Flp-In293 cells. While this was expected for Mut-1 and Mut-2 from human data (Rottbauer et al., 1997; present unpublished data Figure 3.3), the absence of detection of the WT mini-protein was not. Only after large-scale culture of WT and Mut-1 Flp-In293 cell lines followed by immunoprecipitation with the anti-myc antibody could a band of the expected molecular weight for the myc-WT mini-protein be immunoprecipitated. On the other hand, a band of the expected molecular weight for myc-Mut-1 was found in the detergent-insoluble pellet fraction. The reason for the low protein level is unclear. The Flp-In system is adapted for the expression of mammalian genes and was shown to express constructs at both the mRNA and protein levels (Wakabayashi et al., 2006; Roy et al., 2007). The promoter present in the expression vector was the polypeptide chain elongation factor 1 α (pEF-1 α). The associated gene promotes the GTP-dependent binding of an aminoacyl-tRNA to ribosomes (80S) in the cytosol and is expressed in almost all kinds of mammalian cells (Uetsuki et al., 1989). It has been shown that the human EF-1 α promoter is strong in nuclear extracts from HeLa cells (Uetsuki et al. 1989) and that proteins derived from minigenes are also expressed under the control of pEF-1 α

promoter (Tan et al., 2000). Sequencing confirmed the integration of the correct sequences, including the myc-tag and the Kozak sequence (Kozak, 1987). The presence of only one myc-tag may have been not sufficient to detect low amounts of translated proteins in stable cell lines, in contrast to cardiac myocytes transduced with adenovirus expressing myc-cMyBP-Cs under the control of a strong promoter (Sarikas et al., 2005; Mearini et al., 2010). Since the steady-state level of proteins depends on the balance between translation and degradation, it was hypothesized that mini-proteins are unstable and quickly degraded. Eukaryotic cells possess two major proteolytic systems, the autophagy-lysosome pathway and the UPS (for reviews, see Levine et al., 2008; Schlossarek et al. 2011). The UPS is a highly selective degradation pathway of cytosolic, nuclear and myofibrillar proteins and requires polyubiquitination of the target protein prior to its degradation by the 26S proteasome (for review, see Zolk, 2006). Inhibition of proteasomal activities with specific inhibitors has been shown to increase the steady-state level of ubiquitinated proteins in cells or *in vivo* (Sarikas et al., 2005; Vignier et al., 2009). To test the possibility that mini-proteins are degraded by the UPS, stable WT and Mut-2 Flp-In293 cell lines as well as untransfected cells were treated with various concentrations (0 to 10 μ M) of the proteasome inhibitor MG132 for 24 hours. Interestingly, whereas the steady-state level of ubiquitinated proteins increased with increasing concentrations of MG132 in untransfected Flp-In293 cells, WT and Mut-2 cells did not show any accumulation of ubiquitinated proteins. Furthermore, WT and Mut-2 mini-proteins were not detected. Treatment of WT, Mut-1 and Mut-2 stable cell lines with higher concentrations of MG132 (10 to 100 μ M) resulted in accumulation of ubiquitinated proteins, but not of WT, Mut-1 and Mut-2 proteins. These data clearly indicate that the stable Flp-In293 cell lines are less sensitive to proteasome inhibition than pure Flp-In293 cells, but that the different cMyBP-C mini-proteins are not subject to proteasomal degradation. It is also possible that the concentrations of mini-RNAs were already too low to give rise to relevant/detectable concentrations of mini-proteins. Further protein analyses, including protein fractionations are needed to evaluate whether mini-proteins are detected after treatment with high concentrations of MG132. In addition, an antibody directed against epitopes of exon 29 or exon 30, present in all minigenes, is required to specifically identify mini-proteins.

In conclusion, the findings support the view that mutated *MYBPC3* minigenes in stable Flp-In293 cells behave similarly to identical mutated *MYBPC3* genes in myocardial tissue of HCM patients, at least for the expression at the level of mRNA. This provides the first evidence that stable Flp-In293 cells can be used as a cell-based system for screening

the expression of human *MYBPC3* mutations. Further experimental studies are nevertheless needed i) to improve the detection of the mini-proteins by adding additional tags and/or using protein fractionation, and ii) to evaluate the contribution of the NMD and the UPS in this system, for example by using higher concentrations and/or adjusting time of application of specific drugs.

4.2 Modified antisense oligoribonucleotides induce exon skipping in cardiac myocytes from wild-type and *Mybpc3*-knock-in mice

The second aim of my thesis was to evaluate the feasibility and efficacy of 2'-*O*-methyl phosphorothioate (2OMePS) AONs to promote altered splicing that leads to in-frame skipping of the mutated exon in mRNA of cardiac myocytes isolated from *Mybpc3*-targeted KI mice. The expected result was a stable protein lacking the mutated exon with near-normal function that would be able to rescue the molecular and functional phenotype. This so-called 'exon-skipping strategy' is part of a larger research program in our team investigating several RNA-based approaches as tools for HCM therapy.

The homozygous *Mybpc3*-targeted KI mice, which were studied in this work, developed marked left ventricular hypertrophy, diastolic and systolic dysfunction, as well as interstitial fibrosis (Vignier et al., 2009). Therefore they can be considered as a good model for testing therapies against cardiac hypertrophy and dysfunction. KI mice carry a G>A transition on the last nucleotide of exon 6, which is part of the consensus splice donor site sequence and results in three different mutant mRNAs, which are expressed at low levels: missense (mut-1), nonsense lacking exon 6 (mut-2), and one lacking exon 6 and containing part of intron 8 (mut-3). Although pathophysiological mechanisms are still not fully elucidated, evidence indicates that NMD and UPS regulate the expression of genes bearing the mutation, resulting in low levels of mutant proteins that we believe, contribute to the KI phenotype. Therefore, the hypothesis was that strategies aiming to increase mRNA and/or protein levels could rescue the phenotype in KI mice.

The development of AONs as therapeutic molecules was first described by Zamecnik et al. (1978). They could knockdown viral gene expression by targeting the mRNA and therefore prevented protein translation or induced mRNA degradation. Subsequently, AONs were used to interfere with the pre-mRNA splicing machinery in order to correct altered exon splicing in β -thalassemia (Dominski et al., 1993). This

technique is currently being evaluated in clinical research, particularly to treat Duchenne Muscular Dystrophy (DMD), a fatal muscle wasting disease caused by mutations in the dystrophin gene (*DMD*). It was demonstrated that AONs have the potential to efficiently restore the open reading frame of *DMD*. Different groups showed that AONs modified by 2OMePS and directed against exonic splicing enhancer (ESE) sequences cause the specific skipping of mutated exons in DMD patient-specific muscle cell cultures, as well as in mouse (mdx) and dog (GRMD) disease models (for review, see Le Roy et al., 2009). Duchenne patients were treated with 2OMePS AONs by local administration or systemic injections (van Deutekom et al., 2007; Kinali et al., 2009; Goemans et al., 2011). Systemic injection of the 2OMePS AON Pro051 for 5 weeks weekly (Prosensa Therapeutics, Leiden, Netherlands) induced the specific skipping of exon-51 and new dystrophin expression (60-100% dystrophin-expressing muscle fibers; 15.6% of the expression in healthy muscle) in DMD patients. After a 12-week extension phase of weekly injections there was an improvement of ~35 meter in the 6-minute walk test. The application showed no serious adverse effects (Goemans et al., 2011).

In order to remove the mutated exon 6, but to keep the reading frame, it was necessary to target both exons 5 and 6 of *Mybpc3* simultaneously. Interestingly, in addition to the three mutant mRNAs, an mRNA lacking exons 5 and 6 was detected in both KI-NMCM and also in WT-NMCM, but only after two rounds of PCR. This suggested the existence of a naturally spliced *Mybpc3* isoform, which was never described in the literature and that we named variant-4 (var-4). The presence of variant-4 in WT, even at a very low level, strongly prompted us to produce this isoform. Variant-4 protein is expected to contain all major interacting domains and an intact MyBPC motif, including the phosphorylation sites. Gene transfer in HEK293 cells resulted in a stable variant-4 protein in contrast to mutant-2, and AAV-mediated transduction of cardiac myocytes exhibited correct incorporation of variant-4 into the sarcomeric A-band. These data suggest that the variant-4 protein is likely functional and enhancing its level may be a good therapeutic goal. To achieve the in-frame deletion of exons 5 and 6, AONs complementary to ESE sequences in exon 5 and/or 6 were designed. Natural unmodified phosphodiester AONs are rapidly degraded by exonuclease activity (Eder et al., 1991). Therefore, AONs were modified by 2OMePS, which has been shown to slow their degradation by RNases or other nucleases, and to increase the transport through lipid bilayers due to their negative charge (Aartsma-Rus et al., 2002). At first, transfection of cardiac myocytes with Cy3-AON-5 revealed Cy-3-positive dots in the cytoplasm and nuclei, indicating that AONs enter the

cells and may target the pre-mRNAs. Furthermore, AON-5, AON-6 or AON-5+6 induced skipping of the corresponding exons from WT-*Mybpc3* mRNA, indicating that the strategy works in NMCMs. This supports recent findings obtained in cardiac myocytes from neonatal mdx mice transfected with 2OMePS AON directed against ESE of mutated *Dmd* exon (Wang Q. et al., 2010). Interestingly, in KI-NMCMs treatment with either AON-5+6 or with AON-5 alone increased the synthesis of variant-4 mRNA. Based on the results obtained in WT-NMCMs this was not expected for AON-5 alone. It suggests that the G>A transition weakened the splice donor site such that exon 6 is no longer defined as a proper exon by the spliceosome, and skipped together with the targeted exon 5. Strikingly, variant-4 mRNA was markedly produced and even prevented completely the synthesis of the other mutant mRNAs in some cases in KI cardiac myocytes treated with AON-5 or AON-5+6 for 24 h up to 5 weeks. These data provide evidence that AONs directed against ESEs of exon 6 and/or exon 5 are sufficient to produce a “therapeutic mRNA”. Quantitative PCR using specific Taqman probes and primers confirmed these data, although AON-5 was more efficient than AON-5+6 in increasing the level of variant-4 mRNA. The lower level of produced variant-4 mRNA in NMCMs treated with AON-5+6 than with AON-5 alone was not expected. The finding could be explained by a potential competition between both AONs for cell delivery, resulting in the presence of either AON-5 or AON-6 in some cells. This is further supported by the detection of mRNA without exon 5, exon 6 or both exons 5+6 after treatment of WT-NMCMs with AON5+6 (Figure 3.29). In addition, previous data also showed that AONs directed against two different exons result in the skipping of both exons as well as the skipping of the single exons in myotubes derived from human patients (Aartsma-Rus et al., 2004).

The data also showed that the total level of *Mybpc3* mRNAs was 30% lower in AON-treated than in mock-transfected myocytes, suggesting that the AONs and/or the 2OMePS chemistry had toxic side effects in NMCMs. If breakdown of 2OMePS AONs occur monomers with a free phosphorothioate group are released, which can be cell toxic due to non-specific protein-phosphorothioate interactions, because of the negative charge delocalisation at the internucleotide thioate bound (Crooke et al., 1995; Crooke 2000). Furthermore it has been described that oligonucleotides modified by numerous phosphorothioate groups are “sticky” and have the tendency to bind to non-complementary sequences/proteins, which can cause cell toxicity (Crooke 2000; Dias et al., 2002; <http://www.sigmaaldrich.com/life-science/custom-oligos/custom-dna/learningcenter/phosphorothioates.html>). Nonetheless, Yoo et al., 2004 showed that non-specific effects of

phosphorothioate-modified oligodeoxynucleotides targeting *bcl-2* mRNA were reduced by using 2OMePS oligodeoxynucleotides in T24 human bladder cancer cells. To circumvent the problem of cell toxicity, the amount of phosphorothioate linkages should be minimized in the AONs. To slow degradation from the ends and to reduce the amount of released phosphorothioates, it seems sufficient to protect the ends and the middle part of the oligos (guideline Sigma Aldrich; <http://www.sigmaaldrich.com/life-science/custom-oligos/custom-dna/learning/center/phosphorothioates.html>). For prospective syntheses of 2OMePS-AONs this should be considered.

The next obvious question was whether variant-4 mRNA is translated into protein and whether treatment with AON-5 or AON-5+6 can increase the amount of variant-4 protein. In KI-NMCMs two cMyBP-C bands of apparent molecular weight of 150 kDa and 139 kDa were detected. The 150-kDa-band corresponds to mutant-1 and/or mutant-3 described previously (Vignier et al, 2009). The 139-kDa-band migrates at a molecular weight similar to variant-4 protein expressed in HEK293 cells, suggesting that it could be the variant-4 protein. To further confirm this hypothesis, both bands were excised and analysed by mass spectrometry. However, this analysis failed to detect cMyBP-C in both samples, presumably due to its low abundance in KI cardiac myocytes as compared to WT. We hope to resolve this issue with the development of a specific antibody directed against the new amino acids that result from the boundary between exon 4 and 7 formed in this mutant mRNA. Despite the lack of confirmation that the 139-kDa-band is the variant-4 protein, we analysed its abundance vs. total cMyBP-C or vs. calsequestrin. Interestingly, whereas variant-4 protein represents 10% of total cMyBP-C in mock-transfected KI myocytes, it reached ~20% of total in AON-5-treated cells. In contrast, AON5+6 treatment stabilized both variant-4 and mut-1/mut-3 proteins, therefore variant-4 still represented 10% of total. Normalization to calsequestrin revealed that variant-4 levels were 2-fold and 3-fold higher, respectively, in AON-5- and AON-5+6-treated cells relative to scram-treated cells. Interestingly, while levels of mutant-1/mutant-3 and of total cMyBP-C did not differ between AON-5- and scram-treated cells, they were >4-fold higher in AON-5+6- than in scram-treated KI cells. The reason is not yet known. One possibility is that AON-6 by itself favours the production of at least mut-3 mRNA, which lacks exon 6, but retains some part of intron 8, and this mRNA is then translated into a mut-3 protein. The other possibility is that AON-6 is complementary to a sequence, which contains not only an ESE but also a silencer sequence (ESS). However, results obtained in WT-NMCMs at least did not support this hypothesis, since mRNA lacking exon 6 was present and no major

stabilisation of WT mRNA was observed.

4.2.1 Outlook

In conclusion, this proof-of-principle study provides evidence that targeted 2'-*O*-methyl phosphorothioate AON treatment stimulates the synthesis of at least the putative variant-4 protein in KI-NMCM. Whether the quantity of this “therapeutic protein” is enough to rescue the KI phenotype cannot be evaluated in NMCMs. Therefore future experiments will test the exon-skipping strategy in KI engineered heart tissue and *in vivo* to answer this question. Furthermore, the functionality and toxicity of the variant-4 protein will be tested in both engineered heart tissue and *Mybpc3*-WT mice using an adeno associated virus (AAV). In addition, an AAV encoding AON-5+6 in the U7 snRNA backbone will be produced, which allows the expression of antisense sequences (Goyenvalle et al., 2004). These AAVs will be systemically delivered in mice by tail injection and cardiac function will be evaluated at different post-natal time windows.

4.2.2 Summary

Hypertrophic cardiomyopathy (HCM) is the most frequent inherited cardiac disease and lacks effective treatment. It is commonly caused by mutations in the *MYBPC3* gene encoding cardiac myosin-binding protein C (cMyBP-C). About 61% of *MYBPC3* mutations are frameshift or nonsense mutations, which are expected to produce C-terminal truncated proteins. However, these proteins were undetectable in myocardial tissue of HCM patients or after adenoviral gene transfer in cardiac myocytes. The absence of detection suggested that aberrant mRNAs or proteins are highly unstable and degraded by NMD and/or the UPS. This may result in cMyBP-C haploinsufficiency, which is assumed to cause HCM. The evaluation of expression of human mutations is restricted by difficulties to access human tissue samples or to develop mouse models. Therefore the first goal of this study was to establish a cell-based system in HEK293 cells to analyse the expression of *MYBPC3* mutations. We focused on two mutations that result in C-terminal truncated cMyBP-C proteins, which, when stabilized by specific drugs still contain the important functional domains required for sarcomeric incorporation. The major findings of the first part were: modified HEK293 cells stably expressing human *MYBPC3* minigenes i) allow study of the expression of mutations at the level of mRNA and ii) reproduce data obtained in humans at the mRNA level. This provides the first evidence that stable HEK293 cells can be used as a cell-based system for screening the expression of human *MYBPC3* mutations.

The second part of the study was based on a targeted *Mybpc3*-knock-in (KI) mouse model, which develops left ventricular hypertrophy. KI mice carry a homozygous G>A transition on the last nucleotide of exon 6, which results in 3 different mRNAs: one missense, one nonsense lacking exon 6, and one lacking exon 6 and containing part of intron 8. The goal was to evaluate the feasibility and efficiency of antisense oligoribonucleotides (AONs) to remove the mutated exon in KI cardiac myocytes by skipping both exons 5 and 6 and thereby force the expression of a newly-discovered spliced isoform variant-4, which is predicted to be functional. Two modified AONs were designed to target exonic splicing enhancer sequences in exon 5 (AON-5) and exon 6 (AON-6). Isolated and cultivated cardiac myocytes from wild-type-(WT) and KI mice were subsequently treated with AONs for ≥ 8 day. The major findings of the study were: i) Cy3-tagged AON-5 exhibited both a nuclear and cytosolic localisation, suggesting that

AONs can enter the cells and may target pre-mRNAs, ii) AONs induced skipping of the corresponding exons in wild-type- and KI cardiac myocytes and iii) the levels of variant-4 mRNA and protein were higher in AON-treated than scram- or mock-transfected cells. This part provides the first proof-of-concept that the exon-skipping strategy works in *Mybpc3*-KI cells and therefore can be envisioned to be a functional *in vivo* approach to remove mutated exons in the context of HCM.

4.2.1 Zusammenfassung

Die hypertrophe Kardiomyopathie (HCM) stellt die am häufigsten auftretende vererbte Herzerkrankung dar, für die es bislang jedoch keine effektiven Behandlungsmöglichkeiten gibt. Eine der häufigsten Ursachen der HCM sind Mutationen im *MYBPC3* Gen, das für das kardiale Myosin-bindende Protein C (cMyBP-C) kodiert. Bei etwa 61% der *MYBPC3* Mutationen handelt es sich um *frameshift* oder *nonsense* Mutationen, die C-terminal verkürzte Proteine erwarten lassen. Dennoch konnten diese verkürzten Proteine nicht im Myokardgewebe von HCM-Patienten oder nach adenoviraler Überexpression in Kardiomyozyten nachgewiesen werden. Grund für die fehlende Detektion ist der Abbau der sehr instabilen aberranten mRNAs oder Proteine über das NMD und/oder UPS. Dies kann eine cMyBP-C Haploinsuffizienz bedingen, die vermutlich an der Entstehung der HCM beteiligt ist. Die Analyse der Expression humaner Mutationen ist aufgrund der Erschwernis, humane Gewebeproben zu erhalten oder Mausmodelle zu entwickeln, eingeschränkt. Das erste Ziel dieser Arbeit bestand daher in der Etablierung eines zellbasierten Systems in HEK293 Zellen, um die Expression von *MYBPC3* Mutationen zu untersuchen. Der Fokus lag auf zwei Mutationen, die jeweils in C-terminal verkürzten cMyBP-C Proteinen resultieren und welche, wenn durch bestimmte Substanzen stabilisiert, die wichtigen funktionellen Proteindomänen besitzen, die für eine sarkomerische Integration notwendig sind. Die wichtigsten Ergebnisse des ersten Teiles waren: modifizierte HEK293 Zellen, die stabil humane *MYBPC3*-Minigene exprimieren, ermöglichten eine Untersuchung der Expression von Mutationen auf mRNA-Ebene und die Reproduktion von Daten, die in Patienten erhoben wurden. Dies lieferte den ersten Beweis dafür, dass stabil exprimierende HEK293 Zellen als zellbasiertes System für die Untersuchung der Expression humaner *MYBPC3* Mutationen genutzt werden können.

Der zweite Teil dieser Arbeit basierte auf einem *Mybpc3-Knock-in* (KI) Mausmodell, das eine linksventrikuläre Hypertrophie entwickelt. KI-Mäuse weisen am letzten Nukleotid des Exons 6 eine homozygote G>A Transition auf, die in drei verschiedenen mRNS resultiert: Einer *missense* mRNS, einer *nonsense* mRNS, die aus dem Überspringen des Exons 6 resultiert und einer mRNS, die aus dem Überspringen des Exons 6 resultiert, jedoch einen Teil des Introns 8 beibehält. Das Ziel dieses Teiles der Arbeit war es, die Durchführbarkeit und Effizienz von Antisense Oligoribonukleotiden (AON) hinsichtlich des Überspringens der Exons 5 und 6 in KI-Kardiomyozyten zu evaluieren, und somit die Expression der kürzlich entdeckten Spleißvariante (Variante-4) zu forcieren, die vermutlich funktionell ist. Zwei modifizierte AON wurden designt, die gegen exonische spleißverstärkende Sequenzen in Exon 5 (AON-5) und 6 (AON-6) gerichtet sind. Mit den AON wurden anschließend kultivierte, aus WT- und KI-Mäusen isolierte Kardiomyozyten für ≥ 8 Tage behandelt. Die wichtigsten Ergebnisse dieses Teiles waren: i) Die Transfektion mit dem Cy3-getaggten AON-5 zeigte eine nukleäre und cytosolische Lokalisation, einen Hinweis darauf gebend, dass AON in die Zellen gelangen und an der prä-mRNS wirken könnten, ii) AON induzierten das Überspringen der jeweiligen Exons in WT- und KI-Kardiomyozyten und iii) die Menge der mRNS und Proteine von Variante-4 war höher in AON-behandelten als in *scram-* oder *mock-*transfizierten Zellen. Dieser Teil der Arbeit lieferte den ersten Nachweis dafür, dass die *exon-skipping*-Methode in *Mybpc3* KI-Zellen durchführbar ist und auch *in vivo* im Rahmen der HCM angewendet werden könnte, um das mutierte Exon zu entfernen.

5 Appendix

5.1 Material

5.1.1 Adenovirus

The *Mybpc3* variant-4 cDNA (deleted of exons 5 and 6) was cloned into the pGG2 expression vector and sent to Paris for production of an adeno-associated virus serotype 6 (collaboration with Dr. Luis Garcia).

5.1.2 Antibodies

Table 5.1. Antibodies used for Western blotting.

Investigated protein	Primary antibody	Company	Dilution	Secondary antibody	Company	Dilution
cMyBP-C (Minigenes)	c-myc, polyclonal	Sigma	1:1000	anti-rabbit IgG	Exacta Cruz Dianova	1:2000 1:6000
Ubiquitinated proteins	Ubiquitin (FK2), monoclonal	Biomol	1:50 000	anti-mouse IgG	Dianova	1:6000
GFP	GFP, polyclonal	Santa Cruz	1:2000	anti-rabbit IgG	Dianova	1:6000
cMyBP-C (NMCMS)	cMyBP-C-2-14aa, polyclonal	Gift of S. Sadayappan	1:15 000	anti-rabbit IgG	Dianova	1:5000
Calsequestrin	Cardiac CSQ, polyclonal	Dianova	1:1000	anti-rabbit IgG	Sigma	1:6000

Table 5.2. Antibodies used for immunofluorescence staining.

Investigated protein	Primary antibody	Company	Dilution	Secondary antibody	Company	Dilution
cMyBP-C (Minigenes)	MyBP-C motif, polyclonal	Gift of W. Linke	1:500	anti-rabbit IgG, Alexa Fluor-546	Molecular Probes	1:500
cMyBP-C (NMCMs)	cMyBP-C-2-14aa, polyclonal	Gift of S. Sadayappan	1:10 000	anti-rabbit IgG, Alexa Fluor-546	Molecular Probes	1:800
Flag-tag	Flag, monoclonal	Sigma	1:800	anti-mouse IgG, Alexa Fluor-488	Molecular Probes	1:800
Z1-domain of titin	Titin-Z1, polyclonal	Gift of S. Labeit	1:200	anti-rabbit IgG, Alexa Fluor-546	Molecular Probes	1:800

5.1.3 Bacterial strains

Bacterial strain	Company
Chemical competent TOP10 cells	Invitrogen
Epicurian Coli® XL1-Blue supercompetent cells	Stratagene
One Shot® TOP10 chemically competent <i>E. coli</i>	Invitrogen

5.1.4 Chemicals

Chemicals	Company	Place of business
Acrylamide/bis solution (29:1)	Bio-Rad	München
Agarose	Invitrogen	Carlsbad, USA
A/G PLUS-Agarose beads	Santa Cruz	Heidelberg
Ammonium persulfate (APS)	Bio-Rad	München
Ampicillin trihydrate	Serva	Heidelberg
AmpliTaq Gold® polymerase	Applied Biosystems	Carlsbad, USA
Aqua ad iniectabilia	Baxter GmbH	Unterschleißheim
Bacto™ Agar	Becton Dickinson	Heidelberg

Bacto™ Tryptone	Becton Dickinson	Heidelberg
Bacto™ Yeast extract	Becton Dickinson	Heidelberg
5-bromo-4-chloro-3-indolyl-β-D-galactopyranoside (X-Gal)	Sigma Aldrich	Taufkirchen
Bovine serum albumin (BSA)	Sigma	Taufkirchen
Bromphenol blue	Merck	Darmstadt
Calf intestinal alkaline phosphatase (CIP) with corresponding buffer	New England Biolabs	Frankfurt am Main
Calf intestinal alkaline phosphatase FastAP™	Fermentas	St. Leon-Rot
Collagenase type II	Worthington	Lakewood, USA
Complete mini-proteases inhibitor cocktail	Roche Diagnostics	Mannheim
Coomassie Brilliant Blue G-250 reagent	Bio-Rad	München
Cycloheximide	Sigma	Taufkirchen
Deoxyribonucleotide triphosphate (dNTP) mix (dATP, dCTP, dGTP, dTTP)	Applied Biosystems	Carlsbad, USA
Dimethyl sulfoxide (DMSO)	Sigma	Taufkirchen
Dithiothreitol (DTT)	Sigma	Taufkirchen
Dulbecco's modified Eagle medium (DMEM) with 4.5 g/L glucose and without pyruvate	Gibco	Carlsbad, USA
ECL plus Western blotting detection system	Amersham Biosciences	München
Emetine	Sigma	Taufkirchen
Ethidium bromide	Fluka	Oberhaching
Ethylenediaminetetraacetic acid (EDTA)	Sigma	Taufkirchen
Fast AP™	Fermentas	St. Leon-Rot
Fetal bovine or calf serum (FBS or FCS)	Biochrom	Berlin
Gene Ruler™ 100 bp, 1 kb, 1 kb plus DNA ladder;	Fermentas	St. Leon-Rot
Glycerol	Merck	Darmstadt
Glycine	Roth	Karlsruhe
Hank's balanced salt solution (HBSS),	Gibco	Carlsbad, USA

calcium/magnesium-free		
Horse serum	Biochrom	Berlin
Hydrochloric acid (HCl)	Merck	Darmstadt
4-(2-hydroxyethyl)piperazine-1-ethanesulfonic acid (HEPES)	Roth	Karlsruhe
Hygromycin	Invitrogen	Carlsbad, USA
Immunoglobulin G	Sigma	Taufkirchen
Isotonic 0.9% sodium chloride solution	Baxter GmbH	Unterschleißheim
Laminin	Roche Diagnostics	Mannheim
Loading dye, 6x	Fermentas	St. Leon-Rot
M199 with Earl's salt and L-glutamine	Gibco	Carlsbad, USA
MassRuler™ DNA ladder	Fermentas	St. Leon-Rot
Maxima Probe/ROX qPCR	Fermentas	St. Leon-Rot
Maxima SYBR green ROX qPCR Master mix	Fermentas	St. Leon-Rot
Methanol	J. T. Baker	Griesheim
MG132	Calbiochem	Darmstadt
MG262	Biomol	Hamburg
Milk powder	Roth	Karlsruhe
Minimum essential medium (MEM) with Hank's salt and L-glutamine	Gibco	Carlsbad, USA
Mowiol 4-88	Hoechst	Frankfurt
Penicillin-streptomycin	Gibco	Carlsbad, USA
PrimeStar®HS DANN polymerase	Takara	Otsu, Japan
Phosphate buffered saline (PBS)	Biochrom	Berlin
Phosphocreatine	Calbiochem	Darmstadt
Phosphocreatinekinase	Sigma	Taufkirchen
Ponceau S	Serva	Heidelberg
Potassium chloride (KCl)	Merck	Darmstadt
Potassium hydrogen carbonate (KHCO ₃)	Merck	Darmstadt

Potassium dihydrogen phosphate (KH ₂ PO ₄)	Merck	Darmstadt
Precision Plus Protein Standard™	Bio-Rad	München
Sodium chloride (NaCl)	J. T. Baker	Griesheim
Sodium dodecyl sulfate (SDS)	Roth	Karlsruhe
Sodium fluoride (NaF)	Merck	Darmstadt
Sodium hydrogen carbonate (NaHCO ₃)	Merck	Darmstadt
Sodium hydroxide (NaOH)	Merck	Darmstadt
SuperSignal® West Dura extended duration substrate	Pierce	Bonn
T4 DNA ligase with corresponding buffer	New England Biolabs	Frankfurt am Main
TaqMan® Universal PCR Master Mix	Applied Biosystems	Carlsbad, USA
Tetramethylethylenediamine (TEMED)	Bio-Rad	München
TO-PRO-3®	Molecular Probes	Carlsbad, USA
Trishydroxymethylaminomethane (Tris) base	Sigma	Taufkirchen
Tris hydrochloride (Tris-HCl)	Promega	Mannheim
Trisodium citrate dihydrate	Merck	Darmstadt
Triton X-100	Sigma	Taufkirchen
TurboFect™	Fermentas	St. Leon-Rot
Polyoxyethylene (20) sorbitan monolaurate (Tween® 20)	Sigma	Taufkirchen
Wortmannin	Sigma	Taufkirchen
Zeocin™	Invitrogen	Carlsbad, USA

5.1.5 Consumable material

Materials	Company
Blotting paper (Whatman 3MM)	Schleicher & Schuell
Cell scraper	Sarstedt AG & Co.
Cell strainer	Becton Dickinson

Coverslips (Ø 10 mm)	Glaswarenfabrik Karl Hecht KG
Cuvettes (10 x 4 x 45 mm)	Sarstedt AG & Co.
Culture flasks (T75)	Sarstedt AG & Co.
Culture plates (6-well)	Greiner Bio-One GmbH
Culture plates (12-well)	Nalge Nunc International
Falcon tubes (15 and 50 ml)	Sarstedt AG & Co.
Glassware	Schott Duran
Latex gloves	Paul Hartmann AG
Microscope slides	Paul Marienfeld GmbH
Micro tubes (1.5, 2.0 ml)	Sarstedt AG & Co.
Microtiter well plate (96-well)	Sarstedt AG & Co.
Nitrile gloves	Ansell
Nitrocellulose membrane (Protran® BA 85)	Schleicher & Schuell
Nylon membrane (Hybond N+)	Amersham Biosciences
PCR tubes	Sarstedt AG & Co.
Pipette tips (for 10, 100 and 1000 µl pipettes)	Sarstedt AG & Co.
Serological pipettes (2, 5, 10 and 25 ml)	Sarstedt AG & Co.
Serological pipettes (10 ml, wide tip)	Becton Dickinson
Sterile filter (0.22 µm)	Sarstedt AG & Co.
Snap cap	Sarstedt AG & Co.

5.1.6 Kits

Kit	Company
NucleoSpin® plasmid kit	Macherey-Nagel
NucleoBond® Xtra Maxi preparation kit	Macherey-Nagel
pEF5/FRT/V5 Directional TOPO®	Invitrogen
PureLink™ HiPure Plasmid Filter Purification kit	Invitrogen
QIAquick gel extraction kit	Qiagen

QIAquick PCR purification kit	Qiagen
SV Total RNA Isolation Kit	Promega
SuperScript™ III First-Strand Synthesis System for RT-PCR	Invitrogen

5.1.7 Laboratory equipment

Equipment	Company
Accu-jet pipetting aid	Brand GmbH
Analytical balance (GENIUS)	Sartorius AG
Benchtop centrifuge	Sarstedt AG & Co.
Blotting system (Mini Trans-Blot® cell)	Bio-Rad
Centrifuge (5810 R)	Eppendorf AG
Chemie Genius ² Bio imaging system with Gene Tools software	Syngene
Electrophoresis system (Sub-Cell GT)	Bio-Rad
Electrophoresis system (Mini PROTEAN® 3 electrophoresis cell)	Bio-Rad
Ice machine	Scotsman
Incubators (B 5050 E and Hera cell 240)	Heraeus Instruments
Incubator shaker (C25 classic)	New Brunswick Scientific
Magnetic stirrer (IKAMAG® RCT)	Janke & Kunkel GmbH
Microcentrifuge (5415 R)	Eppendorf AG
Microscope (Axiovert 25)	Zeiss
Microscope (Axiovert 200 M) with a 40x-oil objective and with a LSM 5 image system	Zeiss
Microwave	Sharp
Nano Drop spectrometer	ThermoFisher scientific
Neubauer chamber	Glaswarenfabrik Karl Hecht KG
PCR cycler (GeneAmp® PCR system 9700)	Applied Biosystems

PCR sprint thermal cycler	Thermo Hybaid
pH-meter	Knick GmbH
Pipettes (10, 100, 1000 µl)	Eppendorf AG
Portable balance (Scout™ Pro)	Ohaus
Power supply	Bio-Rad
Precision balance (Precision Advanced)	Ohaus
Spectrophotometer (Smart Spec™ 3000)	Bio-Rad
Sterile work bench (Lamin Air HB 2448)	Heraeus Instruments
Surgical instruments	Karl Hammacher GmbH
Taqman ABI Prism 7900HT sequence detection system with ABI 7900HT SDS 2.4 software	Applied Biosystems
Thermomixer comfort	Eppendorf AG
Ultra-pure water system Milli-Q plus	Millipore
Vortexer (Vibrofix VF1)	Janke & Kunkel GmbH
Water bath	GFL

5.1.8 Restriction enzymes

Enzyme with supplied buffer	Company
<i>AvrII</i>	New England Biolabs, Frankfurt am Main
<i>AvrII</i> , Fast digest	Fermentas, St. Leon Rot
<i>BamHI</i>	New England Biolabs
<i>BamHI</i> , Fast digest	Fermentas
<i>EcoRV</i>	New England Biolabs
<i>HindIII</i>	New England Biolabs
<i>KpnI</i>	New England Biolabs
<i>NdeI</i>	New England Biolabs
<i>NdeI</i> , Fast digest	Fermentas

<i>NheI</i> , Fast digest	Fermentas
<i>NotI</i> , Fast digest	Fermentas
<i>PmlI</i> , Fast digest	Fermentas
<i>SalI</i>	New England Biolabs
<i>SbfI</i>	New England Biolabs
<i>SbfI</i> , Fast digest	Fermentas
<i>SfoI</i>	New England Biolabs
<i>SpeI</i>	New England Biolabs
<i>XbaI</i> , Fast digest	Fermentas

5.1.9 Oligonucleotides

All primers and probes were designed using the the “Primer3 version 0.4.0” program, which is online available (<http://frodo.wi.mit.edu/primer3/>), and purchased from the MWG Biotech AG. Human *MYBPC3* and GAPDH primers and probes were designed according to the NCBI gene accession numbers Y10129 and NM_002046.3, respectively. Mouse *Mybpc3* and GalphaS (GNAS) primers and probes were designed according to the NCBI gene accession numbers NC_000068.6 and NM_022000.2, respectively.

All antisense oligoribonucleotides (AON) were designed using the “ESE finder 3.0” program (Krainer Lab and Zhang Lab), which is online available (http://rulai.cshl.edu/cgi-bin/tools/ESE3/ese_finder.cgi?process=home) and purchased from Eurogentec.

5.1.9.1 *MYBPC3* primers and probes

Primers for directional TOPO® cloning (5' to 3'):

WT forward: CACCATGGAGCAAAAAGCTTATTAGCGAGGAAGATCTG

WT reverse: AGGGCTCAGCCACTGACTT

Primers for site-directed mutagenesis (5' to 3'):

Mut-2 forward: CTTTATCCCCAGACCAgTG

Mut-2 reverse: TGAGGGTACAGCAiCTGGTC

Mut-1 forward: CAGGAGTGagtGTTcACCGTCTT

Mut-1 reverse: CAAGACGGTGAACcactCACT CC

Primers for RT-PCR (5' to 3'):

Exon 30 forward: AGCTCTGGGGGTACACAGT

Exon 31 forward: TGGTTGGCTTTAGTGACAGA

Exon 31 reverse: GAAGACGCGGAAGTAGTAGC
Exon 32 reverse: GCCTCGGAGAAGTCCAG
human GAPDH forward: CCTCAAGATCATCAGCAATGCC
human GAPDH reverse: ATGTTCTGGAGAGCCCCGC

pEF5/FRT/V5 primers for RT-PCR (5' to 3'):

Hygromycin forward: TGTCGGCGTACACAAAT
SV40 reverse: TGAGTTTGGACAAACCACAAC

pEF5/FRT/V5 primers for sequencing (5' to 3'):

T7 forward: TAATACGACTCACTATAGGG
BGH reverse: TAGAAGGCACAGTCGAGG

Primers and probe for RT-qPCR:

Exon 32 forward: GAACCGCTCGGTCATC
Exon 33 reverse: AGAGTCAACACTCCCTGCTT
Probe exon 32/exon 33: FAM-TAGCCCCAAGCCCAAGATTTC-TAMRA

Human GAPDH forward: ATGTTTCGTCATGGGTGTGAA
Human GAPDH reverse: TGAGTCCTTCCACGATACCA
Probe human GAPDH: FAM-CAGCCTCAAGATCATCAGCAATGC-TAMRA

GFP forward: GAG CAA GGG CGA GGA GCT GTT C
GFP reverse: ATG AAC TTC AGG GTC AGC TT
Probe GFP: ACG TAA ACG GCC ACA AGT TC

5.1.9.2 *Mybpc3* primers and probes

Primers for RT-PCR (5' to 3'):

Exon 4 forward: TCTCGGTAACCCAGGATGG
Exon 7 reverse: GCTGATCTGAGGTCCAGGTCT

Exon 4 forward: TCTTTCTGATGCGACCACAG
Exon 9 reverse: TCCAGAGTCCCAGCATCTTC

murine GAPDH forward: ATTCAACGGCACAGTCAAG
murine GAPDH forward: TGGCTCCACCCTTCAAGT

Primers and probe for RT-qPCR:

Mutant-1 forward: GTGTCTACCAAGGACAAATTTGACA

Mutant-1 reverse: GCTGATCTGAGGTCCAGGTCT

Probe variant-1: VIC-CTCACTGTCCATAAGG-MGB

Variant-4 forward: TCTCGGTAACCCAGGATGG

Variant-4 reverse: GCTGATCTGAGGTCCAGGTCT

Probe variant-4: FAM-TGAGGTGACCGTGGAGGCCAT-TAMRA

GalphaS forward: CAAGGCTCTGTGGGAGGA

GalphaS reverse: CGAAGCAGGTCCCTGGTCACT

Probe for GalphaS: FAM-GCTGATTGACTGTGCCCACTTTCCT-TAMRA

Primers for SYBR green:

Exon 2 forward: GATGCGAGCCCTGATGAC

Exon 3 reverse: GACTTGAGACACTTTCTTCC

5.1.9.3 Antisense oligoribonucleotide sequences

(Cy3-)AON-5 (5' to 3'): (Cy3-)CCAGCCACUCGGGCUGAGAAGACAA

AON-6 (5' to 3'): AAGUGGUCUGAGCAUCUGUGAUGUG

Scrambled AON (5' to 3'): GGAACACGCCACGCGACCGUUGAAA

5.1.10 Vectors

Vector	Company
pEF5/FRT/V5	New England Biolabs, Frankfurt am Main
pOG44	Fermentas, St. Leon Rot
pGG2	Gift of Dr. Louis Garcia, Paris

5.2 Protein and DNA markers

For Western blot analysis the Precision Plus Protein™ Standard (BIO-RAD) was used (Figure 5.2 (A)). The utilized marker for all PCR runs was the Gene Ruler™ 1 kb DNA Ladder or 100 bp DNA Ladder (Fermentas; see Figure 5.2 (B) and (C)).

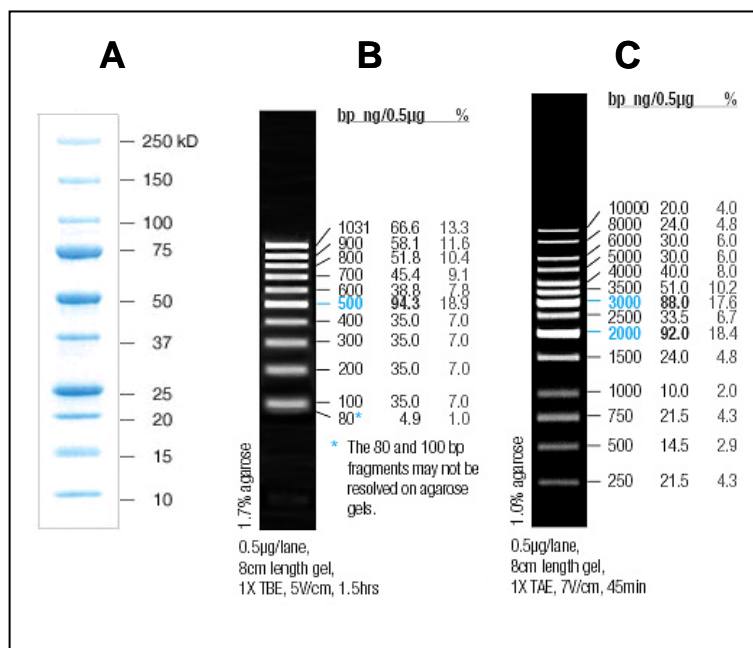


Figure 5.1. Markers.

(A) Precision Plus Protein™ Standards, BIO-RAD. (B) Gene Ruler™ 100 bp DNA Ladder, Fermentas. (C) Gene Ruler™ 1 kb DNA Ladder, Fermentas.

5.3 List of abbreviations

A	Ampere
Aa	Amino acid
ADP	Adenosine diphosphate
AON	Antisense oligoribonucleotide
AraC	Arabinofuranosyl cytidine
APS	Ammonium persulphate
ATP	Adenosine triphosphate
AU	Arbitrary unit
bp	Base pair(s)
MHC	β-myosin light chain
BSA	Bovine serum albumin
°C	Degree Celsius
cDNA	Complementary deoxyribonucleic acid

CSQ	Calsequestrin
C _t	Threshold Cycle
Cy3	Cyanine-3
D	Day
Da	Dalton
DMEM	Dulbecco's Modified Eagle's Medium
DMSO	Dimethyl sulfoxide
DNA	Deoxyribonucleic acid
dNTP	Deoxynucleoside triphosphate
DTT	Dithiothreitol
ECL	Enhanced chemiluminescence
EDTA	Ethylene diamine tetraacetic acid
e.g.	<i>exempli gratia</i> (for example)
EGFP	Enhanced green fluorescent protein
<i>et al.</i>	<i>et alii</i> (and others)
ESE	Exonic splicing enhancer
ESS	Exonic splicing silencer
FAM	Carboxyfluorescein
FCS	Foetal calf serum
g	Gram
GAPDH	Glyceraldehyde 3-phosphate dehydrogenase
GFP	Green fluorescent protein
h	Hour
HCM	Hypertrophic cardiomyopathy
HBSS	Hank's Balanced Salt Solution
HEK	Human embryonic kidney cells
HEPES	4-(2-Hydroxyethyl)-1-piperazineethanesulfonic acid
Het	Heterozygous
Hz	Hertz
i.e.	<i>id est</i> (that is)
IgG	Immunoglobulin G
Inc.	Incorporation
kb	Kilobase
kDa	Kilo Dalton
KI	Knock-in
KO	Knock-out
l	Liter
m	Milli- (1 x 10 ⁻³)
M	Molar
mA	Milliampere

mg	Milligram
min	Minutes
ml	Milliliter
mM	Millimolar
µg	Microgram
µl	Microliter
µM	Micromolar
MOI	Multiplicity of infection
Mut	Mutant
MW	Molecular weight
mRNA	Messenger ribonucleic acid
MyBP-C	Myosin-binding protein-C
c MyBP-C	Cardiac Myosin-binding protein-C
<i>MYBPC3</i>	human cMyBP-C gene
<i>Mybpc3</i>	mouse cMyBP-C gene
µ	Micro (1×10^{-6})
N	Amino-
NaF	Sodium fluoride
NaOH	Sodium hydroxide
NCBI	National Center for Biotechnology Information
NIH	National Institutes of Health
nm	Nanometer
nM	Nanomolar
NMCM	Neonatal mouse cardiac myocytes
NMD	Nonsense-mediated mRNA decay
no.	Number
oligo(dT)	Oligodeoxythymidylic acid
2OMePS	2- <i>O</i> -methyl phosphorothioate
ORF	Open reading frame
P _i	Anorganic phosphat
PAGE	Polyacrylamide gel electrophoresis
PBS	Phosphate buffered saline
PCR	Polymerase chain reaction
PTC	Premature termination codon
RNA	Ribonucleic acid
rpm	Rotation per minute
RT	Room temperature
RT-PCR	Reverse transcriptase-PCR
SD	Standard deviation
SDS	Sodium dodecyl sulfate

sec	Seconds
SEM	Standard error of the mean
TAE	Tris acetate EDTA
TAMRA	Tetramethylrhodamine
TBS	Tris buffered saline
TBS-T	Tris buffered saline with tween-20
TEMED	N, N, N', N'-Tetramethylethylenediamine
Tm	Tropomyosin
Tn	Troponin
TO-PRO-3	Quinolinium,4-[3-(3-methyl-2(3H)-benzothiazolydene)-1-propenyl]-1-[3-(trimethylammonio)propyl]-,diiodide
Tris	Tris-(hydroxymethyl)-aminoethane
U	Unit
UPS	Ubiquitin-proteasome system
UV	Ultraviolet
V	Voltage
Var	Variant
vs.	Versus
wks	Weeks
WT	Wild type

Nucleotide bases

A	Adenine	G	Guanine
C	Cytosine	T	Thymine
U	Uracil		

Amino acids

Ala (A) Alanine	Leu (L) Leucine
Arg (R) Arginine	Lys (K) Lysine
Asn (N) Asparagine	Met (M) Methionine
Asp (D) Aspartic acid	Phe (F) Phenylalanine
Cys (C) Cysteine	Pro (P) Proline
Gln (Q) Glutamine	Ser (S) Serine
Glu (E) Glutamic acid	Thr (T) Threonine
Gly (G) Glycine	Trp (W) Tryptophan
His (H) Histidine	Tyr (Y) Tyrosine
Ile (I) Isoleucine	Val (V) Valine

6 Literature

- Aartsma-Rus, A., M. Bremmer-Bout, et al. (2002). "Targeted exon skipping as a potential gene correction therapy for Duchenne muscular dystrophy." *Neuromuscul Disord* **12 Suppl 1**: S71-77.
- Aartsma-Rus, A., A. A. Janson, et al. (2004). "Antisense-induced multiexon skipping for Duchenne muscular dystrophy makes more sense." *Am J Hum Genet* **74**(1): 83-92.
- Aartsma-Rus, A. and G. J. van Ommen (2010). "Progress in therapeutic antisense applications for neuromuscular disorders." *Eur J Hum Genet* **18**(2): 146-153.
- Adelstein, R. S. (1983). "Regulation of contractile proteins by phosphorylation." *J Clin Invest* **72**(6): 1863-1866.
- Aktories K., Förstermann U., Hofmann F., Starke K. (2009). "Allgemeine und spezielle Pharmakologie und Toxikologie", Elsevier, 10. circulation: 413-415.
- Alcalai, R., J. G. Seidman, et al. (2008). "Genetic basis of hypertrophic cardiomyopathy: from bench to the clinics." *J Cardiovasc Electrophysiol* **19**(1): 104-110.
- Andersen, P. S., O. Havndrup, et al. (2004). "Genetic and phenotypic characterization of mutations in myosin-binding protein C (MYBPC3) in 81 families with familial hypertrophic cardiomyopathy: total or partial haploinsufficiency." *Eur J Hum Genet* **12**(8): 673-677.
- Bahrudin, U., H. Morisaki, et al. (2008). "Ubiquitin-proteasome system impairment caused by a missense cardiac myosin-binding protein C mutation and associated with cardiac dysfunction in hypertrophic cardiomyopathy." *J Mol Biol* **384**(4): 896-907.
- Baralle, M., D. Baralle, et al. (2003). "Identification of a mutation that perturbs NF1 gene splicing using genomic DNA samples and a minigene assay." *J Med Genet* **40**(3): 220-222.
- Barefield, D. and S. Sadayappan (2010). "Phosphorylation and function of cardiac myosin binding protein-C in health and disease." *J Mol Cell Cardiol* **48**(5): 866-875.
- Barnard, D. C., J. Li, et al. (2002). "Regulation of alternative splicing by SRp86 through coactivation and repression of specific SR proteins." *Rna* **8**(4): 526-533.
- Bennett, P., R. Craig, et al. (1986). "The ultrastructural location of C-protein, X-protein and H-protein in rabbit muscle." *J. Muscle Res. Cell Motil.* **7**: 550-567.
- Bourgeois, C. F., F. Lejeune, et al. (2004). "Broad specificity of SR (serine/arginine) proteins in the regulation of alternative splicing of pre-messenger RNA." *Prog Nucleic Acid Res Mol Biol* **78**: 37-88.
- Bradford, M. M. (1976). "A rapid and sensitive method for the quantitation of microgram quantities of protein utilizing the principle of protein-dye binding." *Anal Biochem* **72**: 248-254.
- Carrier, L. (2007). "Cardiac myosin-binding protein C in the heart." *Arch Mal Coeur Vaiss* **100**(3): 238-243.
- Carrier, L., G. Bonne, et al. (1997). "Organization and sequence of human cardiac myosin binding protein C gene (MYBPC3) and identification of mutations predicted to produce truncated proteins in familial hypertrophic cardiomyopathy." *Circ Res* **80**: 427-434.
- Carrier, L., S. Schlossarek, et al. (2010). "The ubiquitin-proteasome system and nonsense-mediated mRNA decay in hypertrophic cardiomyopathy." *Cardiovasc Res* **85**(2): 330-338.
- Cartegni, L., S. L. Chew, et al. (2002). "Listening to silence and understanding nonsense: exonic mutations that affect splicing." *Nat Rev Genet* **3**(4): 285-298.
- Cartegni, L., J. Wang, et al. (2003). "ESEfinder: A web resource to identify exonic splicing enhancers." *Nucleic Acids Res* **31**(13): 3568-3571.
- Carter, M. S., J. Doskow, et al. (1995). "A regulatory mechanism that detects premature nonsense codons in T-cell receptor transcripts in vivo is reversed by protein synthesis inhibitors in vitro." *J Biol Chem* **270**(48): 28995-29003.
- Chang, Y. F., J. S. Imam, et al. (2007). "The nonsense-mediated decay RNA surveillance pathway." *Annu Rev Biochem* **76**: 51-74.
- Charron, P., O. Dubourg, et al. (1998). "Clinical features and prognostic implications of familial hypertrophic cardiomyopathy related to the cardiac myosin-binding protein C gene." *Circulation* **97**(22): 2230-2236.
- Ciechanover, A. and P. Brundin (2003). "The ubiquitin proteasome system in neurodegenerative diseases: sometimes the chicken, sometimes the egg." *Neuron* **40**(2): 427-446.
- Clark, D. P. (2006). "Molecular biology", Elsevier, 1. circulation: 310-312.
- Colson, B. A., T. Bekyarova, D. P. Fitzsimons, T. C. Irving & R. L. Moss (2007) Radial displacement of myosin cross-bridges in mouse myocardium due to ablation of myosin binding protein-C. *J Mol Biol*, 367, 36-41.

- Colson, B. A., M. R. Locher, et al. (2010). "Differential roles of regulatory light chain and myosin binding protein-C phosphorylations in the modulation of cardiac force development." *J Physiol* **588**(Pt 6): 981-993.
- Craig, R. and G. Offer (1976). "The localization of C-protein in rabbit skeletal muscle." *Proc. Royal. Soc. Lond.* **B192**: 451-454.
- Crooke, R. M., M. J. Graham, et al. (1995). "In vitro pharmacokinetics of phosphorothioate antisense oligonucleotides." *J Pharmacol Exp Ther* **275**(1): 462-473.
- Crooke, R. M., M. J. Graham, et al. (2000). "Metabolism of antisense oligonucleotides in rat liver homogenates." *J Pharmacol Exp Ther* **292**(1): 140-149.
- Cuello, F., S. C. Bardswell, et al. (2010). "A novel role for p90 ribosomal S6 kinase in the regulation of cardiac myofilament phosphorylation." *J Biol Chem.*
- Czaplinski, K., M. J. Ruiz-Echevarria, et al. (1998). "The surveillance complex interacts with the translation release factors to enhance termination and degrade aberrant mRNAs." *Genes Dev* **12**(11): 1665-1677.
- Deinum, J., J. M. van Gool, et al. (2001). "Angiotensin II type 2 receptors and cardiac hypertrophy in women with hypertrophic cardiomyopathy." *Hypertension* **38**(6): 1278-1281.
- Dias, N. and C. A. Stein (2002). "Antisense oligonucleotides: basic concepts and mechanisms." *Mol Cancer Ther* **1**(5): 347-355.
- DiMarco, J. P. (2003). "Implantable cardioverter-defibrillators." *N Engl J Med* **349**(19): 1836-1847.
- Dominski, Z. and R. Kole (1993). "Restoration of correct splicing in thalassemic pre-mRNA by antisense oligonucleotides." *Proc Natl Acad Sci U S A* **90**(18): 8673-8677.
- Dreumont, N., S. Hardy, et al. (2010). "Antagonistic factors control the unproductive splicing of SC35 terminal intron." *Nucleic Acids Res* **38**(4): 1353-1366.
- Dreyfuss, G., V. N. Kim, et al. (2002). "Messenger-RNA-binding proteins and the messages they carry." *Nat Rev Mol Cell Biol* **3**(3): 195-205.
- Dujardin, G., D. Commandeur, et al. (2011). "Splicing defects in the CFTR gene: Minigene analysis of two mutations, 1811+1G>C and 1898+3A>G." *J Cyst Fibros.*
- Eder, P. S., R. J. DeVine, et al. (1991). "Substrate specificity and kinetics of degradation of antisense oligonucleotides by a 3' exonuclease in plasma." *Antisense Res Dev* **1**(2): 141-151.
- Fischel-Ghodsian, N. (2005). "Genetic factors in aminoglycoside toxicity." *Pharmacogenomics* **6**(1): 27-36.
- Flashman, E., C. Redwood, et al. (2004). "Cardiac myosin binding protein C: its role in physiology and disease." *Circ Res* **94**(10): 1279-1289.
- Fougerousse, F., A. L. Delezoide, et al. (1998). "Cardiac myosin binding protein C gene is specifically expressed in heart during murine and human development." *Circ Res* **82**(1): 130-133.
- Freiburg, A. and M. Gautel (1996). "A molecular map of the interactions between titin and myosin-binding protein C. Implications for sarcomeric assembly in familial hypertrophic cardiomyopathy." *Eur J Biochem* **235**(1-2): 317-323.
- Friedrich, F. W., P. Bausero, et al. (2009). "A new polymorphism in human calmodulin III gene promoter is a potential modifier gene for familial hypertrophic cardiomyopathy." *Eur Heart J* **30**(13): 1648-1655.
- Fukushige, S. and B. Sauer (1992). "Genomic targeting with a positive-selection lox integration vector allows highly reproducible gene expression in mammalian cells." *Proc Natl Acad Sci U S A* **89**(17): 7905-7909.
- Gautel, M., D. O. Furst, et al. (1998). "Isoform transitions of the myosin binding protein C family in developing human and mouse muscles: lack of isoform transcomplementation in cardiac muscle." *Circ Res* **82**(1): 124-129.
- Gautel, M., O. Zuffardi, et al. (1995). "Phosphorylation switches specific for the cardiac isoform of myosin binding protein-C: a modulator of cardiac contraction?" *Embo J* **14**(9): 1952-1960.
- Gil, A., P. A. Sharp, et al. (1991). "Characterization of cDNAs encoding the polypyrimidine tract-binding protein." *Genes Dev* **5**(7): 1224-1236.
- Goemans, N. M., M. Tulinus, et al. (2011). "Systemic administration of PRO051 in Duchenne's muscular dystrophy." *N Engl J Med* **364**(16): 1513-1522.
- Gong, Q., L. Zhang, et al. (2007). "Nonsense mutations in hERG cause a decrease in mutant mRNA transcripts by nonsense-mediated mRNA decay in human long-QT syndrome." *Circulation* **116**(1): 17-24.
- Goyenvallé, A., A. Vulin, et al. (2004). "Rescue of dystrophic muscle through U7 snRNA-mediated exon skipping." *Science* **306**(5702): 1796-1799.
- Graham, F. L., J. Smiley, et al. (1977). "Characteristics of a human cell line transformed by DNA from human adenovirus type 5." *J Gen Virol* **36**(1): 59-74.

- Graveley, B. R., K. J. Hertel, et al. (2001). "The role of U2AF35 and U2AF65 in enhancer-dependent splicing." *RNA* **7**(6): 806-818.
- Gregorio, C. C., H. Granzier, et al. (1999). "Muscle assembly: a titanic achievement?" *Curr Opin Cell Biol* **11**(1): 18-25.
- Gruen, M. and M. Gautel (1999). "Mutations in beta-myosin S2 that cause familial hypertrophic cardiomyopathy (FHC) abolish the interaction with the regulatory domain of myosin binding protein-C." *J Mol Biol* **286**: 933-949.
- Gruen, M., H. Prinz, et al. (1999). "cAPK-phosphorylation controls the interaction of the regulatory domain of cardiac myosin binding protein C with myosin-S2 in an on-off fashion." *FEBS Lett.* **453**: 254-259.
- Hacihanefioglu, A., P. Tarkun, et al. (2008). "Acute severe cardiac failure in a myeloma patient due to proteasome inhibitor bortezomib." *Int J Hematol* **88**(2): 219-222.
- Hedhli, N. and C. Depre (2010). "Proteasome inhibitors and cardiac cell growth." *Cardiovasc Res* **85**(2): 321-329.
- Hentze, M. W. and A. E. Kulozik (1999). "A perfect message: RNA surveillance and nonsense-mediated decay." *Cell* **96**(3): 307-310.
- Herrmann, J., A. Ciechanover, et al. (2004). "The ubiquitin-proteasome system in cardiovascular diseases—a hypothesis extended." *Cardiovasc Res* **61**(1): 11-21.
- Hirawat, S., E. M. Welch, et al. (2007). "Safety, tolerability, and pharmacokinetics of PTC124, a nonaminoglycoside nonsense mutation suppressor, following single- and multiple-dose administration to healthy male and female adult volunteers." *J Clin Pharmacol* **47**(4): 430-444.
- Hofmann, P. A., M. L. Greaser, et al. (1991). "C-protein limits shortening velocity of rabbit skeletal muscle fibres at low levels of Ca²⁺ activation." *J Physiol* **439**: 701-715.
- Ishigaki, Y., X. Li, et al. (2001). "Evidence for a pioneer round of mRNA translation: mRNAs subject to nonsense-mediated decay in mammalian cells are bound by CBP80 and CBP20." *Cell* **106**(5): 607-617.
- Kass, D. A. and R. J. Solaro (2006). "Mechanisms and use of calcium-sensitizing agents in the failing heart." *Circulation* **113**(2): 305-315.
- Kinali, M., V. Arechavala-Gomez, et al. (2009). "Local restoration of dystrophin expression with the morpholino oligomer AVI-4658 in Duchenne muscular dystrophy: a single-blind, placebo-controlled, dose-escalation, proof-of-concept study." *Lancet Neurol* **8**(10): 918-928.
- Kozak, M. (1987). "An analysis of 5'-noncoding sequences from 699 vertebrate messenger RNAs." *Nucleic Acids Res* **15**(20): 8125-8148.
- Kulikovskaya, I., G. McClellan, et al. (2003). "Effect of MyBP-C binding to actin on contractility in heart muscle." *J Gen Physiol* **122**(6): 761-774.
- Kulikovskaya, I., G. B. McClellan, et al. (2007). "Multiple forms of cardiac myosin-binding protein C exist and can regulate thick filament stability." *J Gen Physiol* **129**(5): 419-428.
- Labeit, S., M. Gautel, et al. (1992). "Towards a molecular understanding of titin." *EMBO J.* **11**: 1711-1716.
- Laemmli, U. K. (1970). "Cleavage of structural proteins during the assembly of the head of bacteriophage T4." *Nature* **227**: 680-685.
- Laugwitz, K. L., A. Moretti, et al. (2005). "Postnatal Isl1+ cardioblasts enter fully differentiated cardiomyocyte lineages." *Nature* **433**(7026): 647-653.
- Lavigne, A., H. La Branche, et al. (1993). "A splicing enhancer in the human fibronectin alternate ED1 exon interacts with SR proteins and stimulates U2 snRNP binding." *Genes Dev* **7**(12A): 2405-2417.
- Le Roy, F., K. Charton, et al. (2009). "RNA-targeting approaches for neuromuscular diseases." *Trends Mol Med* **15**(12): 580-591.
- Lejeune, F., Y. Ishigaki, et al. (2002). "The exon junction complex is detected on CBP80-bound but not eIF4E-bound mRNA in mammalian cells: dynamics of mRNP remodeling." *EMBO J* **21**(13): 3536-3545.
- Levine, B. and G. Kroemer (2008). "Autophagy in the pathogenesis of disease." *Cell* **132**(1): 27-42.
- Linke, W. A., D. E. Rudy, et al. (1999). "I-band titin in cardiac muscles is a three-element molecular spring and is critical for maintaining thin filament structure." *J. Cell. Biol.* **146**: 631-644.
- Linke, W. A. (2000). "Stretching molecular springs: elasticity of titin filaments in vertebrate striated muscle." *Histol Histopathol* **15**(3): 799-811.
- Liu, W., Y. Xiong, et al. (2006). "Stability and homogeneity of transgene expression in isogenic cells." *J Mol Med* **84**(1): 57-64.
- Long, J. C. and J. F. Caceres (2009). "The SR protein family of splicing factors: master regulators of gene expression." *Biochem J* **417**(1): 15-27.

- Lottspeich F. and Engels J. W. (2006). "Bioanalytik", Elsevier, 2. circulation: 649.
- Luther, P. K., P. M. Bennett, et al. (2008). "Understanding the organisation and role of myosin binding protein C in normal striated muscle by comparison with MyBP-C knockout cardiac muscle." *J Mol Biol* **384**(1): 60-72.
- Maciolek, N. L., W. L. Alward, et al. (2006). "Analysis of RNA splicing defects in PITX2 mutants supports a gene dosage model of Axenfeld-Rieger syndrome." *BMC Med Genet* **7**: 59.
- Maquat, L. E. (1995). "When cells stop making sense: effects of nonsense codons on RNA metabolism in vertebrate cells." *RNA* **1**(5): 453-465.
- Maron, B. J., J. M. Gardin, et al. (1995). "Prevalence of hypertrophic cardiomyopathy in a general population of young adults. Echocardiographic analysis of 4111 subjects in the CARDIA Study. Coronary Artery Risk Development in (Young) Adults." *Circulation* **92**(4): 785-789.
- Maron, B. J. (2002). "Hypertrophic cardiomyopathy: a systematic review." *Jama* **287**(10): 1308-1320.
- Marston, S., O. Copeland, et al. (2009). "Evidence from human myectomy samples that MYBPC3 mutations cause hypertrophic cardiomyopathy through haploinsufficiency." *Circ Res* **105**(3): 219-222.
- Martinez-Contreras, R., P. Cloutier, et al. (2007). "hnRNP proteins and splicing control." *Adv Exp Med Biol* **623**: 123-147.
- McKeehan, W. and B. Hardesty (1969). "The mechanism of cycloheximide inhibition of protein synthesis in rabbit reticulocytes." *Biochem Biophys Res Commun* **36**(4): 625-630.
- Mearini, G., C. Gedicke, et al. (2010). "Atrogin-1 and MuRF1 regulate cardiac MyBP-C levels via different mechanisms." *Cardiovasc Res* **85**(2): 357-366.
- Mearini, G., S. Schlossarek, et al. (2008). "The ubiquitin-proteasome system in cardiac dysfunction." *Biochim Biophys Acta* **1782**(12): 749-763.
- Meiners, S., H. Dreger, et al. (2008). "Suppression of cardiomyocyte hypertrophy by inhibition of the ubiquitin-proteasome system." *Hypertension* **51**(2): 302-308.
- Mingeot-Leclercq, M. P. and P. M. Tulkens (1999). "Aminoglycosides: nephrotoxicity." *Antimicrob Agents Chemother* **43**(5): 1003-1012.
- Mitchell, G. A. (1953). "The innervation of the heart." *Br Heart J* **15**(2): 159-171.
- Miura, K., H. Nakagawa, et al. (2002). "Epidemiology of idiopathic cardiomyopathy in Japan: results from a nationwide survey." *Heart* **87**(2): 126-130.
- Moolman-Smook, J., E. Flashman, et al. (2002). "Identification of novel interactions between domains of Myosin binding protein-C that are modulated by hypertrophic cardiomyopathy missense mutations." *Circ Res* **91**(8): 704-711.
- Moolman, J. A., S. Reith, et al. (2000). "A newly created splice donor site in exon 25 of the MyBP-C gene is responsible for inherited hypertrophic cardiomyopathy with incomplete disease penetrance." *Circulation* **101**: 1396-1402.
- Mullis, K. B. and F. A. Faloona (1987). "Specific synthesis of DNA in vitro via a polymerase-catalyzed chain reaction." *Methods Enzymol* **155**: 335-350.
- Nagy, E. and L. E. Maquat (1998). "A rule for termination-codon position within intron-containing genes: when nonsense affects RNA abundance." *Trends Biochem Sci* **23**(6): 198-199.
- Nanni, L., M. Pieroni, et al. (2003). "Hypertrophic cardiomyopathy: two homozygous cases with "typical" hypertrophic cardiomyopathy and three new mutations in cases with progression to dilated cardiomyopathy." *Biochem Biophys Res Commun* **309**(2): 391-398.
- Niimura, H., L. L. Bachinski, et al. (1998). "Mutations in the gene for cardiac myosin-binding protein C and late-onset familial hypertrophic cardiomyopathy." *N. Engl. J. Med.* **338**: 1248-1257.
- O'Gorman, S., D. T. Fox, et al. (1991). "Recombinase-mediated gene activation and site-specific integration in mammalian cells." *Science* **251**(4999): 1351-1355.
- Oakley, C. E., B. D. Hambly, et al. (2004). "Myosin binding protein C: structural abnormalities in familial hypertrophic cardiomyopathy." *Cell Res* **14**(2): 95-110.
- Offer, G., C. Moos, et al. (1973). "A new protein of the thick filaments of vertebrate skeletal myofibrils: extraction, purification and characterization." *J. Mol. Biol.* **74**: 653-676.
- Okagaki, T., F. E. Weber, et al. (1993). "The major myosin-binding domain of skeletal muscle MyBP-C (C protein) resides in the COOH-terminal, immunoglobulin C2 motif." *J. Cell. Biol.* **123**: 619-626.
- Olsen, A. S., A. E. Geddis, et al. (1991). "High levels of expression of a minigene version of the human pro alpha 1 (I) collagen gene in stably transfected mouse fibroblasts. Effects of deleting putative regulatory sequences in the first intron." *J Biol Chem* **266**(2): 1117-1121.
- Olson, T. M., S. Illenberger, et al. (2002). "Metavinculin mutations alter actin interaction in dilated cardiomyopathy." *Circulation* **105**(4): 431-437.

- Osterop, A. P., M. J. Kofflard, et al. (1998). "AT1 receptor A/C1166 polymorphism contributes to cardiac hypertrophy in subjects with hypertrophic cardiomyopathy." *Hypertension* **32**(5): 825-830.
- Paillusson, A., N. Hirschi, et al. (2005). "A GFP-based reporter system to monitor nonsense-mediated mRNA decay." *Nucleic Acids Res* **33**(6): e54.
- Palmer, B. M., D. Georgakopoulos, et al. (2004). "Role of Cardiac Myosin Binding Protein C in Sustaining Left Ventricular Systolic Stiffening." *Circ Res* **94**: 1249-1255.
- Pohlmann, L., I. Kroger, et al. (2007). "Cardiac myosin-binding protein C is required for complete relaxation in intact myocytes." *Circ Res* **101**(9): 928-938.
- Ramburan, Korkie and Moolman-Smook (2010). "Cardiac myosin binding protein C, adrenergic stimulation and cardiac contractility." *SA Heart Journal*, Vol 7, No 1.
- Razumova, M. V., J. F. Shaffer, et al. (2006). "Effects of the N-terminal domains of myosin binding protein-C in an in vitro motility assay: Evidence for long-lived cross-bridges." *J Biol Chem* **281**(47): 35846-35854.
- Rehwinkel, J., J. Raes, et al. (2006). "Nonsense-mediated mRNA decay: Target genes and functional diversification of effectors." *Trends Biochem Sci* **31**(11): 639-646.
- Richard, P., P. Charron, et al. (2003). "Hypertrophic Cardiomyopathy: Distribution of disease genes, spectrum of mutations and implications for molecular diagnosis strategy." *Circulation* **107**: 2227-2232.
- Richard, P., E. Villard, et al. (2006). "The genetic bases of cardiomyopathies." *J Am Coll Cardiol* **48**(9 Suppl): A79-89.
- Richardson, P., W. McKenna, et al. (1996). "Report of the 1995 World Health Organisation/International Society and Federation of Cardiology task force on the definition and classification of cardiomyopathies." *Circulation* **93**: 841-842.
- Rome, E., G. Offer, et al. (1973). "X-ray diffraction of muscle labelled with antibody to C-protein." *Nat New Biol* **244**(135): 152-154.
- Rottbauer, W., M. Gautel, et al. (1997). "Novel splice donor site mutation in the cardiac myosin-binding protein-C gene in familial hypertrophic cardiomyopathy. Characterization of cardiac transcript and protein." *J Clin Invest* **100**: 475-482.
- Roy, S., M. Rached, et al. (2007). "Differential regulation of the human adrenocorticotropin receptor [melanocortin-2 receptor (MC2R)] by human MC2R accessory protein isoforms alpha and beta in isogenic human embryonic kidney 293 cells." *Mol Endocrinol* **21**(7): 1656-1669.
- Sadayappan, S., J. Gulick, et al. (2005). "Cardiac myosin-binding protein-C phosphorylation and cardiac function." *Circ Res* **97**(11): 1156-1163.
- Sadayappan, S., H. Osinska, et al. (2006). "Cardiac myosin binding protein c phosphorylation is cardioprotective." *Proc Natl Acad Sci U S A* **103**(45): 16918-16923.
- Sanchez, L., D. Vasquez, et al. (1977). "Genetics and biochemistry of cryptopleurine resistance in the yeast *Saccharomyces cerevisiae*." *Mol Gen Genet* **156**(3): 319-326.
- Sarikas, A., L. Carrier, et al. (2005). "Impairment of the ubiquitin-proteasome system by truncated cardiac myosin binding protein C mutants." *Cardiovasc Res* **66**(1): 33-44.
- Sauer, B. (1994). "Site-specific recombination: developments and applications." *Curr Opin Biotechnol* **5**(5): 521-527.
- Schlossarek, S. and L. Carrier (2011). "The ubiquitin-proteasome system in cardiomyopathies." *Curr Opin Cardiol* **26**(3): 190-195.
- Schlossarek, S., G. Mearini, et al. (2011). "Cardiac myosin-binding protein C in hypertrophic cardiomyopathy: mechanisms and therapeutic opportunities." *J Mol Cell Cardiol* **50**(4): 613-620.
- Schneider-Poetsch, T., J. Ju, et al. (2010). "Inhibition of eukaryotic translation elongation by cycloheximide and lactimidomycin." *Nat Chem Biol* **6**(3): 209-217.
- Schulte, H. D., H. Gramsch-Zabel, et al. (1999). "[Hypertrophic cardiomyopathy (HCM). Surgical versus drug therapy]." *Z Kardiol* **88**(3): 163-172.
- Shaw, G., S. Morse, et al. (2002). "Preferential transformation of human neuronal cells by human adenoviruses and the origin of HEK 293 cells." *FASEB J* **16**(8): 869-871.
- Smith, C. W. and J. Valcarcel (2000). "Alternative pre-mRNA splicing: the logic of combinatorial control." *Trends Biochem Sci* **25**(8): 381-388.
- Smith, P. J., C. Zhang, et al. (2006). "An increased specificity score matrix for the prediction of SF2/ASF-specific exonic splicing enhancers." *Hum Mol Genet* **15**(16): 2490-2508.
- Solaro, R. J., K. A. Sheehan, et al. (2010). "The curious role of sarcomeric proteins in control of diverse processes in cardiac myocytes." *J Gen Physiol* **136**(1): 13-19.
- Spirito, P., P. Bellone, et al. (2000). "Magnitude of left ventricular hypertrophy and risk of sudden death in hypertrophic cardiomyopathy." *N. Engl. J. Med.* **342**: 1778-1785.

- Squire, J. M., P. K. Luther, et al. (2003). "Structural evidence for the interaction of C-protein (MyBP-C) with actin and sequence identification of a possible actin-binding domain." *J Mol Biol* **331**(3): 713-724.
- Stelzer, J. E., J. R. Patel, et al. (2007). "Differential roles of cardiac myosin-binding protein C and cardiac troponin I in the myofibrillar force responses to protein kinase A phosphorylation." *Circ Res* **101**(5): 503-511.
- Sugden, B., B. De Troy, et al. (1975). "Agarose slab-gel electrophoresis equipment." *Anal Biochem* **68**(1): 36-46.
- Tan, Y., M. R. Demeter, et al. (2000). "BAD Ser-155 phosphorylation regulates BAD/Bcl-XL interaction and cell survival." *J Biol Chem* **275**(33): 25865-25869.
- Tanaka, K., T. Yoshimura, et al. (1988). "Proteasomes (multi-protease complexes) as 20 S ring-shaped particles in a variety of eukaryotic cells." *J Biol Chem* **263**(31): 16209-16217.
- Teare, D. (1958). "Asymmetrical hypertrophy of the heart in young adults." *Br. Heart. J.* **20**: 1-8.
- Tesson, F., C. Dufour, et al. (1997). "The influence of the angiotensin I converting enzyme genotype in familial hypertrophic cardiomyopathy varies with the disease gene mutation." *J. Mol. Cell. Cardiol.* **29**: 831-838.
- Uetsuki, T., A. Naito, et al. (1989). "Isolation and characterization of the human chromosomal gene for polypeptide chain elongation factor-1 alpha." *J Biol Chem* **264**(10): 5791-5798.
- Usuki, F., A. Yamashita, et al. (2006). "Specific inhibition of nonsense-mediated mRNA decay components, SMG-1 or Upf1, rescues the phenotype of Ullrich disease fibroblasts." *Mol Ther* **14**(3): 351-360.
- Valencia-Sanchez, M. A., J. Liu, et al. (2006). "Control of translation and mRNA degradation by miRNAs and siRNAs." *Genes Dev* **20**(5): 515-524.
- van Deutekom, J. C., A. A. Janson, et al. (2007). "Local dystrophin restoration with antisense oligonucleotide PRO051." *N Engl J Med* **357**(26): 2677-2686.
- van Dijk, S. J., D. Dooijes, et al. (2009). "Cardiac myosin-binding protein C mutations and hypertrophic cardiomyopathy: haploinsufficiency, deranged phosphorylation, and cardiomyocyte dysfunction." *Circulation* **119**(11): 1473-1483.
- Van Driest, S. L., V. C. Vasile, et al. (2004). "Myosin binding protein C mutations and compound heterozygosity in hypertrophic cardiomyopathy." *J Am Coll Cardiol* **44**(9): 1903-1910.
- Vignier, N., S. Schlossarek, et al. (2009). "Nonsense-mediated mRNA decay and ubiquitin-proteasome system regulate cardiac myosin-binding protein C mutant levels in cardiomyopathic mice." *Circ Res* **105**(3): 239-248.
- Wakabayashi, K., H. Nakagawa, et al. (2006). "Identification of cysteine residues critically involved in homodimer formation and protein expression of human ATP-binding cassette transporter ABCG2: a new approach using the flp recombinase system." *J Exp Ther Oncol* **5**(3): 205-222.
- Wang, L., J. G. Seidman, et al. (2010). "Narrative review: harnessing molecular genetics for the diagnosis and management of hypertrophic cardiomyopathy." *Ann Intern Med* **152**(8): 513-520, W181.
- Wang, Q., H. Yin, et al. (2010). "In vitro evaluation of novel antisense oligonucleotides is predictive of in vivo exon skipping activity for Duchenne muscular dystrophy." *J Gene Med* **12**(4): 354-364.
- Weiss, J. N., M. Nivala, et al. (2011). "Alternans and arrhythmias: from cell to heart." *Circ Res* **108**(1): 98-112.
- Wilkinson, K. D. (1999). "Ubiquitin-dependent signaling: the role of ubiquitination in the response of cells to their environment." *J Nutr* **129**(11): 1933-1936.
- Wilschanski, M., L. L. Miller, et al. (2011). "Chronic ataluren (PTC124) treatment of nonsense mutation cystic fibrosis." *Eur Respir J.*
- Wilschanski, M., Y. Yahav, et al. (2003). "Gentamicin-induced correction of CFTR function in patients with cystic fibrosis and CFTR stop mutations." *N Engl J Med* **349**(15): 1433-1441.
- Wilton, S. D., A. M. Fall, et al. (2007). "Antisense oligonucleotide-induced exon skipping across the human dystrophin gene transcript." *Mol Ther* **15**(7): 1288-1296.
- Yoo, B. H., E. Bochkareva, et al. (2004). "2'-O-methyl-modified phosphorothioate antisense oligonucleotides have reduced non-specific effects in vitro." *Nucleic Acids Res* **32**(6): 2008-2016.
- Yu, B., J. A. French, et al. (1998). "Molecular pathology of familial hypertrophic cardiomyopathy caused by mutations in the cardiac myosin binding protein C gene." *J. Med. Genet.* **35**: 205-210.
- Zamecnik, P. C. and M. L. Stephenson (1978). "Inhibition of Rous sarcoma virus replication and cell transformation by a specific oligodeoxynucleotide." *Proc Natl Acad Sci U S A* **75**(1): 280-284.
- Zolk, O., C. Schenke, et al. (2006). "The ubiquitin-proteasome system: focus on the heart." *Cardiovasc Res* **70**(3): 410-421.

7 Acknowledgement

First of all I would like to thank Prof. Dr. med. Thomas Eschenhagen, who gave me the opportunity to perform my Ph.D. research in the Department of Experimental Pharmacology and Toxicology of the University Medical Center Hamburg-Eppendorf. Furthermore I thank Prof. Dr. Wolfgang Streit from the Biocenter Klein Flottbek, University of Hamburg, for accepting the supervision of my Ph.D. thesis.

I am very grateful to Prof. Dr. Lucie Carrier for providing me two projects, which were both challenging and suspenseful. I am thankful for her scientific guidance, support, encouragement and inspiring motivation during all the time. Thank you Lucie!!!

I am also very thankful to Dr. Kent Duncan, who corrected this thesis from the viewpoint of a native speaker.

Moreover, I would like to thank Dr. Patrick Dreyfus and Dr. Stéphanie Lorain (Paris, France) for their cooperative work and support in all questions of exon skipping. Furthermore I thank Dr. Sakthivel Sadayappan (Chicago, IL) for the anti-cMyBP-C antibody he sent us.

Thanks to the whole Institute of Pharmacology for the wonderful working atmosphere and its helpful cooperative colleagues. I thank particularly the members of the research group of Lucie Carrier (Elisabeth Krämer, Dr. Saskia Schlossarek, Dr. Giulia Mearini, Doreen Khajetoorians, Birgit Geertz and especially Silke Reischmann, Verena Behrens and Felix Friedrich) for all their support and engagement.

This work was supported by grants to Lucie Carrier from the DFG Forschergruppe 604 (CA 618/1-2), Fritz Thyssen Stiftung (Az. 10.09.1.139) and EU-FP7-Health-F2-2009-241577 (BIG-Heart).